Fall 2020

Investigating the Timing of initial Louann Salt Flow and Its Relationship with the Gilbertown Fault Zone, Southwest Alabama

Avery Rosenbalm

INVESTIGATING THE TIMING OF INITIAL LOUANN SALT FLOW AND ITS RELATIONSHIP WITH THE GILBERTOWN FAULT ZONE, SOUTHWEST ALABAMA

by

Avery Rosenbalm

A Thesis
Submitted to the Graduate School,
the College of Arts and Sciences
and the School of Biological, Environmental, and Earth Sciences
at The University of Southern Mississippi
in Partial Fulfillment of the Requirements
for the Degree of Master of Science

Approved by:

Dr. Jeremy Deans, Committee Chair
Dr. T. Markham Puckett
Mr. Tony Stuart

December 2020

Published by the Graduate School

ABSTRACT

The Mesozoic Louann Salt extends through the northern GOM, extending onshore from eastern Texas to western Alabama and Florida. Along the landward terminus of the salt is a system of peripheral faults, including the Gilbertown Fault Zone bordering the Mississippi Interior Salt Basin to the north and east. This study sought to constrain the timing of fault movement and determine its relationship to the baswinward evacuation of Louann Salt through the use of a 3D seismic survey and well logs. By mapping Mesozoic formations and the peripheral fault system, lateral changes in formation thickness were used to generate fault expansion indices (FEI) and formation thickness charts, whereas well logs were utilized for finding formation tops and density. Through comparing the timing of fault slip, salt evacuation, lateral differential loading, and density changes, this study suggests the evacuation of salt flow initiated before an average stratigraphic density inversion formed and before more faults slipped. This indicates that faults moved as a passive response to salt evacuation. Multiple peaks in fault slip along all of the faults are observed through the Mesozoic with some differences in timing and magnitude, but patterns of slip across all faults indicate main slip events during the deposition of the Cotton Valley Group, the Mooringsport Formation, and the Eutaw Formation. The record of fault motion makes clear that salt evacuation is episodic and increased during periods of greater deposition and density inversion.

ACKNOWLEDGMENTS

I would like to express my gratitude to Savannah Oil and Gas Company, LLC and their associates for the donation of the Gilbertown 3D seismic survey. Their generosity made this study possible. I would like to thank my committee members, Dr. Puckett and Mr. Tony Stuart for their assistance with this project, and my committee chair, Dr. Deans, for his endless patience and guidance.

TABLE OF CONTENTS

LIST OF TABLES

LIST OF ILLUSTRATIONS

LIST OF ABBREVIATIONS

FEI	Fault Expansion Index
GFS	Gilbertown Fault System
GOM	Gulf of Mexico
MFS	Melvin Fault System
MISB	Mississippi Interior Salt Basin
WBFS	West Bend Fault System

CHAPTER I – INTRODUCTION

This study focused on the temporal relationship between the initiation of movement of the Louann Salt and the initiation and movement of the regional peripheral fault zone, the Gilbertown Fault Zone, by investigating the wedgeward terminus of the Louann Salt and associated Mesozoic sedimentary deposits using well logs and a 3D seismic survey. Salt tectonism of the Louann Salt has been influential in the subsurface structures of the Gulf of Mexico (GOM) region and integral to the basin's development and evolution by increasing accommodation space and helping develop the petroleum system. The (GOM) is divided into several smaller salt basins, one being the Mississippi Interior Salt Basin (MISB) which extends through southwestern Alabama to southern Mississippi and into much of Louisiana (Mancini and Puckett, 2000). The MISB has Louann Salt overlying basement (Dobson and Buffler, 1997) with alternating siliciclastic and carbonate deposits filling the basin (Puckett and Mancini, 1999). The wedgeward terminus of the Louann Salt is closely followed by the peripheral Gilbertown Fault System at the northern edge of the basin (Bishop, 1973; Hughes, 1968; Mancini and others, 1999; Martin, 1978), with some authors suggesting that there is more slip than predicted for the amount of salt evacuation (Hughes, 1968). The basin has as much as 13,000 ft of sediment overlying the Louann Salt (Mancini and others, 1999). The fault system is comprised of largely *en echelon* listric normal faults that extend from western Texas to eastern Florida (Mancini and others, 2001a). Basinward movement of the salt is hypothesized as a cause of the peripheral faults (Bishop, 1973; Martin, 1978). The mechanism driving salt movement and the normal fault system is still largely contested (Eoff and others, 2015; Rowan, 2019), with interpretations including gravity driven

faulting, relict basement faults and topography, differential compaction of sediments, gravity flow of salt, and sediment creep (Bishop, 1973; Fossen, 2016; Hughes, 1968; Jin and others, 2009).

When salt movement initiated is also still under investigation in the MISB. Hughes (1968) suggested salt flow began soon after deposition of the salt, during deposition of the overlying Oxfordian Norphlet Formation; Jackson and Seni (1983) indicated the earliest record of movement occurred later, during Late Jurassic (Tithonian) coincident with Jurassic Cotton Valley Group deposition. Largely, studies leave it ambiguous, suggesting initiation as Early Cretaceous or Late Jurassic (Andrews, 1960; Johnson and others, 2006; Mancini and others, 2001b; Qi and others, 1998; Shah Alam and Pilger, Jr., 1988).

This study focuses on a portion of the peripheral fault system—specifically the Gilbertown Fault Zone imaged in the seismic survey outlined Figure 1—that may have implications for the rest of the peripheral fault system across the GOM. The main hypothesis being, when and why did the Louann Salt begin to evacuate? More specifically, what is the relationship between salt movement, faulting, density inversion, sediment thickness variation, and sediment creep? This study has been granted access to a 100 mi^2 seismic survey in Choctaw County, Alabama, thanks to Savannah Oil & Gas, LLC and its affiliates.

Additionally, the study area and region have significant petroleum reserves, making this study of interest to a wide variety of workers and society. Faulting proximal to mechanically weak layers such as salt can be complex due to the differences in strain response. With several potential contributing factors to induce fault movement,

constraining the timing of initial salt movement is possible, and could also potentially isolate the core driving element(s) of fault initiation. Additionally, the interplay between deposition, faulting, and salt evacuation was evaluated. This study seeks to a) map the geometry of the fault and related fold system in the 3D seismic section, b) use well logs to determine if there are loci of significant deposition such as deltas near the fault system that could induce movement through differential loading, c) measure and compare the thickness of sediments above and below the fault to test the validity of sediment creep using a fault expansion index, and d) determine at what point of sedimentation was the density differential significant enough to initiate salt movement using density logs and compaction curves.

Figure 1.1 *Index Map*

Index map of the extent of the Louann Salt and the peripheral fault zones in the northern Gulf of Mexico region. The donated 3D seismic survey is outlined in red. Modified after Hosman (1996) and Ko (2014).

CHAPTER II – LITERATURE REVIEW

2.1 Geologic Setting

2.1.1 Gulf of Mexico

The GOM formed from the process of Pangaea rifting during the Middle to early Late Jurassic (Worrall and Snelson, 1989). Failure occurred along the former Gondwana-Laurentia boundary, and the more weakly sutured accreted terranes (Eddy and others, 2018). Extension initiated in the Late Triassic (~210 Ma) with the collapse of the Appalachian and Ouachita mountains with rifting trending northwest to southeast with little lateral movement as North America and South America began splitting apart (Bird and others, 2005; Eddy and others, 2014; Eddy and others, 2018; Pindell and others, 2014; Worrall and Snelson, 1989). Shallow seas that form with rifting often provide depositional environments for evaporites, and that proved to be the case in the GOM.

While there is some dispute regarding the timing of the evaporitic sequences deposition of the Werner Anhydrite and the Louann Salt, it is largely agreed that deposition occurred at the end of rifting and prior to seafloor spreading (Bird and others, 2005; Eddy and others, 2014; Eddy and others, 2018) as evidenced by the separation of the northern Louann Salt and the southern Campeche Salt, which are suggested to be the same formation (Worrall and Snelson, 1989). Shortly after evaporite deposition, the Yucatan Peninsula began to rotate, changing the spreading orientation from northwest-southeast to northeast-southwest extension (Bird and others, 2005; Eddy and others, 2014; Eddy and others, 2018; Pindell and others, 2014; Worrall and Snelson, 1989). This rotation, coupled with the seafloor spreading, is attributed to separating the two sections of salt (Eddy and others, 2018).

With the newly formed GOM, transgressive-regressive sequences in the Late Jurassic deposited clastic and carbonate sediments on the salt. During the Cretaceous, the passive-margin region experienced tectonic activity, inducing a series of uplifts across the northern GOM region (Worrall and Snelson, 1989). The Sabine Uplift, Monroe Uplift, and Wiggins Arch are all positive features that arose through the Triassic (Adams, 2009). In this period, the northern GOM largely was composed of gently sloping carbonate shelves, which experienced two cycles of progradation (Worrall and Snelson, 1989). The uplifts, coupled with underlying salt flow, provided Cretaceous formations with structural features optimal for hydrocarbon localization (Worrall and Snelson, 1989).

Cenozoic deposition largely originated from migrating alluvial sources, resulting in characteristic delta to distal marine sequences (Worrall and Snelson, 1989). Structures such as listric faults rooted in older formations continue to have expression in Cenozoic formation. (Worrall and Snelson, 1989).

2.1.2 Stratigraphy

This section will attempt to give an overview of the main Mesozoic units in southwest Alabama and east Mississippi as they pertain to the focus of this study (Figure 2.1). Some disconnect exists between the naming system of subsurface units between state surveys. As the seismic block used for this study was shot just within the Alabama border, the naming system used by the Geological Survey of Alabama will be adhered to.

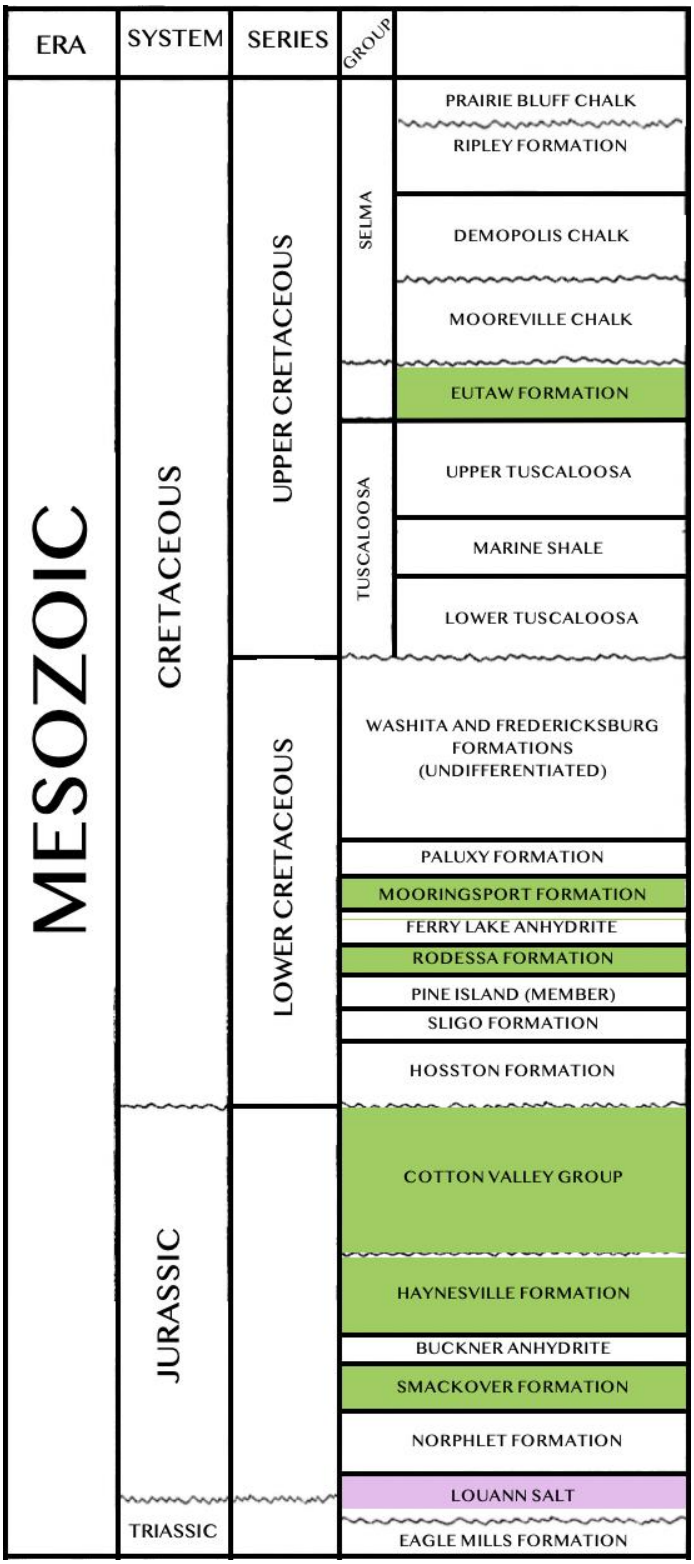

Figure 2.1 *Mesozoic stratigraphic column*

Louann Salt (pink) and other important formations (green) highlighted. Modified after (Wilson, 1976).

The basement of the MISB and the southwest corner of Alabama is crystalline and sedimentary Paleozoic rocks (Dockery, III and Thompson, 2016; Raymond and others, 1988a). Unconformably overlying the Paleozoic basement, is the Eagle Mills Formation, the first Mesozoic formation. This section will start with a description of the Eagle Mills Formation and continue stratigraphically upwards through the Selma Group, and terminate with a description of Cenozoic deposition.

Eagle Mills Formation: The Eagle Mills Formation is a red-bed, non-marine unit of mostly shales, mudstones, and siltstones, with infrequent medium- to coarse-grained sandstones, and identified as Late Triassic by the presence of *Macrotaeniopteris magnifolia*, (Dawson, 1995; Dawson and Callender, 1992; Dockery, III and Thompson, 2016; Raymond, 1989; Salvador, 1991; Scott and others, 1961). While broadly described as a red-bed, the Eagle Mills Formation is described in more detail as mottled red and purple, and frequently gray to green due to the presence of chlorite (Dawson, 1995; Salvador, 1991). Alluvial fan and stream bed deposits are likely the depositional environment for the coarser sections, typically seen in lower parts of the formation, while finer sedimentation dominated the upper formation and is attributed to flood plains or lake beds (Scott and others, 1961). Clast size also appears to increase the further east the formation extends (Scott and others, 1961). The formation has a depositional relationship to graben areas, including that of the peripheral fault system and the Gilbertown Fault Zone (Dockery, III and Thompson, 2016; Scott and others, 1961), though this has yet to be fully explained.

Minor igneous intrusions are observed in the formation. Diabase and basalt dikes and sills from Late Triassic and Early Jurassic rifting cut through the Eagle Mills Formation (Dawson, 1995; Dawson and Callender, 1992; Dockery, III and Thompson, 2016; Raymond, 1989). Clasts of the intrusions are present in the unconformably overlying Werner Conglomerate (Scott and others, 1961), which is noted to be relatively indistinguishable from the Eagle Mills Formation and is often considered one unit (Dawson and Callender, 1992).

Louann Salt*:* The Louann Salt was deposited during the Callovian and Oxfordian and unconformably overlies the Werner Formation (Dockery, III and Thompson, 2016; Mancini and others, 1990; Mancini and others, 2001a; Rhodes and Maxwell, 1993; Wade and Moore, 1993). The salt extends from south of the peripheral fault zone to beyond the shelf break in the GOM, only absent on structural highs such as the Wiggins Arch (Dockery, III and Thompson, 2016; Rhodes and Maxwell, 1993). The salt is considered significantly pure, coarse crystalline halite, with infrequent streaks of sands, shales, or anhydrite (Andrews, 1960; Wade and Moore, 1993). As much as 6,000 feet in thickness was deposited (Bearden and others, 2000; Halbouty and Hardin, Jr., 1956; Hughes, 1968; Mancini and others, 1990; Pindell and others, 2014). In some areas of the Alabama MISB, an anhydrite member of the Louann Salt caps the formation, known as the Pine Hill Anhydrite (Mancini and others, 1990). More on the Louann Salt, its formation, and salt tectonics will be discussed in later sections.

Norphlet Formation*:* The Oxfordian Norphlet Formation varies lithologically across its geographic range, but in the study area, it is primarily composed of continental-derived clastic sediments (Tew and others, 1991). The depositional environment was an extensive

desert plane bounded by Paleozoic and Proterozoic composed highlands (Tew and others, 1991). Deposited conformably on top of the Louann Salt, it exhibits a regressive depositional sequence with four recognized lithofacies: 1) a basal shale representative of lagoons or bays isolated from the shoreline; 2) conglomeratic sandstone found predominately in up-dip areas of the formation, 3) red beds of both sandstone and siltstone downdip of the second lithofacies, interpreted as wadi deposits; and 4) an aeolian quartzose sandstone, the topmost of which experienced marine reworking related to the transgression that began Smackover deposition (Dockery, III and Thompson, 2016; Hunt and others, 2017; Schmoker and Schenk, 1994; Tew and others, 1991; Wade and Moore, 1993). Maximum formation thickness appears to be in the MISB at 900 feet (Mancini and others, 1990), however in Alabama the formation thickness peaks at 800 feet (Tew and others, 1991).

Smackover Formation*:* The Smackover Formation, depending on the location, has either a gradational or an abrupt contact with the underlying Norphlet Formation (Mancini and others, 1990) and an upper contact at the top of the uppermost occurrence of limestone beneath the Buckner Anhydrite (Petty, 2010). Ammonite records date the formation to the late Oxfordian (Mancini and others, 1990). Deposited during two system tracts (Tonietto and Pope, 2013), the Smackover Formation is commonly divided into three lithofacies (Dockery, III and Thompson, 2016; Mancini and others, 1990; Petty, 2010; Wade and Moore, 1993). The lower Smackover Formation, part of a transgressive systems tract, is largely an algal carbonate mudstone laminated with wackestone and packstone packages, likely deposited in a subtidal to intertidal environment (Dockery, III and Thompson, 2016; Mancini and others, 1990; Petty, 2010; Tonietto and Pope, 2013;

Wade and Moore, 1993). The middle Smackover Formation includes shale and siltstone interbedded with packstone (Petty, 2010), still in a transgressive systems tract (Tonietto and Pope, 2013). The upper Smackover Formation exhibits cycles of coarsening upwards, with sequences of fine-grained sandstones to oolitic, peloidal, and oncoidal packstones to grainstones, and shoaling packages across local highs (Dockery, III and Thompson, 2016; Petty, 2010; Tonietto and Pope, 2013; Wade and Moore, 1993) The upper facies was deposited during the highstand systems tract (Tonietto and Pope, 2013). Regionally, the Smackover Formation thickness varies, thinning over paleohighs, and has an average thickness in Alabama of approximately 300 feet (Mancini and others, 1990).

Buckner Anhydrite*:* The Buckner Anhydrite conformably overlies the Smackover Formation, interfingering or gradationally (Mancini and others, 1990; Mann, 1988; Salvador, 1991). Some studies refer to the Buckner Anhydrite as a formation (Bishop, 1971; Dockery, III and Thompson, 2016; Wade and Moore, 1993), while others refer to it as a basal member of the Haynesville Formation (Benson and others, 1996; Mancini and others, 1990; Mann, 1988; Salvador, 1991). Wade and Moore (1993) assert that the Buckner Anhydrite interfingers with the stratigraphically higher Cotton Valley Group sands in Alabama, thus eliminating the Haynesville Formation altogether. The Buckner Anhydrite was predominantly deposited during the highstand systems track at the end of Smackover Formation deposition (Salvador, 1991). The depositional environment is largely interpreted to be shallow waters protected from an open marine environment, in environments such as coastal lagoons and sabkhas (Benson and others, 1996; Mancini and others, 1990; Mann, 1988; Salvador, 1991). The Buckner Anhydrite is characterized by evaporite sequences principally of anhydrite and thin red beds, caused by cycles of

subaqueous deposition until sediment accumulation exceeded sea level for subaerial exposure, then increasing accommodation space to resume the cycle (Benson and others, 1996; Mann, 1988). Halite deposits as thick as 1000 feet (Wade and Moore, 1993) locally cap the Buckner Anhydrite (Mancini and others, 1990; Salvador, 1991). Anhydrite thickness averages 100 – 150 feet in southwest Alabama (Mann, 1988) and locally thins over paleohighs and salt highs, implying salt movement prior to Buckner Anhydrite deposition (Benson and others, 1996; Dockery, III and Thompson, 2016).

Haynesville Group*:* The Haynesville Group—or Formation, depending on sources—was deposited during the late Kimmeridgian to early Tithonian in a highstand systems tract (Hammes and Frébourg, 2012; Salvador, 1991), part of a worldwide episode that deposited organic-rich calcareous mudstones (Hammes and others, 2011). Overlying the Buckner Anhydrite, the Haynesville Group is lithologically variable, and is predominantly interbedded terrigenous clastics and carbonates along the eastern extent with thin anhydrite beds (Mancini and others, 1990; Obid, 2005; Salvador, 1991). Deposition was likely along a wide shelf of the Apalachicola basin (Dobson and Buffler, 1997) in shallow, stratified water (Hammes and others, 2011), with the formation thinning or absent along salt highs (Salvador, 1991). A member of the Haynesville Group, the Frisco City Sandstone, is present in southwest Alabama, indicative of an alluvial fan environment that grades to shoreface deposits downdip (Salvador, 1991). In the MISB region of Alabama, the Haynesville may be as thick as 2,800 feet (Mancini and others, 1990).

Cotton Valley Group*:* Overlying the Haynesville Formation is the Cotton Valley Group, deposited in the Late Jurassic (Forgotson, Jr., 1954; Mann and Thomas, 1964; Moore,

1983; Payeur and others, 2017; Sydboten, Jr. and Bowen, 1987) to potentially the beginning of the Cretaceous (Dobson and Buffler, 1997). While the Cotton Valley Group is divided into four formations—the Bossier Shale, Terryville Sandstone, Hico Shale, and Knowles Limestone—within east Texas and Louisiana (Mann and Thomas, 1964), in the MISB the Cotton Valley Group is largely treated as one formation, though some studies identify two members, the lower Shongaloo Member and an upper Dorcheat Member (Moore, 1983). The Cotton Valley Group has minor interbedded limestones and shales of predominantly course to fine clastic sediments (Sydboten, Jr. and Bowen, 1987). The base of the Cotton Valley Group is picked above the Haynesville Group at the initial appearance of limestone (sometimes referred to as the Knowles Limestone) and picked below the Hosston Formation at the primary shale below gravel (Moore, 1983). The depositional environment has largely been attributed to one or two large deltaic systems that occurred in the MISB, with a higher amount of clastic sediments in the eastern reaches of the MISB attributed to being nearer the source of clastic sediment (Dobson and Buffler, 1997; Sydboten, Jr. and Bowen, 1987) or originating from a nearer source than that of the delta system (Forgotson, Jr., 1954). Influence of salt tectonism on deposition has been demonstrated by thickened wedges along the margins of salt detachments (Payeur and others, 2017). Variable erosion of the Cotton Valley Group is suggested by transitional contacts with the Cretaceous sediments above in some locations and sharp contacts in others (Payeur and others, 2017).

Hosston & Sligo Formations*:* Overlying the Cotton Valley Group are the Hosston and Sligo Formations. The Hosston Formation continues beyond the up-dip limit of the Cotton Valley Group, where it unconformably overlies older Jurassic rocks (Mink and

Mancini, 1995). There is a gradational contact between the updip Hosston Formation and the downdip equivalent Sligo Formation (Mancini and Puckett, 2000). Hauterivian to Aptian in age, the Hosston and Sligo Formations were deposited as a transition from shallow marine (Sligo Formation) to continental clastic (Hosston Formation) (Doolan and others, 2011; Mancini and Puckett, 2000; Thomson, 1978). The Sligo Formation is more limited in the region, only occurring within the southern region of the MISB, where it is mostly beds of shales and fine sandstones; outside of the MISB, the formation is predominantly limestone (Doolan and others, 2011; Mancini and Puckett, 2000). The up-dip Hosston Formation fines upward, but is largely a sandstone unit (Rives, 1961) with interbedded shales and mudstones (Nunnally and Fowler, 1958). In Alabama, the sediments are likely sourced from the Appalachian Mountains to the northeast and deposited in deltaic to beach environments (Doolan and others, 2011; Mink and Mancini, 1995). This results in a large variation in lithology, with conglomeratic sands to nodular mudstones (Nunnally and Fowler, 1958). The Hosston Formation, in central MISB, reaches thicknesses of 3300 feet (Thomson, 1978).

Pearsall Formation*:* In the Gulf Coast region, the Pearsall Formation overlies the Sligo Formation and is composed of three members: the Pine Island Shale, the James Limestone, and the Bexar Shale (Enomoto and others, 2012). In southwest Alabama, the stratigraphic column generally includes only the Pine Island member of the Pearsall Formation (Doolan and others, 2011; Forgotston, Jr., 1963; Wilson and others, 1976) or includes the James Limestone, which only extends into the southern reaches of the MISB (Enomoto and others, 2012; Mancini and others, 2001a). The Pine Island Shale is largely dark calcareous shales intermixed with fissile mudstone and siltstones to fine and

medium grained sandstones (Enomoto and others, 2012; Mancini and others, 2001a). Deposition likely occurred near the source on the shelf in a fluvial or deltaic environment (Forgotston, Jr., 1963). The Pine Island Shale has thicknesses ranging from 640-1262 feet in the MISB (Valentine and others, 2014). The James Limestone occurs as limestone interbedding becomes more pervasive downdip and becomes regionally extensive (Mancini and others, 2001a).

Rodessa Formation*:* Overlying the Pine Island Shale is the Rodessa Formation, a lithologically varied formation that thickens and fines southward (Forgotston, Jr., 1963; Roberts and Lock, 1988). The depositional environment was most likely a shelf with a restricted backreef area (Forgotston, Jr., 1963; Pittman, 1984; Roberts and Lock, 1988) with local sediments sourced from the Appalachian Mountains being deposited in stacked meander belts, indicated by thin fining upwards packages (Esposito and others, 2008). In eastern Mississippi and southwest Alabama the sediments grade from fine micaceous sands to calcareous and biogenic shales, with marine limestones increasing in occurrence basinward (Esposito and others, 2008; Forgotston, Jr., 1963; Roberts and Lock, 1988). The end of Rodessa Formation deposition saw increased shelf restriction from reef development, leading to increased salinity and an increase in evaporites, including an anhydrite bed (Forgotston, Jr., 1963; Pittman, 1984; Roberts and Lock, 1988; Valentine and others, 2014). Rodessa Formation thickness in the MISB has been found to be around 800 feet (Esposito and others, 2008).

Ferry Lake Anhydrite*:* Conformably overlying the Rodessa Formation is the Ferry Lake Anhydrite (Pittman, 1984). Dated to Albian times through ammonite occurrences, its deposition is strongly influenced by the reef growth that restricted circulation during

upper Rodessa Formation deposition (Petty, 1995; Pittman, 1984). The resulting lagoon remained throughout Ferry Lake Anhydrite deposition, with occasional flooding over the reef disrupting the stratopycnal body (Kimball and others, 1989; Petty, 1995; Pittman, 1984). Consequently, the formation of predominantly anhydrite beds includes interbedded shale and carbonates, particularly oolitic limestone (Forgotson, Jr., 1957; Kimball and others, 1989; Pittman, 1984). While observed in southwest Alabama (Wilson and others, 1976), Forgotson (1957) asserts that the Ferry Lake Anhydrite thins to disappears in central Mississippi. Pittman (1985) specifies a thickness of 200-250 feet over most of the region. When absent, the Rodessa Formation is overlain by the Mooringsport Formation.

Mooringsport Formation*:* The Mooringsport Formation conformably overlies the Ferry Lake Anhydrite (Forgotson, Jr., 1957). With a maximum thickness in the MISB of 800 feet, up-dip the formation thins, with a thickness of only 250 feet in eastern Mississippi (Dockery, III and Thompson, 2016; Nunnally and Fowler, 1958). Foraminiferal correlation has dated the Mooringsport Formation as forming during the mid to late Albian (Mancini and Puckett, 2000). The Mooringsport Formation continued deposition of the restricted shelf and lagoonal environment that developed during Rodessa Formation and Ferry Lake Anhydrite deposition (Raymond and others, 1988b). As such, a range of lithologies are observed, with limestones dominant downdip, sandstones up-dip, and shales in the intermediary, though the formation is mostly marine shale and limestone (Mancini and Puckett, 2000; Nunnally and Fowler, 1958). To the northeast of the basin, micaceous fine-grained sandstones, mudstones and shales with minimal limestone nodules dominates the lithology (Nunnally and Fowler, 1958). In some

locations, the absence of limestones can make distinguishing the upper Mooringsport Formation from lower Paluxy Formation nearly impossible (Dockery, III and Thompson, 2016).

Paluxy Formation*:* Conformably overlying the Mooringsport Formation is the Paluxy Formation (Mancini and Puckett, 2000; Nunnally and Fowler, 1958). Divided in two members by Mancini & Scott (2006), the lower member is characterized by fossiliferous clay- and mudstones and very fine-grained sandstones. Their upper member is described as a nonfossiliferous, friable sandstone and interbedded silt- and claystones. This chiefly sand and shale sequence is how the formation is identified, with the top of the formation picked at the lower limestone occurrence of the overlying Fredericksburg Group (Dockery, III and Thompson, 2016; Nunnally and Fowler, 1958). The middle of the formation is largely sandstone, with thinner shale packages, while the upper and lower segments of the formation exhibit thicker shales packages (Mancini and Puckett, 2000). Maximum thickness of the Paluxy Formation is 1500 feet, though in eastern Mississippi, it is 800 feet (Dockery, III and Thompson, 2016).

Washita-Fredericksburg (Undifferentiated)*:* The Washita and Fredericksburg Formations are composed predominantly of limestone and deltaic deposits, and the contact between them is insufficient to easily differentiate them in well logs (Reese, 1975). As a result they are referred to as the Washita-Fredericksburg Undifferentiated (or Wash-Fred) in the MISB, and as the undifferentiated Lower Cretaceous units in Alabama (Swanson and others, 2013). The Fredericksburg Formation begins a cycle of transgressive, onlapping shelf limestones and intermediary lowstand continental clastics (Dockery, III and Thompson, 2016; Swanson and others, 2013; Talbert and Atchley,

2000). As the transgressive cycle ended and the shoreline began to regress due to inland uplift, Washita Formation deposition commenced (Swanson and others, 2013). The Washita Formation sedimentation is largely similar to that of the Fredericksburg Formation, though the sands progress southward as the deltaic systems prograde with the receding shore (Reese, 1975). Across the greater GOM area, the Wash-Fred may include or be subdivided into smaller formations, including the Edwards Limestone, Person Formation, Goodland Limestone, Kiamichi Formation, Kainer Formation, and the Dantzler Formation (Dockery, III and Thompson, 2016; Swanson and others, 2013). The Dantzler Formation caps the Wash-Fred, composed of red shale and sands with some fossiliferous zones (Dockery, III and Thompson, 2016). Thickness for the Wash-Fred is as much as 1500 feet (Dockery, III and Thompson, 2016).

Tuscaloosa Group (Lower, Marine Shale, Upper)*:* The Tuscaloosa Group unconformably overlies the Lower Cretaceous sedimentary rocks, and is divided into three sections: the Lower Tuscaloosa, the Marine Shale, and the Upper Tuscaloosa (Mancini and others, 1987; Winter, 1954). The Lower Tuscaloosa is Cenomian, during which there was a worldwide sea-level rise, and as such upwardly grades from fluvial and deltaic systems to marine shelf systems (Mancini and others, 1987). The Lower Tuscaloosa includes a massive sand unit from barrier island sands, a claystone unit from lagoonal deposits, and sands from the shelf (Dockery, III and Thompson, 2016; Mancini and others, 1987). The Marine Shale is of late Cenomian age, and exhibits glauconitic and carbonaceous claystone that is rich in macrofossils indicative of a shallow marine shelf (Dockery, III and Thompson, 2016; Mancini and others, 1987; Munyan, 1943). As sea level fell, depositional environments similar to those of the Lower Tuscaloosa

resumed, and Upper Tuscaloosa sediments are primarily composed of variegated sands and clays (Munyan, 1943), with a basal gravel layer (Dockery, III and Thompson, 2016).

Eutaw Formation*:* Conformably overlying the Tuscaloosa Group is the Eutaw Formation (Mancini and others, 1987). Comprised of two members, an unnamed lower and the upper Tombigbee Sand, it can reach thicknesses of 350 feet in Alabama (Liu, 2005; Mancini and Soens, 1994). The lower member of the Eutaw Formation has a basal section of chert pebbles, phosphatic nodules, and fragments of permieralized wood and shark teeth, while the remainder of the bed is generally glauconitic and micaceous crossbedded sandstone with clay laminations (Dockery, III and Thompson, 2016; Mancini and Soens, 1994). The Tombigbee Sand is locally highly fossiliferous, and is massive sandstones with glauconite, crossbedding, and laminae (Dockery, III and Thompson, 2016; Liu, 2005; Mancini and Soens, 1994). The Tombigbee Sand likely deposited in nearshore environments of isolated lagoons, deltas, and tidal inlets (Liu, 2005).

Selma Group*:* The Selma Group is a series of shallow marine carbonates, separated into four main formations: the Mooreville Chalk, the Demopolis Chalk, the Ripley Formation, and the Prairie Bluff Chalk (Copeland, 1968; Dockery, III and Thompson, 2016; Heydari, 2000). The oldest, the Mooreville Formation, overlies the Eutaw Formation and is a thin-bedded gray marl, with a very dense section of a few feet at the top of limestone known as the Arcola Limestone Member (Copeland, 1968; Heydari, 2000). The Demopolis Chalk unconformably overlies the Mooreville Formation, and has a lower member of gray marl, and a middle and upper member of argillaceous chalk, of which contains a very high percent of $CaCO_3$ (Copeland, 1968; Heydari, 2000). The Ripley Formation

conformably overlies the Demopolis Chalk and is comprised of calcareous clays, and fossiliferous or micaceous sands (Copeland, 1968). The uppermost member of the Selma Group, the Prairie Bluff Chalk is massive fine and micaceous chalk with variable fossil abundance (Copeland, 1968). In all, the Selma Group reaches thicknesses of 950 feet in western Alabama, and is indicative of a major marine transgression for the area (Dockery, III and Thompson, 2016). Northward, the members grade into continental clastic rocks (Dockery, III and Thompson, 2016).

Cenozoic Sedimentation*:* Unconformably overlying the Selma Group is the Midway Group, which is the first of the Cenozoic sediments (Cushing and others, 1964). The Wilcox Group, Claiborne Group, and Jackson Group comprise the remainder of the main formations in the study area (Cushing and others, 1964) Largely, Cenozoic sediments are unconsolidated sands, clays, and shales, with a maximum thickness of 7,000 feet in the MISB (Cushing and others, 1964).

2.2 Salt Tectonics

Salt, due to its rheological properties, is generally weaker than its overburden and may be induced to evacuate its original deposition extent as a result of mechanisms such as density inversions (buoyancy), gravity spreading, differential loading, local loading, and sediment creep (Hudec and Jackson, 2007; Hughes, 1968; Rowan, 2019; Vendeville, 2005). Sedimentary layers comprised predominantly of halite are referred to as salt deposits, despite potential presence of other evaporites such as anhydrite, or other minerals (Hudec and Jackson, 2007). Pure rock salt has a density of 2.16 g/cc, though lithologic layers defined as salt, due to the aforementioned impurities, is typically 2.20

g/cc (Fossen, 2016; Hudec and Jackson, 2007; Jackson and Hudec, 2017; Warren, 2006). Compaction that occurs during diagenesis from continued deposition increases the density of the overburden, potentially creating a density inversion (Fossen, 2016; Hudec and Jackson, 2007; Jackson and Hudec, 2017; Warren, 2006). Dry salt will deform via dislocation creep, whereas minimal water content weakens the salt and causes movement through diffusion creep (Archer and others, 2012; Fossen, 2016; Hudec and Jackson, 2007). Salt behaves viscoelastically, but under geologic conditions, time scales, and strain rate, elasticity can effectively be ignored and, for modelling purposes, salt may be treated as a viscous fluid (Fossen, 2016; Hudec and Jackson, 2007). Initially, both the salt and the overburden had been modeled as viscous fluids, but research has indicated that the brittle nature of lithified overburden is necessary to incorporate into models (Fossen, 2016; Jackson and Hudec, 2017). In instances of lithified overburden, the salt must overcome the yield strength of overlying sediment and boundary drag, variables not accurately modelled when also treating the overburden as a fluid (Hudec and Jackson, 2007; Vendeville, 2005).

Triggers of salt movement are varied and numerous. Not only must there be one or more triggers for movement initially, but there must also be at least one mechanism that continues to drive movement (Rowan, 2019). Buoyancy was long treated as the dominant mechanism for both triggering and driving salt flow due to density inversions, but other forces have been assessed for their viability in contributing to salt movement. With the 2.20 gm/cc density even after minimal compaction, salt is significantly less dense than its overburden: lithified carbonates can have densities as high as 2.7-2.8 g/cc, and while uncompressed siliciclastic sediments have similar density to salt, after

compression siliciclastic rocks have higher density than salt. Some debate exists as to how much overburden must exist to induce movement (Hughes, 1968; Vendeville, 2005). For the already more dense carbonates, it is possible that movement can begin to occur syndepositionally under unlithified sediments, but this is not thought to be the case for siliciclastics (Hudec and Jackson, 2007; Hughes, 1968; Jackson and Hudec, 2017; Vendeville, 2005). To compress siliciclastic sediments to a density greater than salt, there must be at least 2,000-2,300 feet of overburden for fine-grain sizes, or up to 5,000-10,000 feet for larger grain sizes (Fossen, 2016; Hudec and Jackson, 2007; Rowan, 2019). Once achieved, this density differential may drive the buoyancy of salt to rise towards the surface.

However, it is thought that density alone does not trigger movement. Archer and others (2012) posit that as a viscous liquid, salt can be initiated to flow by small regional dips from gravity, with slopes as little as 0.5%, while Vendeville (2005) asserts the critical angle is less than 1°. Differential loading, whether sedimentary, tectonic, or thermal (Hudec and Jackson, 2007), can also trigger lateral or upward migration (Archer and others, 2012; Fossen, 2016; Jackson and Hudec, 2017; Vendeville, 2005; Warren, 2006; Warsitzka and others, 2013). Variations across the salt in any such differential loading may induce zones of differing pressure, leading to movement of salt to lower pressures. Differential loading is especially significant near focused deposition, such as deltas.

Salt will laterally move from high depositional load towards low depositional loads in a positive feedback cycle: areas of thicker—and therefore heavier—overlying sediment will settle downward into the salt inducing a pressure difference, forcing the salt

to evacuate outward from beneath the load (Hudec and Jackson, 2007; Jackson and Hudec, 2017; Rowan, 2019). This creates surficial basins that will subsequently receive greater sedimentation, increasing the overburden and further expelling the underlying salt from that area. As it is pressure driven, and not density driven, salt flow in such a manner can occur even when there is a lack of density inversion (Vendeville, 2005).

2.3 Louann Salt

The Louann Salt is an integral part of the GOM region's geology and, through subsurface movement and salt structures, has a large influence on the strata. The relative pureness of the salt, mentioned previously, is largely a function of the paleoenvironment it was deposited in. Branson (1915) first proposed the "modified bar theory" to explain how large deposits of gypsum and salt were forming. The modified bar theory suggests that marine waters enter a primary barred basin, where the initial precipitates calcite and gypsum are deposited and the residual water is concentrated brine. Recurring cycles would further concentrate the brine, until sea level rise was sufficient enough to flood the primary barred basin and push the brine into a secondary basin through thin channels, where halite would be deposited. Eventually, there would be a primarily anhydrite/gypsum basin adjacent to a primarily halite basin. Hazzard et al (1945) ascribed this explanation to the Louann Salt. The west Texas Delaware Basin acted as the first basin, where the Permian Castile Formation is a series of alternating layers of calcite and gypsum and minimal halite, while the Gulf Coast Basin was the secondary, depositing the relatively pure Jurassic Louann Salt as basin waters became more saline over time (Halbouty and Hardin, Jr., 1956).

Development of the MISB sub-basin of the Gulf Coast Basin is a function of the paleo-highs. The Wiggins Arch, which has no salt present, and the Adams County High, which has minimal salt, mark the southern bounds of the MISB (Salvador, 1991). To the northwest and west, the Monroe Uplift, LaSalle Arch, and Sabine Uplift separate the MISB from the North Louisiana salt basin, while the Conecuh Ridge is an influential high to the east (Andrews, 1960; Salvador, 1991). The northern termination of the basin is largely a function of up-dip termination, which may be influenced by the Ouachita Belt trending northwest to southeast through north-central Mississippi, and the Appalachian Front trending northeast to southwest through northern Alabama resulting in highlands along the northeast boundary of the MISB (Worrall and Snelson, 1989). This northern limit of the MISB, and the extent of the Louann Salt as a whole, is now marked by a series of peripheral fault zones, regionally being the Pickens-Gilbertown Fault Zone, discussed below (Bishop, 1973; Hughes, 1968).

Salt related subsurface structures follow a typical trend from proximity to the peripheral fault zones to the interior of the basin (Hughes, 1968). In the MISB, structures that form in the thinnest salt, near the up-dip pinch-out and have salt anticlinal thicknesses of 500-2000 feet, are known as peripheral salt ridges. These ridges run parallel to the peripheral fault zones and form as initial salt flow moved up-dip, but are not significant enough to pierce through overlying sediments (Fossen, 2016; Hughes, 1968). Further downdip into the salt basin, low-relief salt pillows are the dominant structure, which typically occur at salt anticlinal thickness of 1000-3500 feet, with a general parallel trend to the peripheral salt ridges and minimal structural effect on formations above the Haynesville Formation (Hughes, 1968). In the central basin area,

anticline thicknesses of 3,500-7,000 feet are intermediate salt anticlines, while those that reach 7000 feet and above Hughes (1968) refers to as high relief salt anticlines. High relief structures may take different shapes, including ridges, stocks, and teardrop diapirs, sometimes referred to as piercement domes (Fossen, 2016). Two domes, Richton and Tatum, have risen to an extent to be within 1000 feet of the surface (Bearden and others, 2000).

What caused salt movement, and when it initiated, is still under investigation. Hughes (1968) suggested salt flow began during Norphlet Formation deposition; Jackson and Seni (1983) indicated the earliest record of movement occurred as late as during Cotton Valley Group deposition. Largely, studies leave it ambiguous, suggesting initiation as Early Cretaceous or Late Jurassic (Andrews, 1960; Johnson and others, 2006; Mancini and others, 2001b; Shah Alam and Pilger, Jr., 1988).

2.4 Peripheral Fault System

The landward periphery of the MISB is marked by a series of related fault zones that approximately mark the extent of the Louann Salt deposition. In Texas, there is the Mexia-Talco Fault Zone; in Arkansas, there is the South Arkansas Fault Zone; in Mississippi and extending into west Alabama there is the Pickens-Gilbertown Fault Zone; in southwest Alabama there is the West Bend-Coffeeville Fault Zone, and extending into the Florida panhandle is the Pollard-Foshee Fault Zone (Bishop, 1973; Copeland, 1976; Mancini and others, 2001a; Mancini and Mink, 1985; Martin, 1978). Within each of these broad fault may be smaller fault systems; for example, the Gilbertown Fault Zone (Figure

2.2) includes both the Melvin Fault System and Gilbertown Fault System (Copeland, 1976; Qi and others, 1998).

These fault zones are extensional systems that typically parallel the regional strike of their area, and are generally listric faults that root in the Louann Salt (Mancini and others, 2001a; Mancini and Mink, 1985; Martin, 1978). The faults are often referred to in literature as contemporaneous faults, in that there is syndepositional movement (Bishop, 1973; Hardin and Hardin, 1961; Hughes, 1968; Quarles, Jr., 1953).

Given the proximity to and rooting in the Louann Salt, the peripheral fault zones are typically associated with and expected to be resultant from salt flow. Bishop (1973) conducted an extensive assessment of regional fault trends and found this to be too simplistic a model. Instead, a compilation of several hypotheses are likely to each influence initiation of salt flow and the evolution of the fault zones. An older series of regional faults is closely associated with the continental margin and the Ouachita orogenic belt, and it is theorized that this older extensional regime continued to influence the younger peripheral fault trend (Bishop, 1973). The Mexia-Talco fault system was compared to the fault zones related to rifting in the East African Rift Zone, and shared common features, including a composition of *en-echelon* half-grabens, antithetic faults, splaying, specific widths and dips, and an overall tensional stress regime (Walthall and Walper, 1967).

Another trend observed in relation to the peripheral faults are flexures (Bishop, 1973), in which regional dip has been apparently amplified downdip of a structure (Hardin and Hardin, 1961). Flexures observed in the Gulf Coast region are attributed to the landward depositional edge of the continental slope, due to the difference in slope

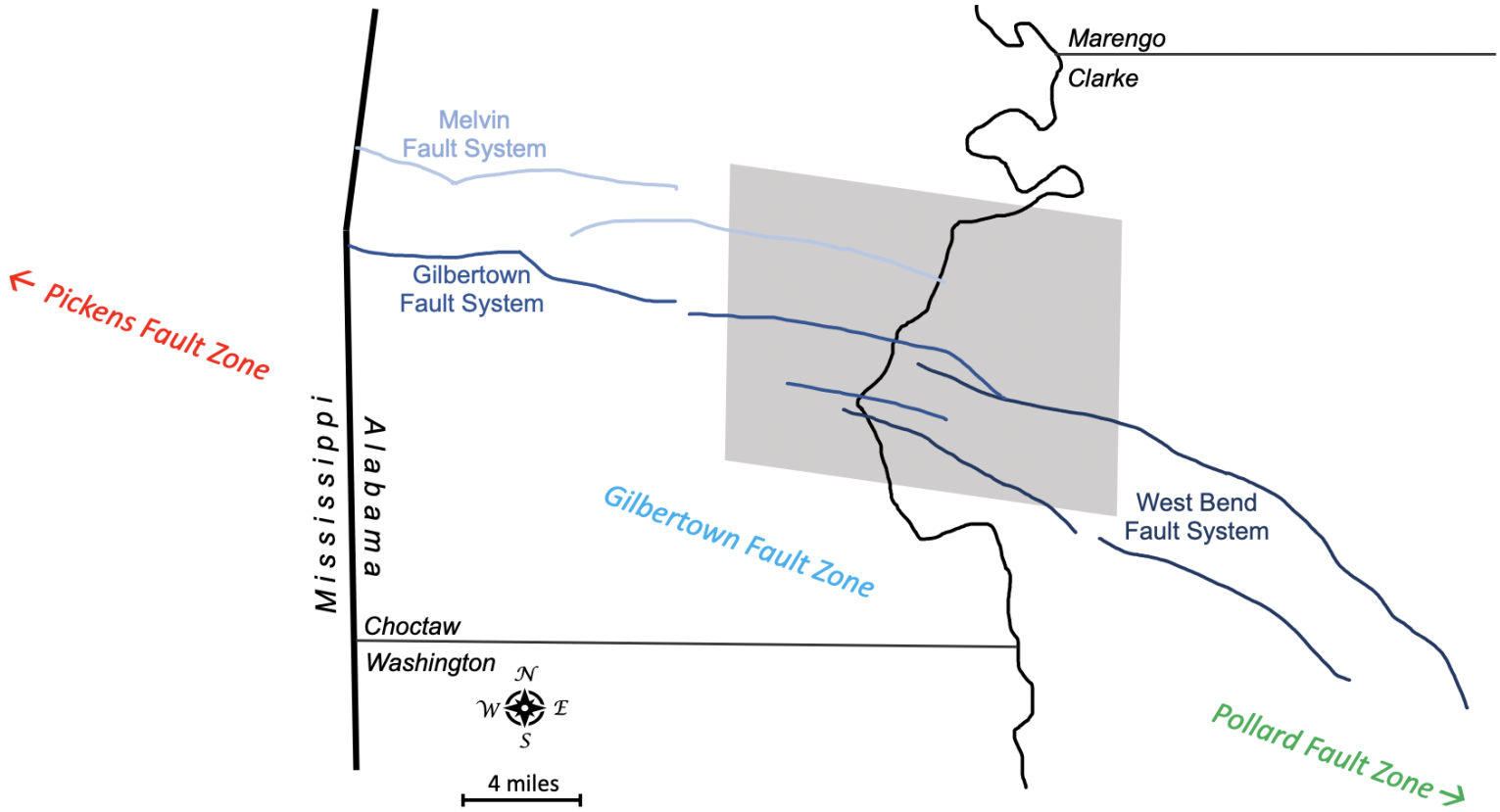

Figure 2.2 *Regional map of the Gilbertown Fault Zone*

Modified after Qi and others (1998) and Pashin and others (1998b).

between it and the continental shelf (Hardin and Hardin, 1961). Flexures in the Gulf Coast area are associated with regional contemporaneous faults (Bishop, 1973; Hardin and Hardin, 1961). As a result of the faults increasing accommodation space, sedimentation must increase downdip, making dip seem more significant. This relationship between flexure and fault thus appears to be more broadly a function of regional dip at the time of deposition. This could indicate basement trends are the underlying influence for flexure-fault association, as specified by Walthall and Walper, (1967).

More frequently referenced as influencing the peripheral fault trend is gravity slip or gravity creep (Bishop, 1973). The regional dip trend, coupled with elastic basin-fill sediments, results in a slow down-dip slip of unlithified sediments (Cloos, 1968). This gravity slide requires a plane upon which the sediments are able to transport along (Quarles, Jr., 1953); in the MISB, this is the Louann Salt. As the sediment sags along the plane of movement, it is breaking away from a stable platform; in the MISB, this is the Paleozoic rocks (Quarles, Jr., 1953). Beyond the up-dip extent of the Louann Salt, a slip surface is not present between Mesozoic and Paleozoic rocks. The depositional extent of the Louann Salt thus provides the plane of movement to break away from the up-dip stable platform where the Louann Salt is not present, whereupon the peripheral fault system can form.

The final factor Bishop (1973) listed as a mechanism of initiating salt movement is salt flow. This follows a similar mechanism to the gravity creep; however, the driving mechanism is not the sediments sliding on a slip plane (the salt) because of a regional dip and the difference between a reliable and unreliable basement, but rather from the salt

being an unreliable basement as a result of salt movement throughout the basin. The difference between the two systems is the salt acting as a passive or as an active agent; through sediment creep, salt flow is passive, with salt flow induced by mobile sediments, while through salt flow, the salt flows and induces movement in the sediments. As described by Hughes (1968), the fault system is initiated from stresses in the overburden due to underlying salt flow. However, Hughes (1968) goes on to clarify that salt movement by itself would likely not be enough to generate the degree of faulting present; instead, the juxtaposition of the weaker salt with the stable Paleozoic basement generated both shear and tensional stresses that induced faulting with minimal salt flow.

CHAPTER III – METHODS

This study first utilized the seismic survey to map the Gilbertown Fault Zone and its surrounding stratigraphy. Through the survey, variation in strata thickness was measured, while well logs were added as control points for correlating the formations. Neutron-density logs were used for calculating formation density. Lastly, compaction curves were coupled with density measurements to calculate overburden pressure.

3.1 Data Collection

This study used a pre-stack time-migrated seismic survey generated by Reservoir Geophysical Corporation, proposed and owned by Savannah Oil & Gas LLC and its affiliates. The survey covers 100 mi^2 across the Gilbertown Fault Zone in Choctaw and Clarke County, Alabama. 625 inlines are oriented north to south, while 550 crosslines are oriented east to west. While shooting the survey, a 2 ms sampling rate was used, with an 8 s two-way travel time. The survey is georeferenced using North American Datum 1927 on the Alabama West 102 projection.

Well logs were imported into IHS Petra®, and formation depths as well as neutron porosity averages were found from these wells. Well logs from within the seismic block were exported into the seismic data within IHS Kingdom® to tie in the subsurface mapping through correlating picked horizons in the seismic section and picked formation tops in the well logs. Wells surrounding the Gilbertown Fault Zone received the primary focus for this study.

3.2 Mapping Fault Geometry

The trace of the fault(s) were mapped through offset of reflectance boundaries. The analyzed well logs within the seismic survey were used to augment fault mapping by using log picked formations along reflectance boundaries in the seismic data. The reflectance of some strata are significantly stronger than others. Among the brightest horizon reflectances are the top of the Selma Chalk Group, the top of the Eutaw Formation, and the top of the Smackover Formation. These were the first to be correlated to the well logs and used as markers across the fault system.

3.3 Lateral Facies Thickness

The thickness of several formations were measured with the goal of determining if there are any loci of local loading. Focus was given to Late Jurassic to Early Cretaceous formations. Thickness measurements were made through the seismic section, and as such are in time (s). The median thickness (in time) for each formation was calculated. The range of thicknesses in the formation were compared to the average, and any thickness outside two standard deviations was noted. Areas with several outliers due to increased lateral thickness were considered as an area of increased depositional load.

3.4 Measure Overburden Thickness Above & Below Fault

Formation thickness was measured throughout the entirety of the survey. Thickness was measured as noted above. Formation thickness was measured at each of the 352 equally spaced measurement points in which the formation was present. To compare across-fault thicknesses, measurements on either side of the fault were averaged

per formation and compared by plotting the average thickness of the formation on the footwall block versus those on the hanging wall block. This comparison technique is called a fault expansion index (FEI) (Thorsen, 1963). Thickness of the formation on the upthrown footwall was divided by the thickness of the formation on the downthrown hanging wall. This ratio was plotted and the greatest ratio is indicative of the largest amount of fault movement. Changes in formation thickness across the fault could indicate fault-controlled deposition. No change (ratio of 1) indicates no fault growth during formation deposition—for the older formations, this could be they were deposited prior to faulting, while for the younger formation it indicates cessation of fault growth (Thorsen, 1963).

Observations of thickened sediments immediately adjacent to the fault trace on the downthrown block were used to suggest growth strata, which can indicate the deposition of the formation was coeval with faulting and differentiate which formations deposited prior to faulting, potentially through observation of drag folds.

3.5 Formation and Overburden Density Inversions

Neutron-density logs were used as a method to determine formation porosity. Given that some rock types have a greater degree of compaction than others (e.g., chalk), standardized formation compaction curves can provide porosity measurements as a function of burial depth. This would allow formation density for each formation to be calculated from deposition to present. The compaction curves from Kim and others, (2018) were used to calculate initial porosity and thickness of the formations through

time with the porosity and thickness measurements. This provided a timeline for when the salt would have moved given only the lithostatic load influencing the salt.

CHAPTER IV – RESULTS

The following section covers the main results from this study: first, the 3D seismic survey was mapped, finding a reflector representative of approximately the top of each formation, as well as marking where faults were observed. Second, thickness measurements for each formation were made and tabulated. Those thicknesses were then used to generate fault expansion indices for all faults mapped. Lastly, formation density measurements and formation thickness (in feet) were collected via well logs to calculate the density of each formation over time.

4.1 Mapping

Bright reflectors within the 3D seismic survey were used for initial mapping of formations (i.e., the Selma Chalk). Remaining formations were mapped via formation tops in well logs embedded within the seismic survey. The following formations were mapped: Norphlet Formation, Smackover Formation, Buckner Anhydrite, Haynesville Formation, Cotton Valley Group, the Hosston and Sligo Formations (combined), Rodessa Formation, Ferry Lake Anhydrite, Mooringsport Formation, Paluxy Formation, the Washita and Fredericksburg Formations (combined), Tuscaloosa Formation, Eutaw Formation, and the Selma Chalk. The Hosston and Sligo Formations and the Washita and Fredericksburg Formations were combined due to their similar composition and subsequent difficulty in identifying their contact both seismically and in wells. Additionally, the Tuscaloosa Formation was picked at the top of the Lower Tuscaloosa as the Lower Tuscaloosa had a stronger reflector. As such, Tuscaloosa Formation thicknesses measured from the seismic data will be thinner than what is traditionally

reported (see Stratigraphy). The lost thickness is attributed to the above Eutaw Formation, which will be proportionally thicker than what is traditionally reported.

Formations dipped uniformly southwest until being intercepted by the fault system, with formations deepest in the subsurface in the southwest of the survey, and shallowest in the northeast corner, as shown with the top of the Norphlet Formation (Figure 4.1). The fault system seen in the survey had little effect on overall strike of the formations, but locally there was shallowing or deepening of the formation around the fault system. Folding near the fault system was also observed, with drag folding present along some of the faults in formations younger than the Rodessa Formation. A rollover anticline is associated with the fault system, as well. The formations older than the main growth phase have folded down, resulting in their absence in the southeast corner of the survey as they slid down the fault scarp.

A fault system (Figure 4.2) extends through the seismic survey from the western edge of the survey through to the eastern edge. The fault system is comprised of five fault segments, trending west-northwest to east-southeast. The northernmost fault, F1, extends (from west to east) through the first third of the survey before terminating. South of F1 is F2, which is traced from the western edge of the survey into the center, where it branches into F3 and F4. F3 continues relatively due east to the eastern edge of the survey, and F4 continues slightly south and east before paralleling F3 to the survey's eastern limit. The last fault, F5, is to the south of F2, extending from the western edge of the survey until it terminates approximately halfway to the eastern edge. While F1, F2, F3, and F4 all extend below the Norphlet Formation to a décollement surface defined by the Louann Salt, F5 only cuts through younger formations, extending down to the Ferry Lake

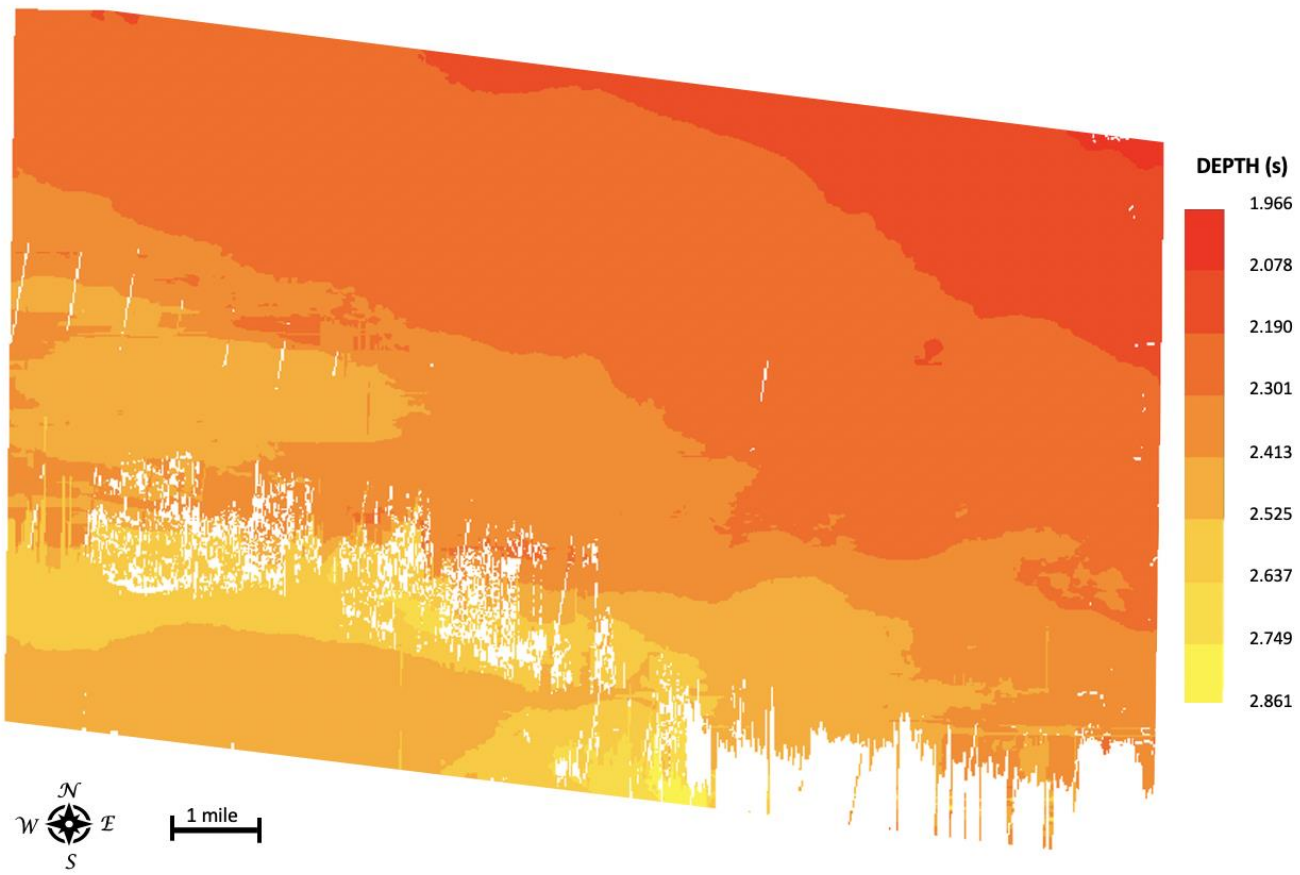

Figure 4.1 *Norphlet Formation horizon*

The top of the Norphlet Formation mapped in the 3D seismic survey. Depth is in travel time, horizontal distance is in miles. General dip towards the SW is shown.

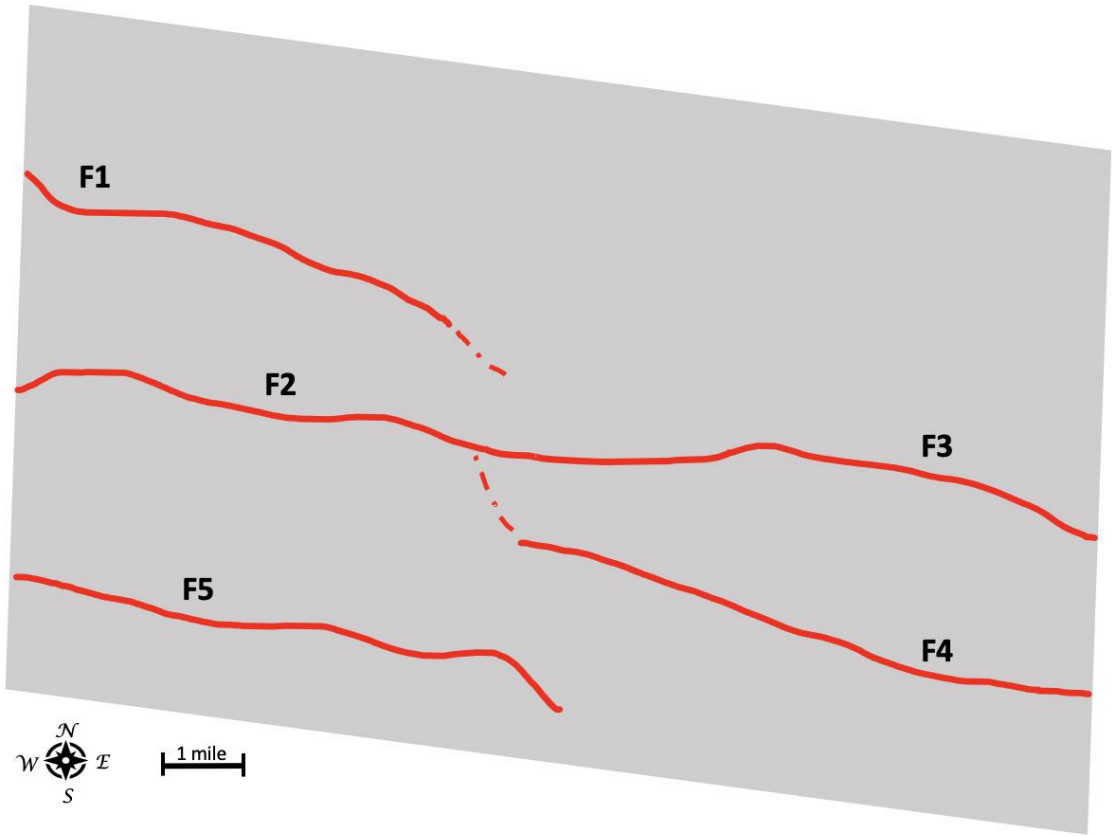

Figure 4.2 *Mapped Faults*

The fault system observed in the 3D seismic survey is shown in red lines as observed in the Selma Chalk (~2,000 feet depth). Dashed red lines represent continuation of the fault that was not directly mapped. The F4 linkage to F2 is investigated in a later section.

Anhydrite. Additionally, F1, F2, F3, and F4 dip southwest into the basin, while F5 dips northeast.

Once the above-mentioned formations and the fault system were mapped, the seismic survey was gridded with 16 northwest-southeast lines (labelled 1 – 16) approximately paralleling the strike of the observed fault system, and 22 northeast-southwest lines (labelled A – V) approximately perpendicular to the strike of the observed fault system, each one 30 survey lines from one another (Figure 4.3). This geometry was chosen so as to visualize and measure attributes relative to the orientation of the faults and provide points of analysis for other data sets (see below). Lines A – V are shown as cross-sections in Appendix A.

4.2 Formation Thickness

To measure thickness of each formation across the seismic survey, thickness was measured at the intersection of each NE-SW and NW-SE line for every formation. Exceptions were made when there was a gap in the survey continuity, as well as when intersections fell within a fault zone and the seismic reflectors were too uncertain to pick formation tops. Additionally, the rollover anticline in the southeast corner of the survey caused some formations to have missing sections and were unable to be measured. Tables with each thickness measurement taken are shown in Appendix B.

Thickness was measured in seconds via the ruler tool in IHS Kingdom. Measurements were made from formation top to formation top, perpendicular to both. As a result, any imperfect picks in the formation tops effected the accuracy of the measurements. Additionally, some formations had very small thicknesses in the survey,

and a minor change in placement of the ruler would cause a significant change in thickness (e.g., a change from 0.017s to 0.019s is a 10% change in thickness). Due to these limitations, individual measurements will not be analyzed, but localized or survey-wide thinning or thickening trends in the data should hold true.

Thickness varied for each formation across the survey. Largely, thicker sediments were observed on the downthrown side of F2, F3, and F4. Thickness for each formation was averaged across the entire survey, and any measurement within the formation that was two standard deviations or greater from said average was highlighted. Across all formations, few measurements were highlighted for being thinner than the average thickness; most highlighted measurements were thicker than the average for that formation.

Multiple highlighted measurements within a single formation that are close in proximity (usually adjacent) to one another form clusters. For thinner than average measurements, only the Washita-Fredericksburg Formation contained a significant cluster, comprised of 10 contiguous measurements in the downthrown block of F4 with several small (2-3 contiguous measurements) clusters nearby in the downthrown blocks of F2 and F4 (Figure 4.4). The majority of measurements two standard deviations away from the mean of their respective

formations were thicker than the mean thickness, and frequently clustered, though most were small clusters of 5 or less measurements. The largest cluster observed is in the Cotton Valley Group on the downthrown side of F2, with 30 contiguous measurements comprising the majority of Cotton Valley Group measurements from the F2 downthrown block (Figure 4.5).

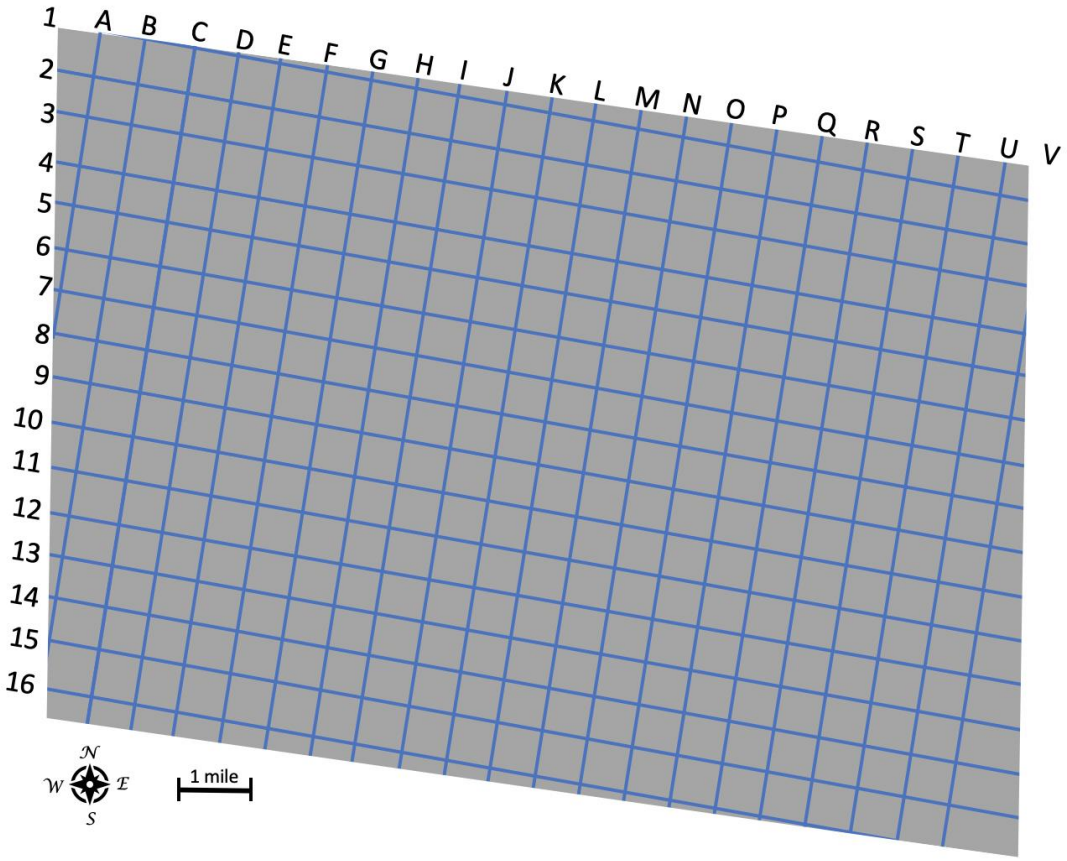

Figure 4.3 *Measurement locations*

3D seismic survey (gray parallelogram) with 22 NE-SW lines (labelled A-V) and 16 NW-SE lines (labelled 1-16) oriented parallel and perpendicular to strike, respectively. Formation thickness measurements were taken at each intersection of the lines.

	A	B	C	D	E	F	G	H	I	J	K	L	M	N	O	P	Q	R	S	T	U	V
1		0.212	0.195	0.212	0.195	0.206	0.202	0.185	0.197	0.185	0.176	0.187	0.176	0.168	0.162	0.153	0.16	0.155	0.159	0.151	0.157	
2	0.205	0.214	0.193	0.21	0.197	0.21	0.21	0.183	0.189	0.183	0.178	0.174	0.17	0.164	0.166	0.158	0.166	0.153	0.162	0.162	0.164	
3	0.212	0.206	0.195	0.195	0.201	0.206	0.208	0.176	0.206	0.193	0.178	0.183	0.174	0.17	0.157	0.16	0.168	0.168	0.17	0.162	0.16	
4	0.199	0.204	0.197	0.202	0.21	0.21	0.208	0.179	0.206	0.178	0.183	0.181	0.172	0.174	0.155	0.151	0.155	0.157	0.166	0.174	0.166	
5	0.186	0.208		0.21	0.21	0.195	0.195	0.189	0.189	0.193	0.181	0.174	0.179	0.174	0.159	0.153	0.145	0.155	0.172	0.172	0.17	0.171
6	0.163		0.128			0.187	0.208	0.199	0.187	0.181	0.185	0.178	0.181	0.166	0.155	0.147	0.162	0.149	0.172	0.172	0.172	0.174
7		0.151	0.122	0.233	0.267	0.284	0.174	0.195	0.164	0.168	0.172	0.178	0.179	0.162	0.172	0.162	0.162	0.16	0.174	0.172	0.168	0.174
8		0.204	0.143	0.235	0.241	0.237	0.155	0.183	0.155	0.168	0.164	0.17	0.185	0.185	0.176	0.155	0.151	0.16	0.176	0.176	0.17	0.168
9		0.21	0.139	0.225	0.214	0.22	0.136	0.187	0.172	0.174	0.174	0.172	0.174	0.168					0.08			0.158
10								0.178							0.185	0.067	0.158	0.176	0.074	0.16	0.189	0.155
11		0.164	0.162	0.17	0.143	0.189	0.084	0.162	0.204	0.164	0.13	0.105	0.162	0.178	0.195	0.082	0.153	0.174	0.174	0.181	0.183	0.168
12		0.138	0.132	0.157	0.113	0.166	0.061	0.105	0.174	0.132	0.092	0.099					0.147	0.162	0.164	0.191	0.162	0.149
13		0.139	0.124	0.132	0.145	0.162	0.065	0.086	0.13	0.118	0.092	0.078	0.143	0.094	0.099	0.17		0.141	0.143	0.185	0.143	
14		0.138	0.168	0.21		0.147	0.109	0.141	0.168	0.176	0.113	0.118	0.138	0.069	0.084	0.113	0.151		0.115	0.143		0.172
15		0.166	0.204	0.227	0.212	0.212	0.082	0.191	0.187	0.172	0.134	0.122	0.116	0.044	0.071	0.097	0.136	0.141	0.084	0.134	0.063	0.118
16			0.225	0.214	0.216	0.216	0.099	0.191	0.187	0.17	0.149	0.134	0.071	0.034	0.063	0.086	0.124	0.143	0.09			

Figure 4.4 *Washita-Fredericksburg Formation thickness measurements*

Thickness measurement cells from the Washita-Fredericksburg Formation. Highlighted cells (bordered in red) indicate measurements two standard deviations away from the mean. Darker green indicates thicker, lighter green indicates thinner. Tan indicates no measurement taken.

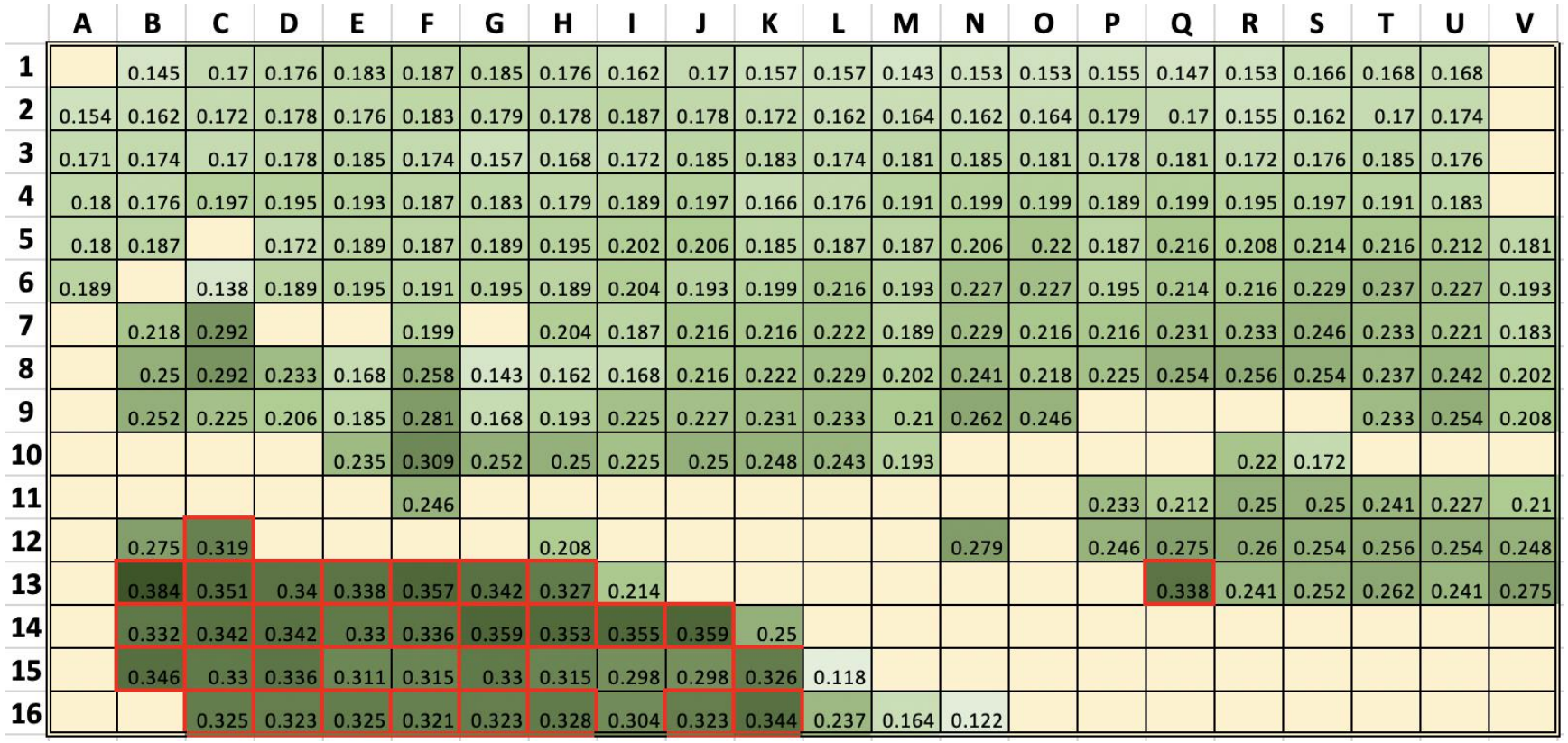

	A	B	C	D	E	F	G	H	I	J	K	L	M	N	O	P	Q	R	S	T	U	V
1		0.145	0.17	0.176	0.183	0.187	0.185	0.176	0.162	0.17	0.157	0.157	0.143	0.153	0.153	0.155	0.147	0.153	0.166	0.168	0.168	
2	0.154	0.162	0.172	0.178	0.176	0.183	0.179	0.178	0.187	0.178	0.172	0.162	0.164	0.162	0.164	0.179	0.17	0.155	0.162	0.17	0.174	
3	0.171	0.174	0.17	0.178	0.185	0.174	0.157	0.168	0.172	0.185	0.183	0.174	0.181	0.185	0.181	0.178	0.181	0.172	0.176	0.185	0.176	
4	0.18	0.176	0.197	0.195	0.193	0.187	0.183	0.179	0.189	0.197	0.166	0.176	0.191	0.199	0.199	0.189	0.199	0.195	0.197	0.191	0.183	
5	0.18	0.187		0.172	0.189	0.187	0.189	0.195	0.202	0.206	0.185	0.187	0.187	0.206	0.22	0.187	0.216	0.208	0.214	0.216	0.212	0.181
6	0.189		0.138	0.189	0.195	0.191	0.195	0.189	0.204	0.193	0.199	0.216	0.193	0.227	0.227	0.195	0.214	0.216	0.229	0.237	0.227	0.193
7		0.218	0.292			0.199		0.204	0.187	0.216	0.216	0.222	0.189	0.229	0.216	0.216	0.231	0.233	0.246	0.233	0.221	0.183
8		0.25	0.292	0.233	0.168	0.258	0.143	0.162	0.168	0.216	0.222	0.229	0.202	0.241	0.218	0.225	0.254	0.256	0.254	0.237	0.242	0.202
9		0.252	0.225	0.206	0.185	0.281	0.168	0.193	0.225	0.227	0.231	0.233	0.21	0.262	0.246					0.233	0.254	0.208
10					0.235	0.309	0.252	0.25	0.225	0.25	0.248	0.243	0.193					0.22	0.172			
11						0.246										0.233	0.212	0.25	0.25	0.241	0.227	0.21
12		0.275	0.319					0.208						0.279		0.246	0.275	0.26	0.254	0.256	0.254	0.248
13		0.384	0.351	0.34	0.338	0.357	0.342	0.327	0.214								0.338	0.241	0.252	0.262	0.241	0.275
14		0.332	0.342	0.342	0.33	0.336	0.359	0.353	0.355	0.359	0.25											
15		0.346	0.33	0.336	0.311	0.315	0.33	0.315	0.298	0.298	0.326	0.118										
16			0.325	0.323	0.325	0.321	0.323	0.328	0.304	0.323	0.344	0.237	0.164	0.122								

Figure 4.5 *Cotton Valley Group thickness measurements*

Thickness measurement cells from the Cotton Valley Group. Highlighted cells (bordered in red) indicate measurements two standard deviations away from the mean. Darker green indicates thicker, lighter green indicates thinner. Tan indicates no measurement taken.

4.3 Faults

Fault expansion indices were generated for each of the five fault segments. For each index, thicknesses were averaged using three NE-SW lines of measurements, with separate averages above and below each fault for each formation. Lines E, F, and G were used to generate indices for F1, F2, and F5. Lines J, K, and L were used to isolate F2. Lines R, S, and T were used to generate an index for F3 and for F4. Simplified cross sections for lines E/F/G (Figure 4.6a), J/K/L (Figure 4.6b), and R/S/T (Figure 4.6c) illustrate the various fault blocks.

Of the three sections, F1 is only present in lines E, F, and G. The expansion index for F1 was created with M2 as the upthrown block, and N1 as the downthrown block. In the FEI for F1 (Figure 4.7), most formations have a ratio very close to one, peaking at 1.57. The first occurrence of a ratio over one in the FEI is with deposition of the Buckner Anhydrite, which has a ratio of 1.15. Expansion in the hanging wall resumed during the Cotton Valley Group, before the peak in the FEI occurred during the Hosston and Sligo Formations, with a ratio of 1.57. Expansion appears to have stopped until the Mooringsport Formation, then again with Washita and Fredericksburg Formations. Expansion continued to a secondary peak during the Tuscaloosa Group with a ratio of 1.31, with final expansion occurring during the Selma Chalk. The overall trend of the F1 expansion index is difficult to ascertain; growth resumes and ceases throughout the depositional sequence.

To the south of F1, also in lines E, F, and G, is F2. The younger formations (Paluxy Formation and younger) in F2's downthrown block are faulted by F5, resulting in the separation of the M1 and S1 block. For the formations deeper than F5

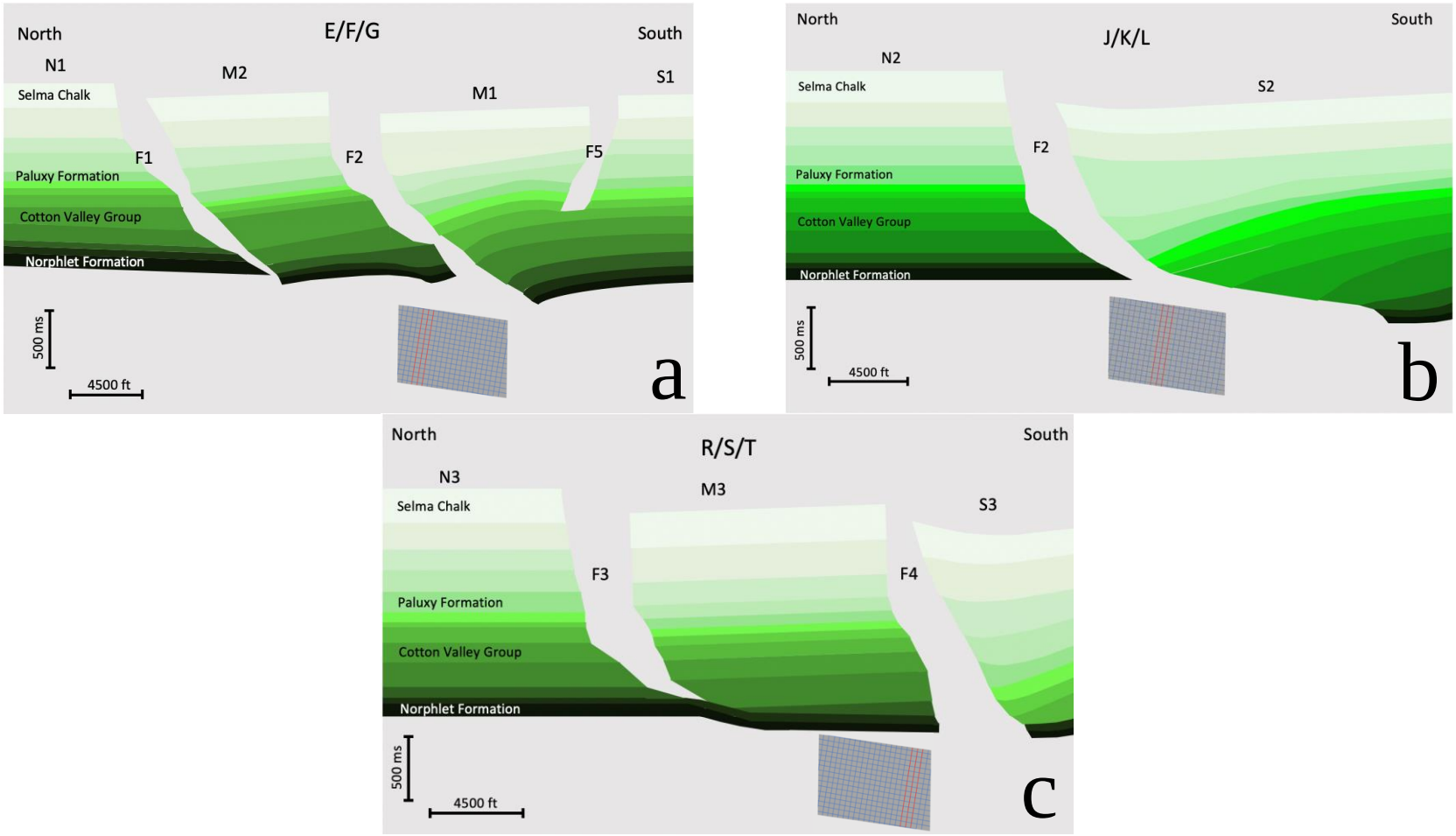

Figure 4.6 *Simplified cross-sections*

Simplified cross sections for a) lines E, F, and G, b) lines J, K, and L, and c) lines R, S, and T.

(Mooringsport Formation and older) in F2's downthrown block, thickness measurements are used from both M1 and S1 indiscriminately. In the formations faulted by F5, thickness measurements for the F2 hanging wall were used only from M1. The footwall used is M2. The FEI for F2 (Figure 4.8) indicates downthrown block expansion began during the Haynesville Formation, which has a ratio of 1.17, increasing in expansion to the Cotton Valley Group. Expansion appears to have paused during the Hosston and Sligo Formations, before resuming in the Rodessa Formation and continuing through the Rodessa Formation. The peak of expansion occurred during the Ferry Lake Anhydrite with a ratio of 1.87. A final occurrence of expansion occurred with the deposition of the Eutaw Formation.

Without knowing if the M2 block faulted from the N1 block prior to the M1 block faulting from M2, an index was also created encompassing both the F1 and F2 faults by comparing M1 (downthrown) to N1 (upthrown) (Figure 4.9). The F1 & F2 index is similar to the F2 index, but has peak expansion during the Cotton Valley Group and lacks a secondary peak in the Eutaw Formation. There is a second expansion peak during the Mooringsport Formation, rather than the Ferry Lake Anhydrite, though these formations do share a contact and as such the expansion is likely proximal in time.

The last fault present in E, F, and G is the back-dipping F5, which only faults the Paluxy Formation and younger. The F5 FEI (Figure 4.10) suggests overall little expansion, with peak expansion occurring during the Eutaw Formation with a ratio of 1.32. While the other formations have ratios of less than one, the highest of them is the Paluxy Formation, with a ratio of 0.90, and may represent an initial expansion during the Paluxy Formation. The Paluxy Formation, Washita-Fredericksburg Formations, and

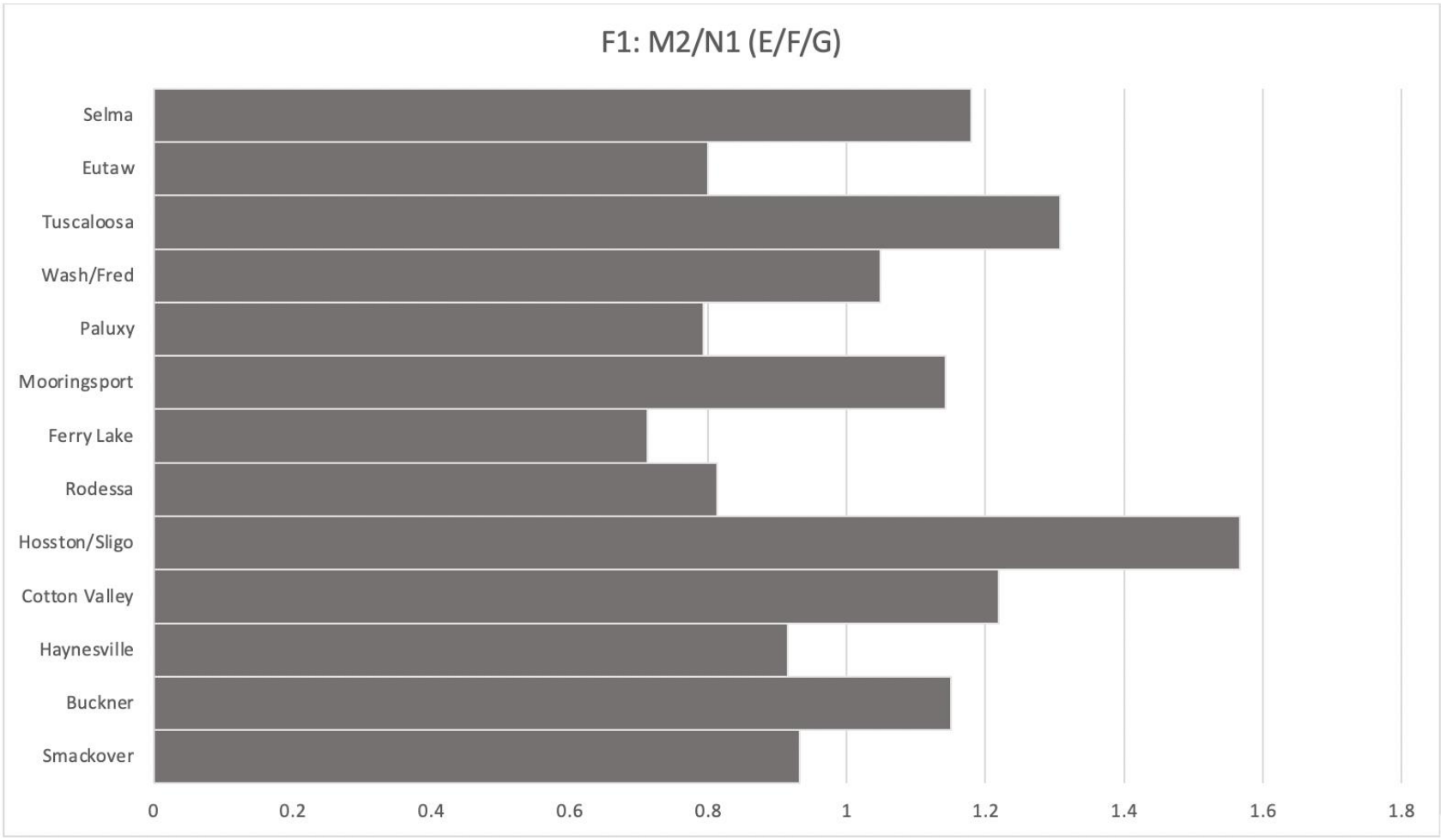

Figure 4.7 *F1 fault expansion index*

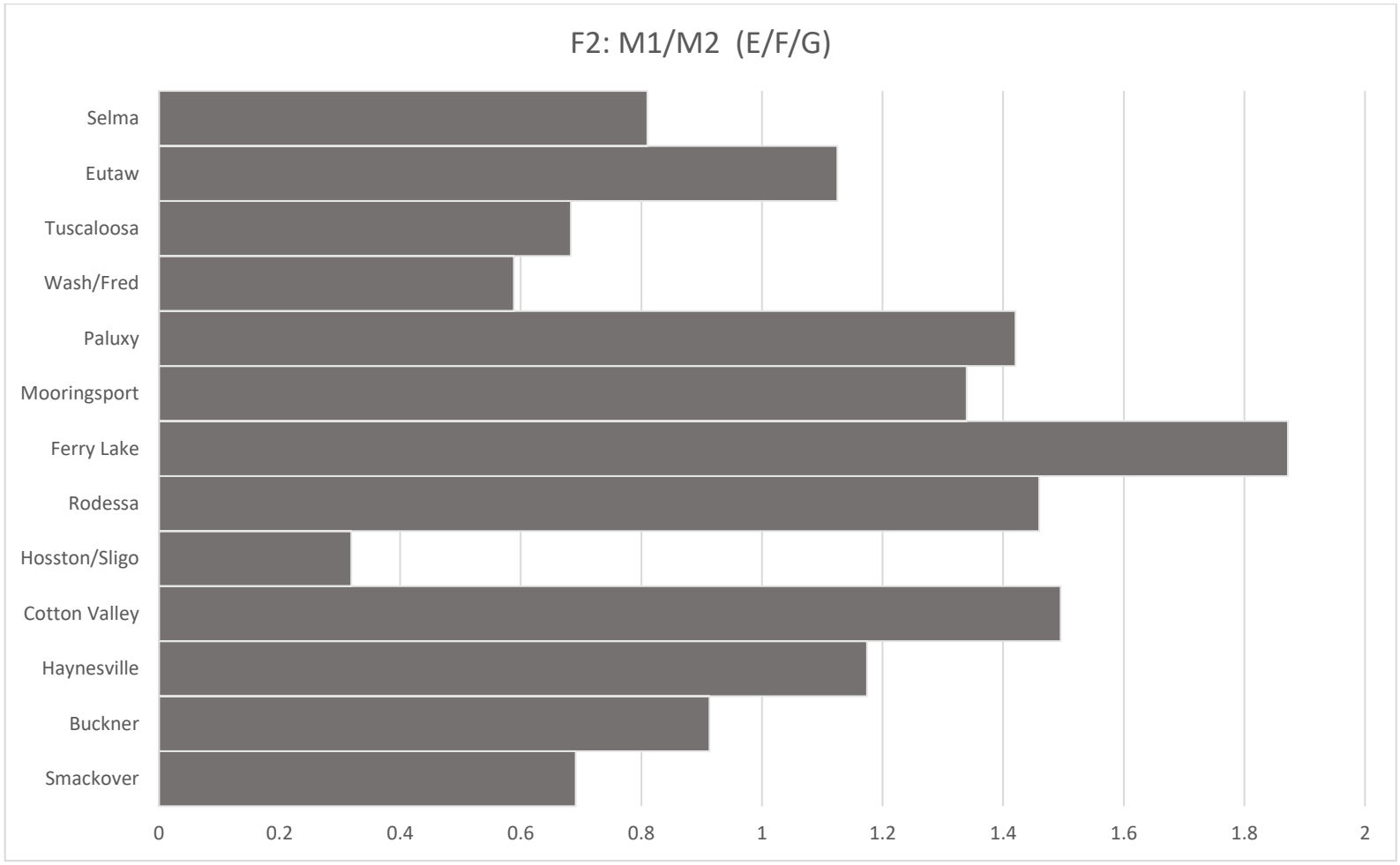

Figure 4.8 *F2 fault expansion index (EFG)*

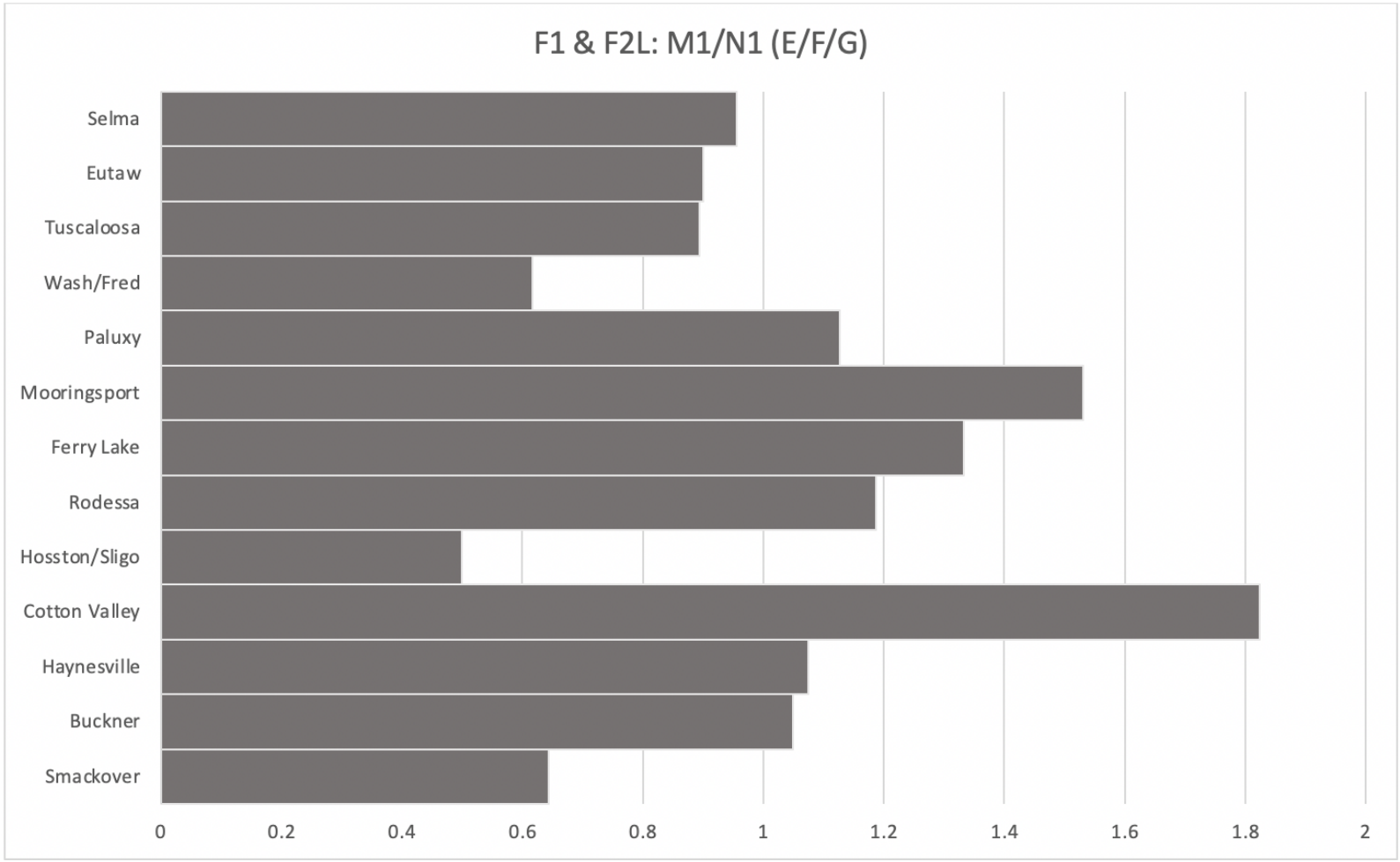

Figure 4.9 *F1 & F2 fault expansion index*

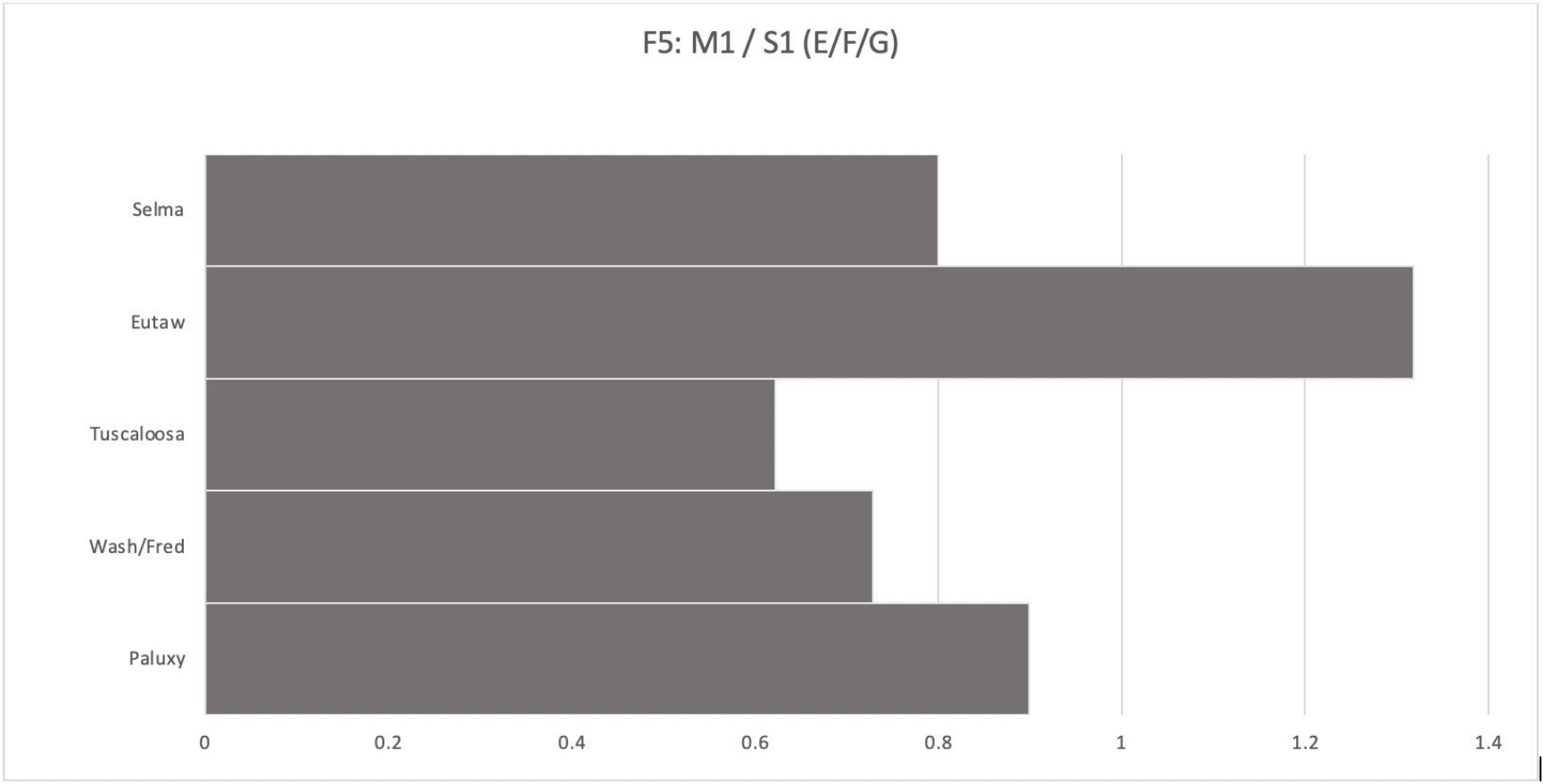

Figure 4.10 *F5 fault expansion index*

Tuscaloosa Group may also all be pre-growth strata, with no expansion in the fault until the Eutaw Formation.

In lines J, K, and L, only one fault is clearly present: F2. Line J may contain the tip line of F1 as its throw approaches 0, and line L may contain F4. Only F2 is present in line K, and is in both lines J and L. As such, the J/K/L section is representative of only F2. The FEI for F2 (Figure 4.11) is created by using S2 block as the downthrown block, and N2 as the upthrown block. The F2 index indicates the initial period of expansion occurred with deposition of the Cotton Valley Group, which is also a peak of expansion with a ratio of 1.41. Expansion appears to have ceased during the Hosston and Sligo Formations, before resuming during the Rodessa Formation and continuing until the peak of expansion during the Mooringsport Formation, with a ratio of 1.48. Minimal to no expansion occurred after the Mooringsport Formation. The overall trend of the F2 index in the J, K, and L lines is an expansion increase through the Cotton Valley Group, quiescence during the Hosston and Sligo Formations, then an expansion increase through the Mooringsport Formation, with little to no subsequent expansion.

In lines R, S, and T, the F3 and F4 fault segments are present. It is likely that at least one of the two is a continuation of F2. The F3 FEI (Figure 4.12) is created with M3 as the downthrown block and N3 as the upthrown block. F3 does not exhibit expansion until deposition of the Haynesville Formation, at a ratio of 1.23. Expansion then slows through the Hosston and Sligo Formations before potentially ceasing during the Rodessa Formation. A short period of expansion occurs during the Mooringsport Formation, and again during the Eutaw Formation and Selma Chalk, with 1.29 expansion peak during the Eutaw Formation. The overall trend of the F3 index involves decreasing expansion

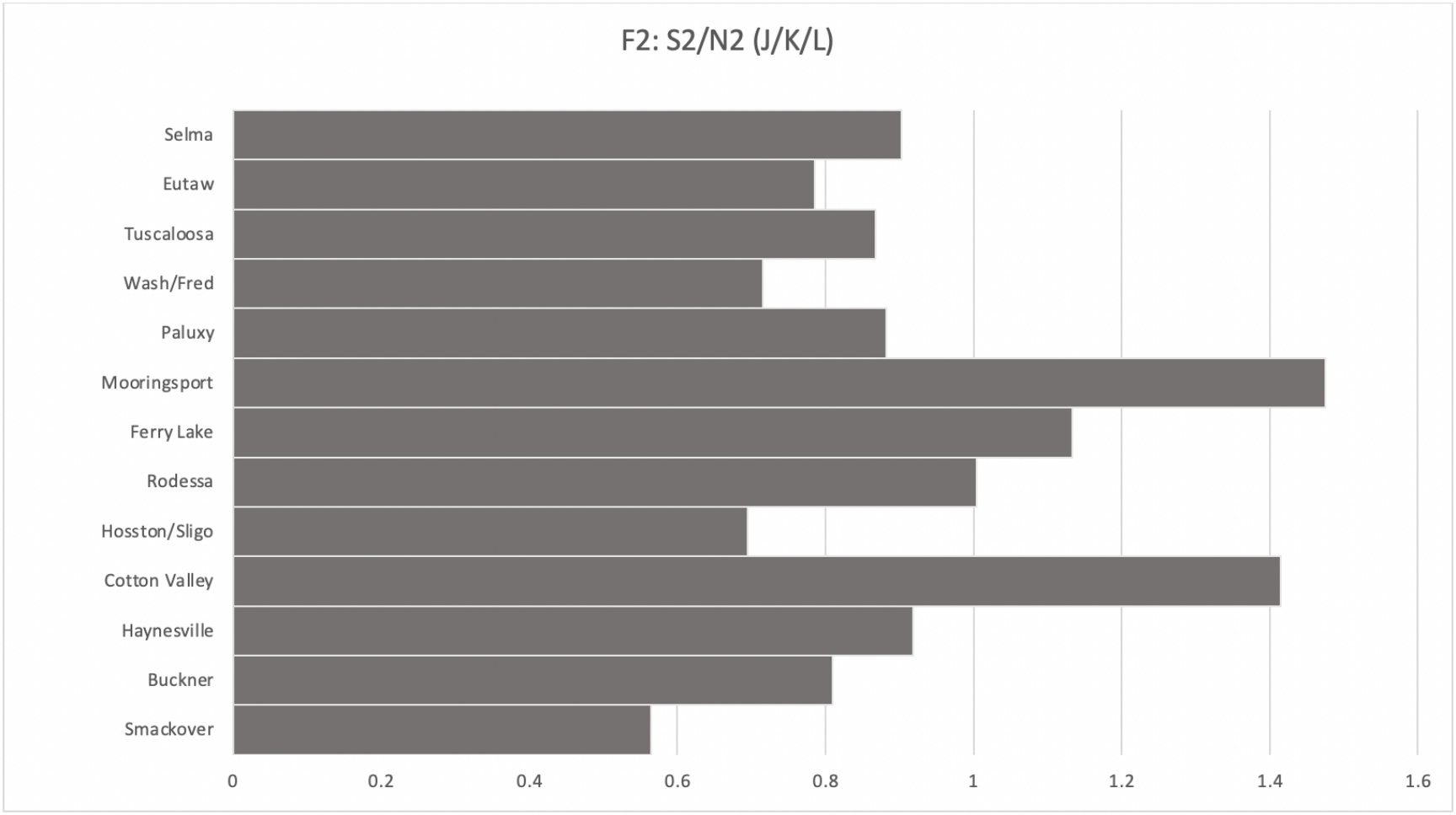

Figure 4.11 *F2 fault expansion index (JKL)*

from the Haynesville Formation, then a peak during the Mooringsport Formation with a subsequent decline, with a main peak of expansion occurring during the Eutaw Formation and Selma Chalk.

The F4 FEI (Figure 4.13) uses S3 as the downthrown block, and M3 as the upthrown block. This index does not have data for the Haynesville Formation, Cotton Valley Group, or Hosston/Sligo Formations as these formations are absent due to the rollover anticline. Initial expansion may have occurred during the Smackover Formation with a ratio of 1.29. Expansion was underway with deposition of the Rodessa Formation, and continued through the Paluxy Formation. The 2.77 peak expansion occurred during this interval with the Mooringsport Formation. Expansion resumed only once more, during the deposition of the Tuscaloosa Group, and is another peak for this index at 2.54. The overall trend for the F4 index is increasing expansion through the Mooringsport Formation, then decreasing, with an exception during the Tuscaloosa Group. F4 has the highest recorded expansion index of any of the faults.

Lastly, without knowing if the M3 block faulted from the N3 block prior to the S3 block faulting from M3, an index was created encompassing both the F3 and F4 faults by comparing S3 as the downthrown block to N3 as the upthrown block (Figure 4.14). Like the F4 index, the F3 and F4 index is missing thickness data from the Haynesville Formation, Cotton Valley Group, and Hosston/Sligo Formations. Also like the F4 index, expansion may have begun with the deposition of the Smackover Formation, but is underway during the Rodessa Formation, and continuing through the high 3.19 peak during the Mooringsport Formation. Expansion then pauses until there is a small resurgence in expansion during the Tuscaloosa and Eutaw Formations. Overall,

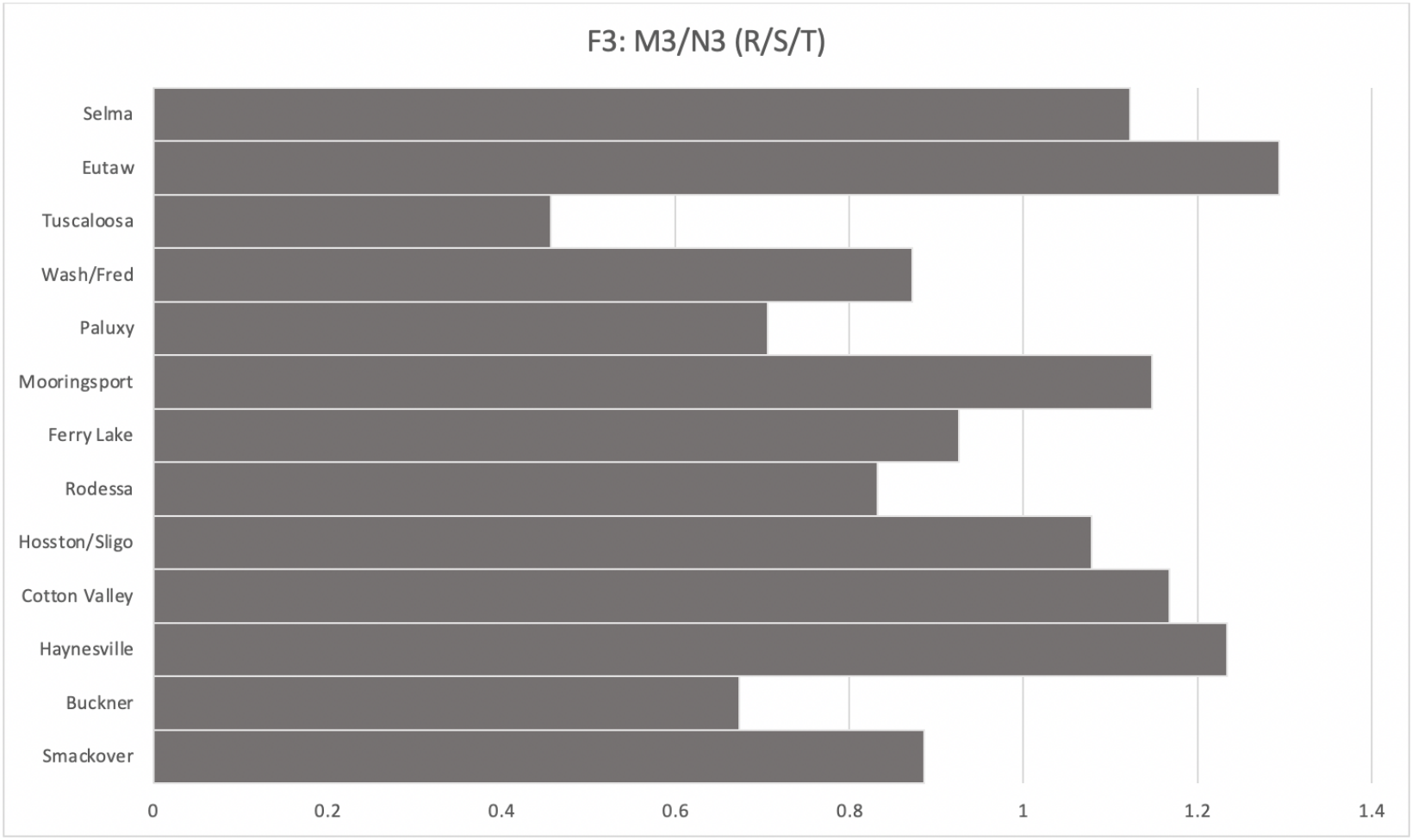

Figure 4.12 *F3 fault expansion index*

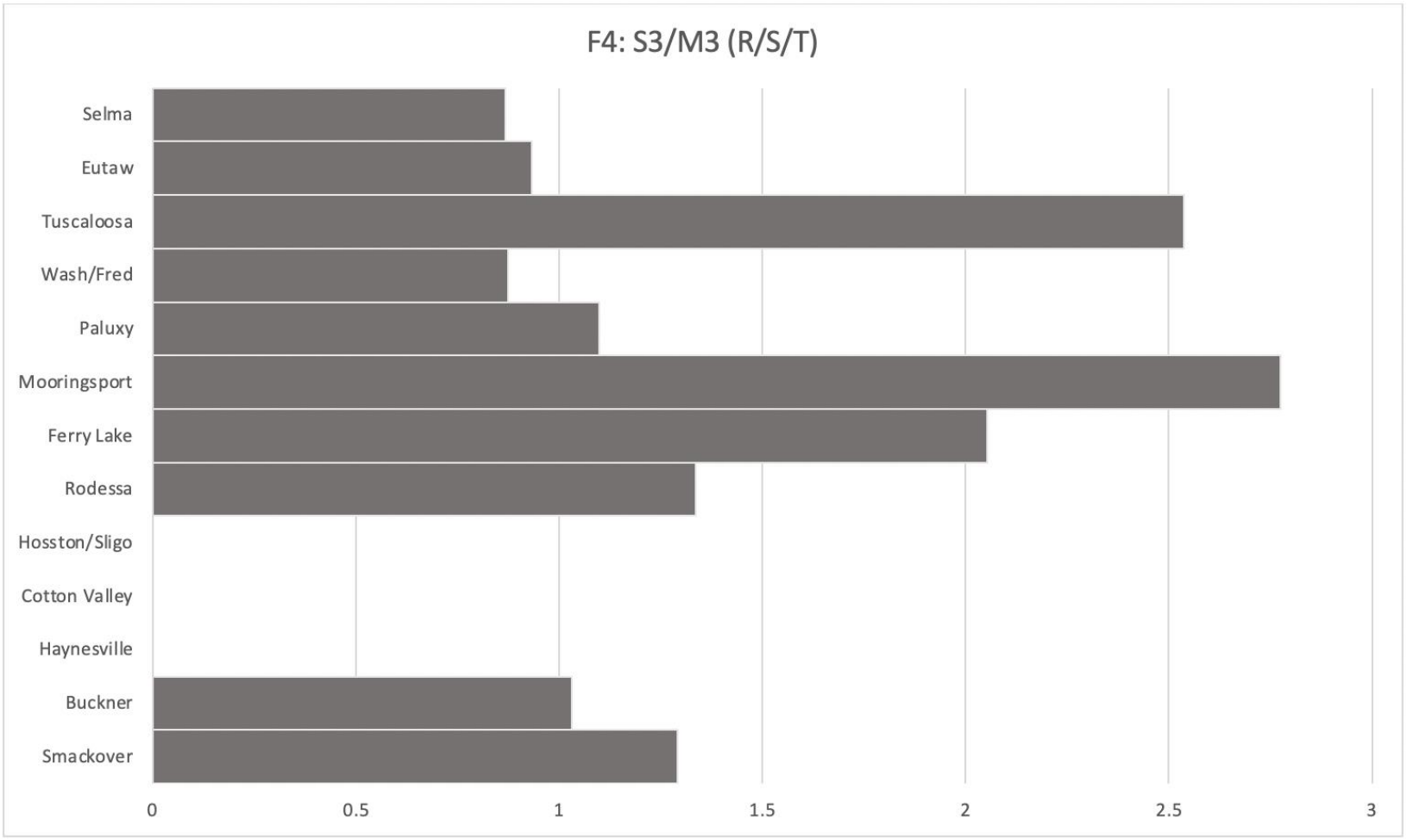

Figure 4.13 *F4 fault expansion index*

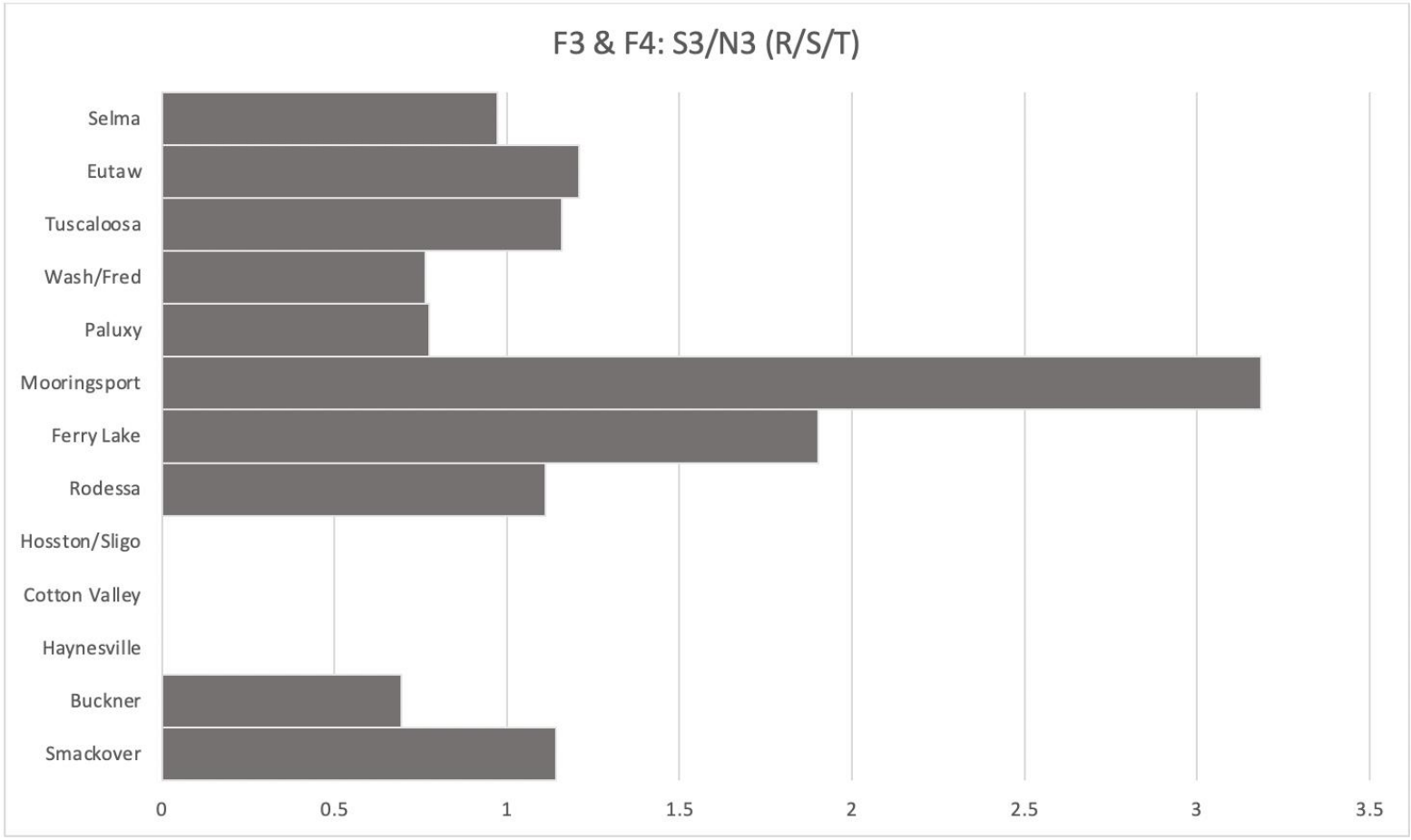

Figure 4.14 *F3 & F4 fault expansion index*

the F3 and F4 index increases to the Ferry Lake Anhydrite, pauses, and then has a secondary stage of expansion during the Tuscaloosa Group and Eutaw Formation. Across all faults, the highest expansion index generally occurs during one or more of three time periods: the Haynesville Formation and Cotton Valley Group, the Ferry Lake Anhydrite and Mooringsport Formation, and the Tuscaloosa Group and Eutaw Formation. A comparison summary of fault expansion initiation and peaks is in Table 4.1. Faults tended to initiate expansion during the Buckner Anhydrite and Haynesville Formation, with peak expansion in three pulses: near the Cotton Valley Group, Mooringsport Formation, and Eutaw Formation.

Fault expansion indices from the three comparisons of the northernmost block to the southernmost block (excepting those made by F5, which is composed of younger sediments) are plotted against each other in Figure 4.15 (F1 and F2 from E, F, and G; F2 from J, K, and L; and F3 and F4 from R, S, and T). While the indices align well, there is an anomalously high value in the Mooringsport Formation for F3 and F4. Acknowledging that the Mooringsport Formation is still a peak for F3 and F4, removing that data point results in trendlines nearly identical.

F2 (J/K/L) and F2 (E/F/G) are expected to be the same fault before it links with the F3 and F4 faults. In Figure 4.16, the two F2 fault indices indicate activity and quiescence at similar times and to similar degrees. Lastly, we can compare F2 to the F3 and F4 faults in an effort to determine the relationship between the three. In Figure 4.17, F2 (J/F/K) is compared to F3 and F4. While F4 has three formations with significantly higher ratios than F2 and an overall higher degree of accommodation, periods of activity between the two fault segments appear synchronous. Conversely, F3 appears to have

Table 4.1 *Fault expansion summary*

Summary of expansion activity for the faults per formation. F1 and F3 are the "north" faults, while F2 and F4 are "south" faults, and so are placed adjacent to one another.

Formation	*F1*	*F3*	*F2 (EFG)*	*F2 (JKL)*	*F4*	*F5*
Selma						
Eutaw		PEAK	PEAK 2			PEAK
Tuscaloosa	PEAK 2				PEAK 2	
Wash/Fred						
Paluxy						
Mooringsport		PEAK		PEAK	PEAK	
Ferry Lake			PEAK			
Rodessa						
H/S	PEAK 1					
CV			PEAK 1	PEAK 1		
Haynesville		PEAK	START			
Buckner	START					
Smackover					START	

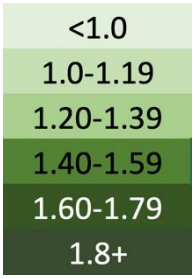

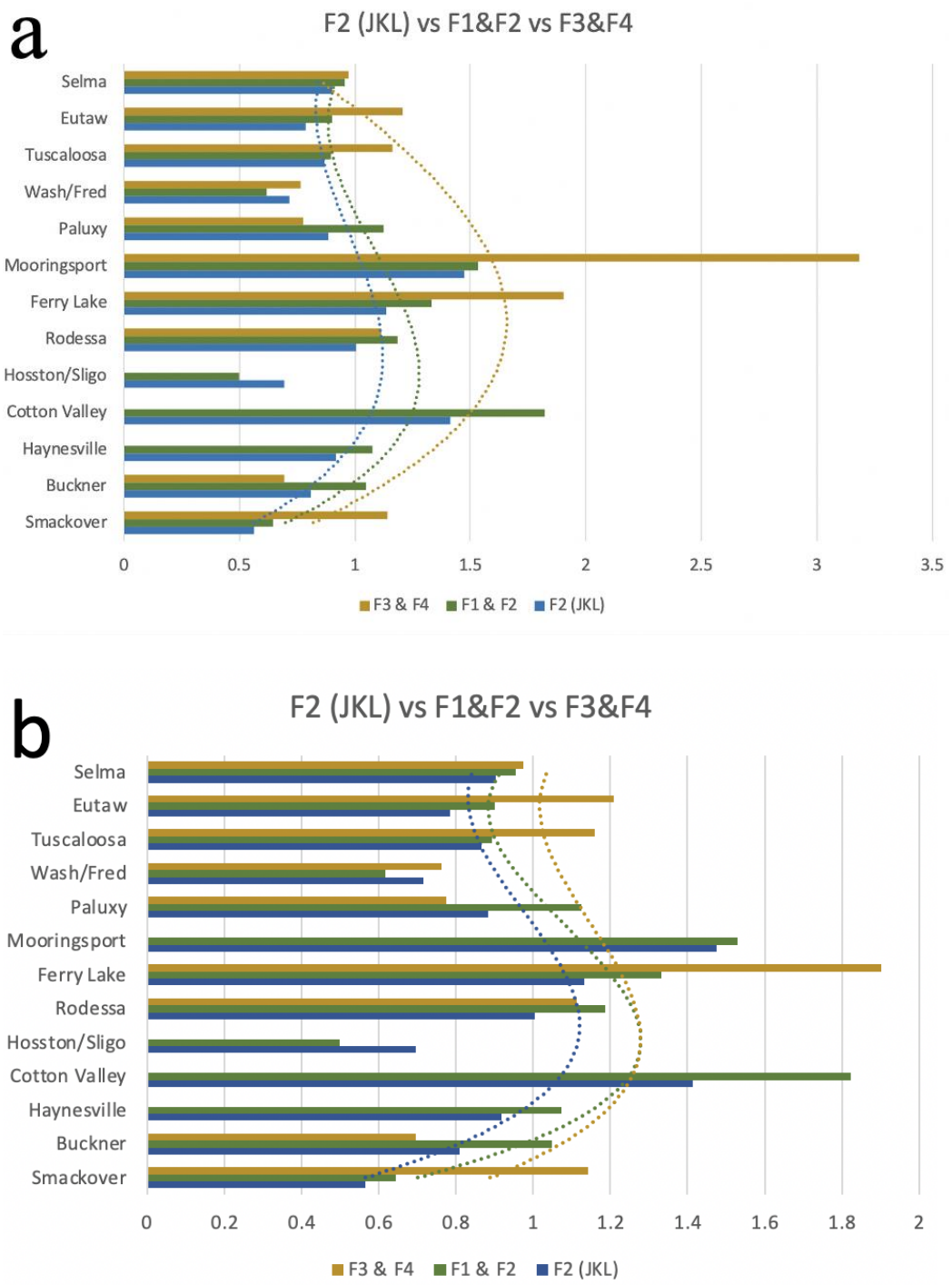

Figure 4.15 *Comparison of fault expansion indices for F2 (JKL), F1 & F2, and F3 & F4*

a) Comparison chart of the F2 (J/K/L), F1&F2, and F3&F4 fault expansion indices. b) With the 3.2 value removed from F3 & F4, the indices follow nearly identical trends (both shown with a power 3 polynomial trendline).

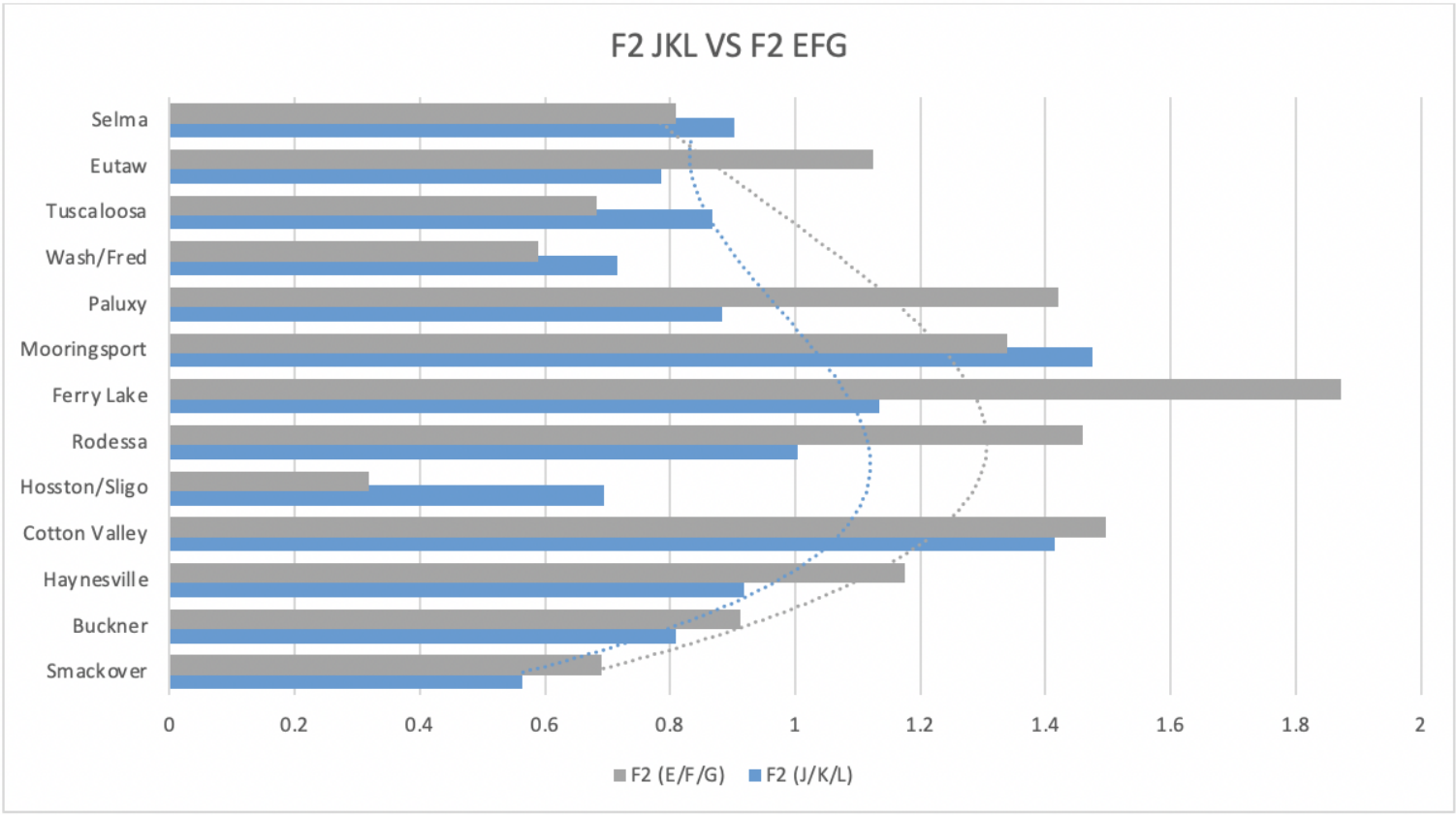

Figure 4.16 *Comparison of fault expansion indices for F2 (EFG) and F2 (JKL)*

Comparison chart of the F2 (E/F/G) and F2 (J/K/L) fault expansion indices, with a power 3 polynomial trend line for each fault.

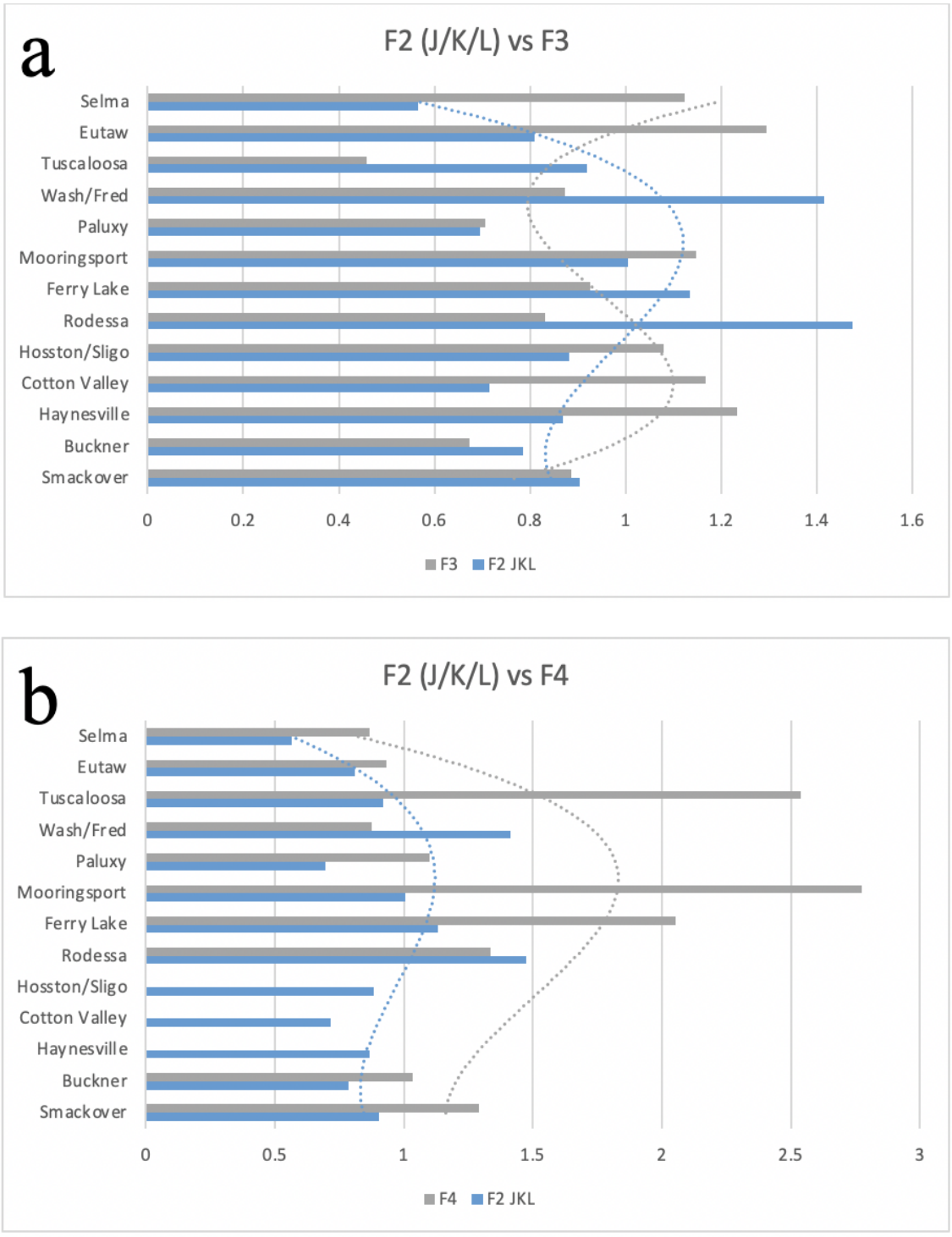

Figure 4.17 *Comparison of fault expansion indices for F2 vs F3 and F2 vs F4*

Comparison of fault expansion indices for F2 (J/K/L) to F3 (a) and F4 (b) with a power 3 polynomial trendline for each fault.

nearly opposite activity periods to those of F2, despite having a similar average expansion ratio along the fault.

4.4 Density

A density inversion is frequently cited as reasoning for salt to initiate flow in a salt-based sedimentary basin (Fossen, 2016; Jackson and Hudec, 2017). The composite compaction curves created by Kim and others (2018) were used to reconstruct formation porosity and thickness through the history of the basin (Appendix C), modelled through the following formula:

$$(1)\quad porosity = porosity_{initial} * exp\,(-depth * coefficient)$$

where the coefficient is based on lithology. This study first required the calculation of the initial porosity of each formation, and so rearranged the equation to

$$(2)\quad porosity_{initial} = porosity / exp\,(-depth * coefficient)$$

To determine the porosity of the formations at the time of their deposition, the current porosity of the formation and depth of the formation are needed, as well as determining the coefficient. The coefficients were gathered from the literature (Kim and others, 2018) and are outlined in Table 4.2.

The porosity of each formation was found via the average value of a neutron porosity log through each formation. The log was taken from California Time Petroleum,

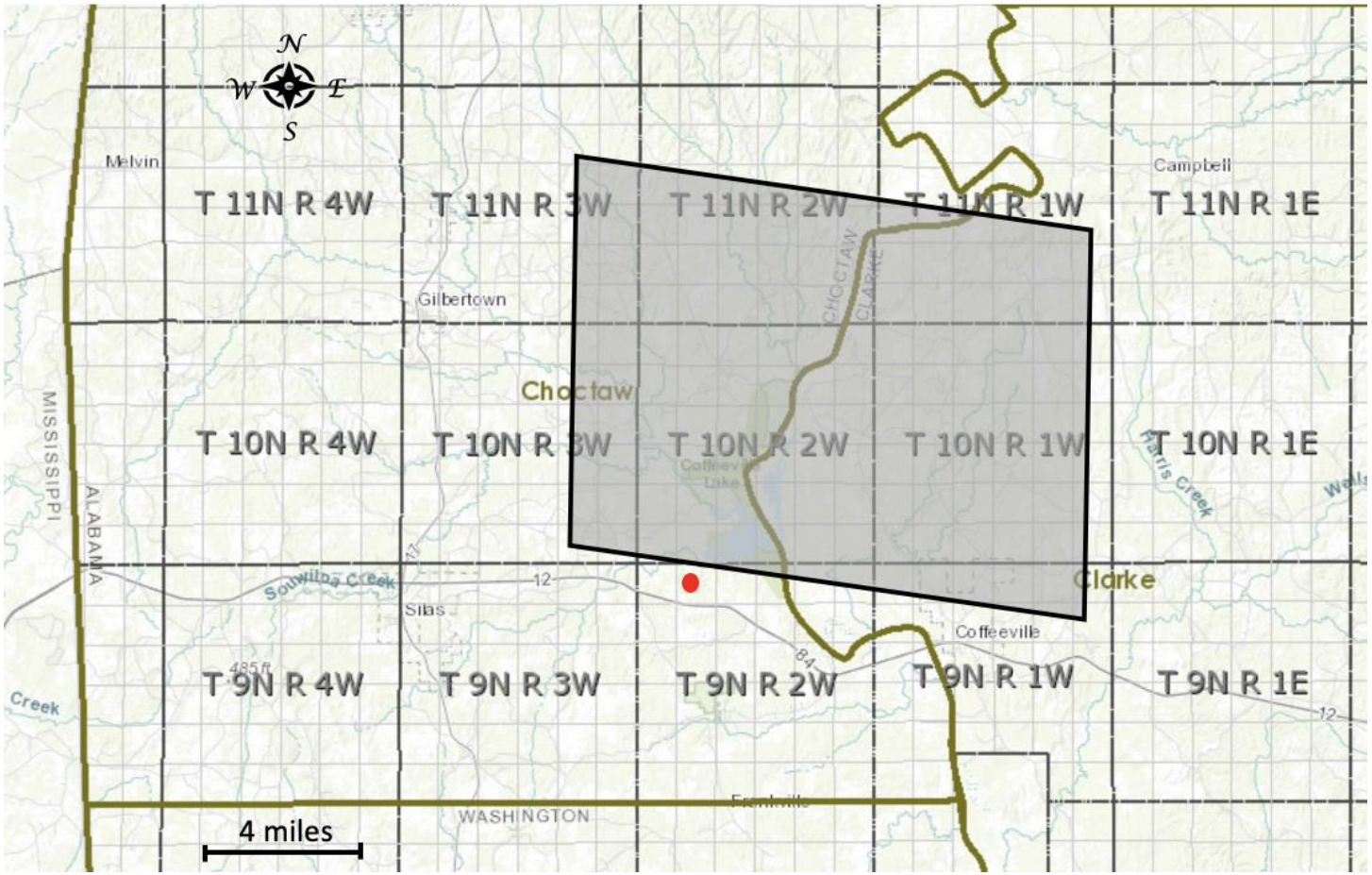

Figure 4.18 *Survey location*

Location of the Altmeyer #1 well (red dot) relative the 3D seismic survey (gray square).

Inc.'s Altmeyer #1 well located in Section 9, Township 5 North Range 2 West, just south of the survey (Figure 4.18). The well is south of the fault zone, in sediments overlying salt. Average neutron porosity values for each formation are shown in Table X.

While the model requires the thickness of each formation in meters, the above thickness measurements (used in the fault expansion indices and local loading) are in seconds. As such, for this formula, the thickness of each formation was averaged using formation top picks from eight wells as well as seismic picks compared to depth from two wells (Figure 4.19). Thicknesses were measured only in the undeformed sediments north of the fault zone to attempt an accurate reconstruction of how the sediments deposited without deformation variables. The thickness for the Norphlet Formation is the only exception, as only one well (Bolinger 19-16 #1) drilled below the Norphlet Formation, and the thickness for the Norphlet Formation was taken from this well. All measured thicknesses were in feet and were subsequently converted to meters. Average thickness values for each formation are shown in Table 4.2.

By using the values in Table 5.2, the initial porosity value was calculated for each formation (Table 5.3). To determine the density of the formations at the time of their deposition, the following equation

$$(3)\ thickness_{initial} = thickness\ (\ 1 + (\ porosity_{initial} - porosity))$$

was used to find first the thickness of the formation once it has deposited. Because formation density changes due to compaction with each successive formation depositing, both the thickness and porosity of each formation are recalculated with every subsequent

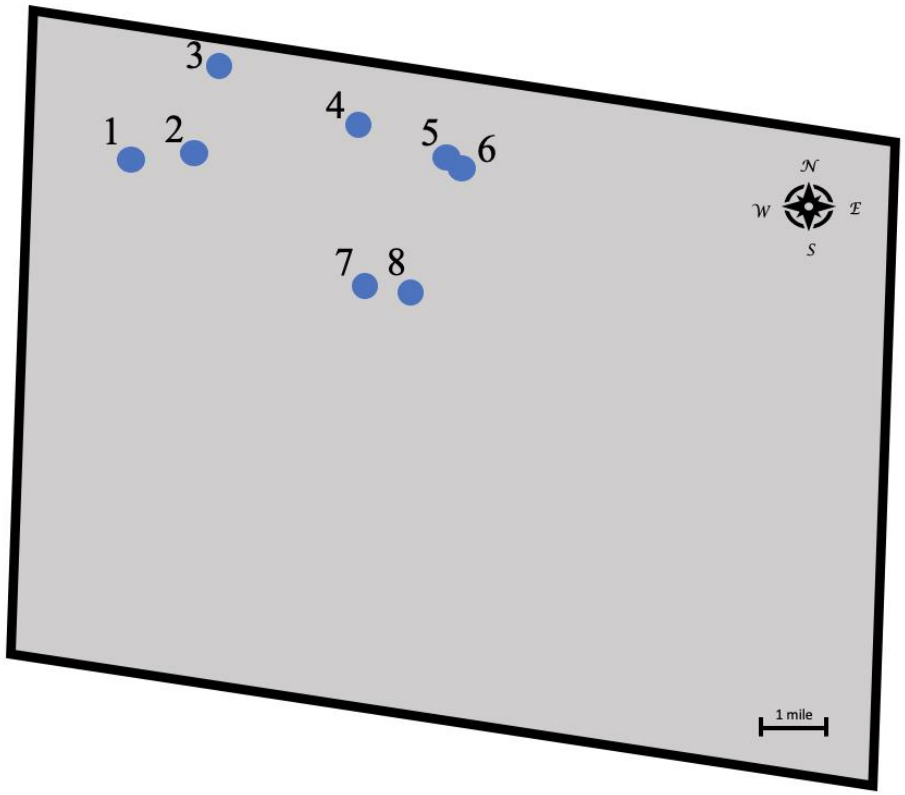

Figure 4.19 *Well locations*

Locations of the nine wells whose formation top picks were used to determine formation thickness in feet. 1) Chappell Unit #1, 2) Bolinger 19-16 #1, 3) Newton 17-5 #1, 4) First National Bank of Laurel #1, 5) William Dansby #1, 6) Clanahan 23-10 #1, 7) Cowan-Scotch Lumber 34-14 #1 8) Elliott Unit 34-16 #1.

Table 4.2 *Initial porosity calculation values*

Current average neutron porosity, thickness, and coefficient values used for each formation. Average neutron porosity values are based on the Altmeyer #1 neutron porosity log.

Formation	Neutron Porosity	Thickness (ft)	Coefficient
Norphlet Formation	0.13	700	2966
Smackover Formation	0.138	302	2599
Buckner Anhydrite	0.16	278	1846
Haynesville Formation	0.125	561	3299
Cotton Valley Group	0.145	1366	2966
Hosston & Sligo Formations	0.15	637	1909
Rodessa Formation	0.135	613	3560
Ferry Lake Anhydrite	0.16	425	1846
Mooringsport Formation	0.16	365	3560
Paluxy Formation	0.16	535	3299
Washita & Fredericksburg Formations	0.18	1025	2966
Tuscaloosa Group	0.24	513	1909
Eutaw Formation	0.32	1414	2966
Selma Chalk	0.14	1258	2574

formation deposition. As the initial thickness and initial porosity for each formation is already determined, thickness through time is calculated by

$$(4)\ thickness = thickness_{initial} / (1 + (porosity_{initial} - [porosity_{initial} * exp (-depth * coefficient])) $$

and those thickness values are then summed to find depth, which is then used for finding the compacted porosity with formula (1). With the porosity and thickness values of each formation as each overlying formation deposits, the density per formation over time is calculated by

$$(5)\ density = (grain\ density * (1 - porosity)) + (1.04 * porosity)$$

where the grain density is the approximate density of the sediments primarily comprising the formation, and 1.04 is the density used for porewater (assuming a saturated formation). The values used are summarized in Table 4.3.

To achieve a density inversion, overlying formations would need to be greater than 2.2 g/cc, the average density of a near-pure halite formation such as the Louann Salt. The initial density of the overlying Norphlet Formation was ~ 2.07 g/cc. It isn't until after deposition of the Cotton Valley Formation that the Norphlet Formation has a density of 2.20 g/cc or higher, at which time it was ~ 2.22 g/cc. The Haynesville Formation deposited with a density of ~2.24 g/cc. However, the average overburden density

(corrected for thickness) is not greater than 2.20 g/cc until the deposition of the Rodessa Formation.

Table 4.3 *Density calculation values*

Grain density used to approximate the density of each formation.

Formation	Initial Porosity	Grain Density
Norphlet Formation	0.36	2.65 g/cc
Smackover Formation	0.42	2.71 g/cc
Buckner Anhydrite	0.74	2.71 g/cc
Haynesville Formation	0.28	2.72 g/cc
Cotton Valley Group	0.31	2.65 g/cc
Hosston & Sligo Formations	0.44	2.68 g/cc
Rodessa Formation	0.22	2.72 g/cc
Ferry Lake Anhydrite	0.41	2.71 g/cc
Mooringsport Formation	0.25	2.72 g/cc
Paluxy Formation	0.25	2.72 g/cc
Washita & Fredericksburg Formations	0.26	2.65 g/cc
Tuscaloosa Group	0.40	2.65 g/cc
Eutaw Formation	0.38	2.65 g/cc
Selma Chalk	0.15	2.71 g/cc

CHAPTER V – DISCUSSION

To determine what may be the cause of salt movement, several things must be chronologically constrained: 1.) When does the density inversion likely occur? 2.) When is there evidence of fault activity? 3.) Does local loading occur, and if so, in what formations? Finally, it must be determined, is there an adequate influence on the salt to cause movement, or would another factor provide a more suitable influence?

Additionally, if a coherent model is to be developed for the relationship between salt movement and fault movement, the following items must also be considered: 1.) When the initial fault movement occurred, 2.) When there were peaks in fault movement, and 3.) Does this movement coincide with a) salt flow initiation, b) the density inversion, c) local loading, and d) current constraints on salt evacuation from other studies?

5.1 Density Inversion

To consider density to be a driving force in initiating salt movement, there must be a formation density of 2.20 g/cc or greater. Hudec and Jackson (2007) indicate that the cumulative overburden must average a density greater than that of salt to initiate salt flow through a density inversion, rather than just a singular formation. Formation density is modelled as the grain density of the formation, modified by the porosity of the formation.

Modelling density as a function of porosity and depth shows a density of 2.20 g/cc or greater is not observed until the deposition of the Haynesville Formation, with the density of the Haynesville Formation at deposition (i.e. no compaction) 2.24 g/cc. The Norphlet Formation, directly overlying the Louann Salt, increases from a depositional

density of 2.07 g/cc to a density of 2.22 g/cc due to decreasing porosity from compaction with the deposition of the Cotton Valley Group. The overburden does not average a density of 2.20 g/cc or greater until the deposition of the Rodessa Formation.

In support of the model indicating an average overburden density inversion was not until Rodessa Formation deposition is the average overburden thickness needed for siliciclastic rocks to have an average density above 2.20 g/cc. Depending on the sediment type in the overburden, typically 2,000 – 6,500ft of burial depth is required to increase siliciclastic sediments to 2.20 g/cc or greater depending on how fine grained the overburden is (Fossen, 2016; Hudec and Jackson, 2007; Rowan, 2019). With Rodessa Formation deposition, the salt has an overburden of 5,000ft, well within the accepted range. The minimum accepted thickness, 2,000ft, is not reached until the deposition of the Haynesville Formation, whereupon the overburden is just shy of 2,300ft.

The earliest point density may have affected the salt is during the deposition of the Haynesville Formation. This is based solely off the minimum suggested overburden thickness to increase siliciclastic sediments to a formation density greater than 2.20 g/cc. More likely, salt was not affected by a density inversion until the deposition of the Rodessa Formation, when both the modelled formation density and the overburden thickness suggest an inversion could occur.

5.2 Faults

5.2.1 Fault Linkages

The history of the fault system is constrained to better correlate the chronological relationship between movement in the Louann Salt and in the fault system. There are five

faults to constrain: F1, F2, F3, F4, and F5. This system is part of the Pickens-Gilbertown-Pollard fault system and can be compared to previous maps of the area (Figure 6.1).

Based on the comparison of regional faults to those mapped in the studies, it is suggested that F1 is the eastward terminus of the Melvin Fault System (MFS), while F2 would be what was previously interpreted to be the eastern terminus of the Gilbertown Fault System (GFS). F3 and F4 can then be associated with the West Bend Fault System (WBFS). While F5 has no corresponding fault in these references, it is a younger fault than the others, not extending to the decollement surface, and is likely to accommodate some of the extensional strain on the footwall of F2.

The Pashin and others (1998a) and Pashin and others (1998b) fault maps were created using wells logs, and so were well constrained only along actively drilled areas at that time. This results in poor constraint of the fault system in areas without high levels of drilled and logged wells, such as the links between the fault systems (i.e., the survey area). The same year, however, Qi and others (1998) mapped the same linkage observed in the 3D seismic (Figure 6.2) as well as linking F1 and F3, using well log data. They do not have the F3 or F4 equivalent faults labelled as part of the WBFS. While the GFS and MFS regionally strike mainly E-W, the WBFS accommodates a bend in the peripheral fault zone, with a strike of WNW-ESE. This transition in strike is captured by the 3D survey. The connection of the two fault systems, whether differentiated by name or strike, may have an influence on the basin through the orientation change affecting the direction of 2D extension perpendicular to the faults. The fault orientation is likely a function of the wedgeward terminus of the salt and not a function of extension direction.

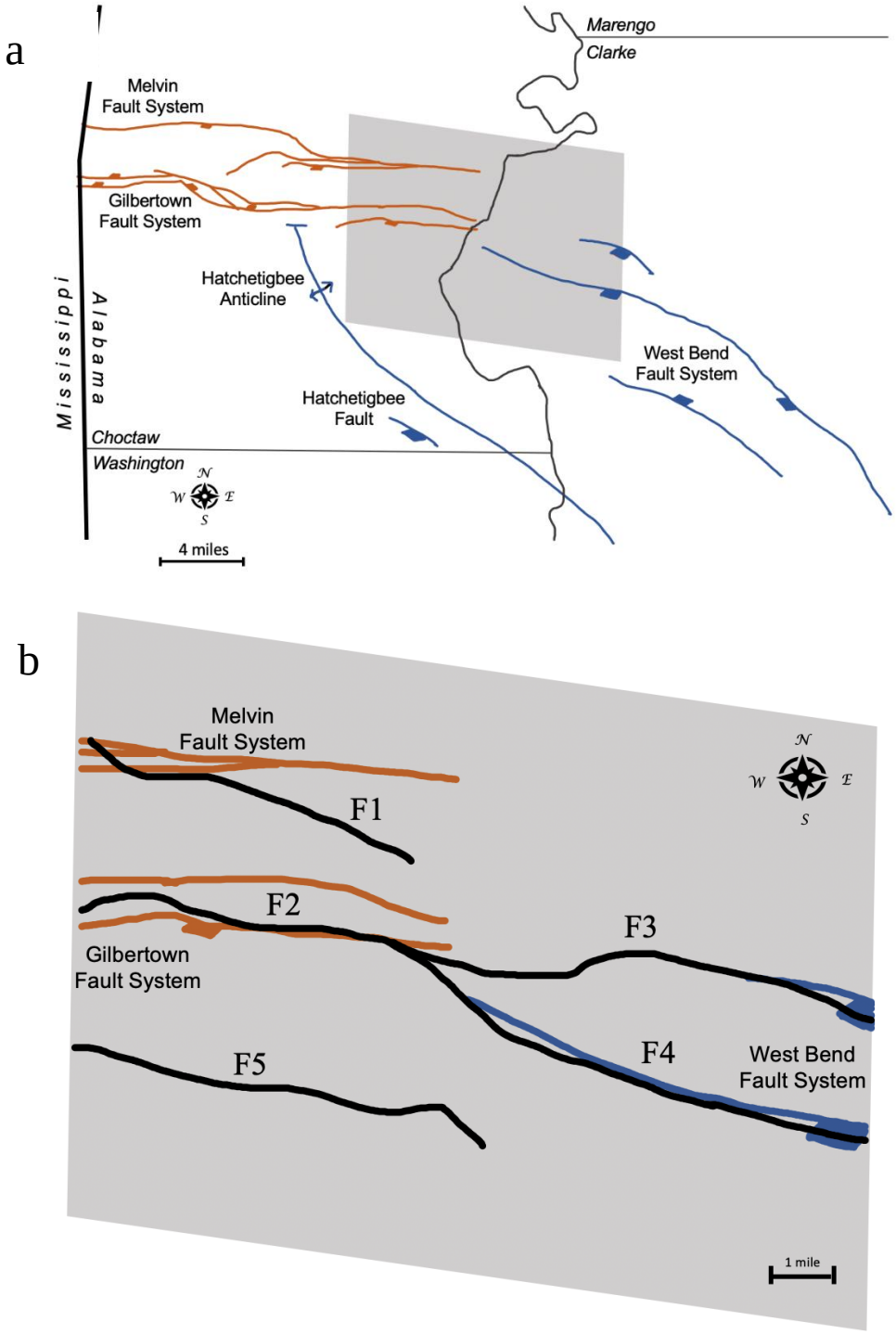

Figure 5.1 *Regional fault system map*

a) Map of the regional fault systems, with the survey shaded grey. b) Survey area with faults mapped from this study (at the top of the Selma Chalk) overlaying previously mapped fault systems. Modified after Pashin and others (1998a), in brown, and Pashin and others (1998b), in blue.

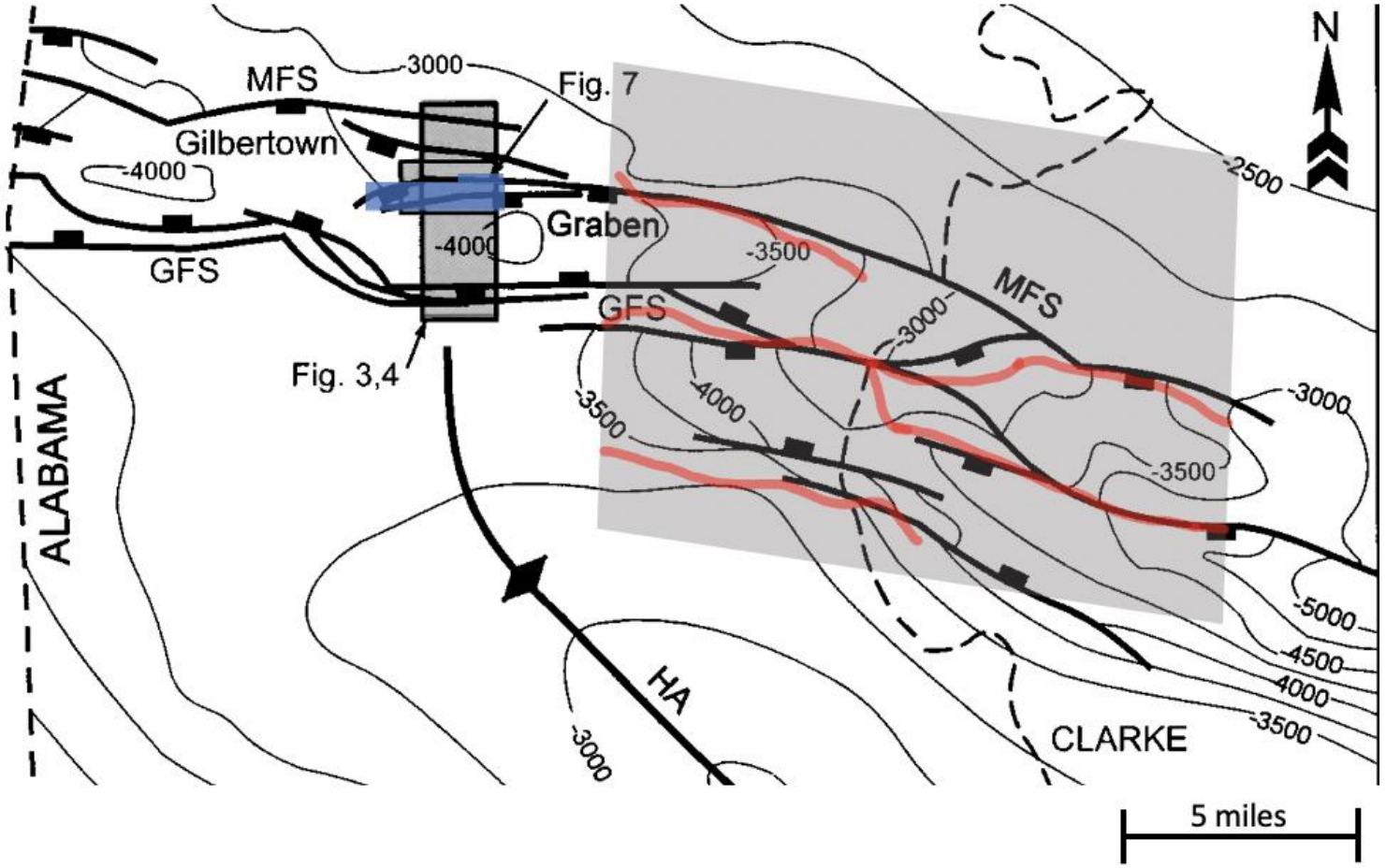

Figure 5.2 *Melvin and Gilbertown Fault Systems*

Comparing 3D mapped faults in this study, red lines, to those mapped by Qi and others (1998), black lines. North Choctaw Ridge Field is in blue. Modified after Qi and others (1998).

The fault set from this study may not be representative of the entire basin; however, the connection of the GFS and WBFS suggests that the subdivision of the peripheral fault zone into various fault systems may be unnecessary aside from geographic blocking and local studies, as the systems all across the basin may be largely synchronous and/or interconnected.

5.2.2 Fault Expansion Index: Timing of Slip

Since all five fault segments are normal faults, there is potential for accommodation space to be generated on downthrown side of the fault. As the formations slip down the listric surface, they increase accommodation space resulting in thicker hanging wall formations as compared to the formation thicknesses in the footwall. These thickened formations in the hanging wall are known as growth strata (e.g., Xiao and Suppe, 1989), as they "grow" with slip, allowing the tracking of fault movement. The FEI (Figure 5.3) is one such way to track fault movement (Thorsen, 1963) and is used here to indicate when the fault first initiated, when peak slip was occurring, when it stopped slipping, and any other recognizable pattern or trend.

The fault expansion indices all had a few formations whose ratios were less than one. In a normal fault system such as this, plotting the downthrown block divided by the upthrown block should result in ratios of 1 or greater. The ratios of less than one are likely predominately a result of potential thickness errors (mentioned previously), as erosive events only impacting the formations to the south of the fault system is unlikely. Additionally, N-S thinning trends in deposition unrelated to the fault system could also cause a ratio of less than 1. As the fault should both begin and end with ratios of approximately one (assuming faulting is no longer active), the values of the lowermost

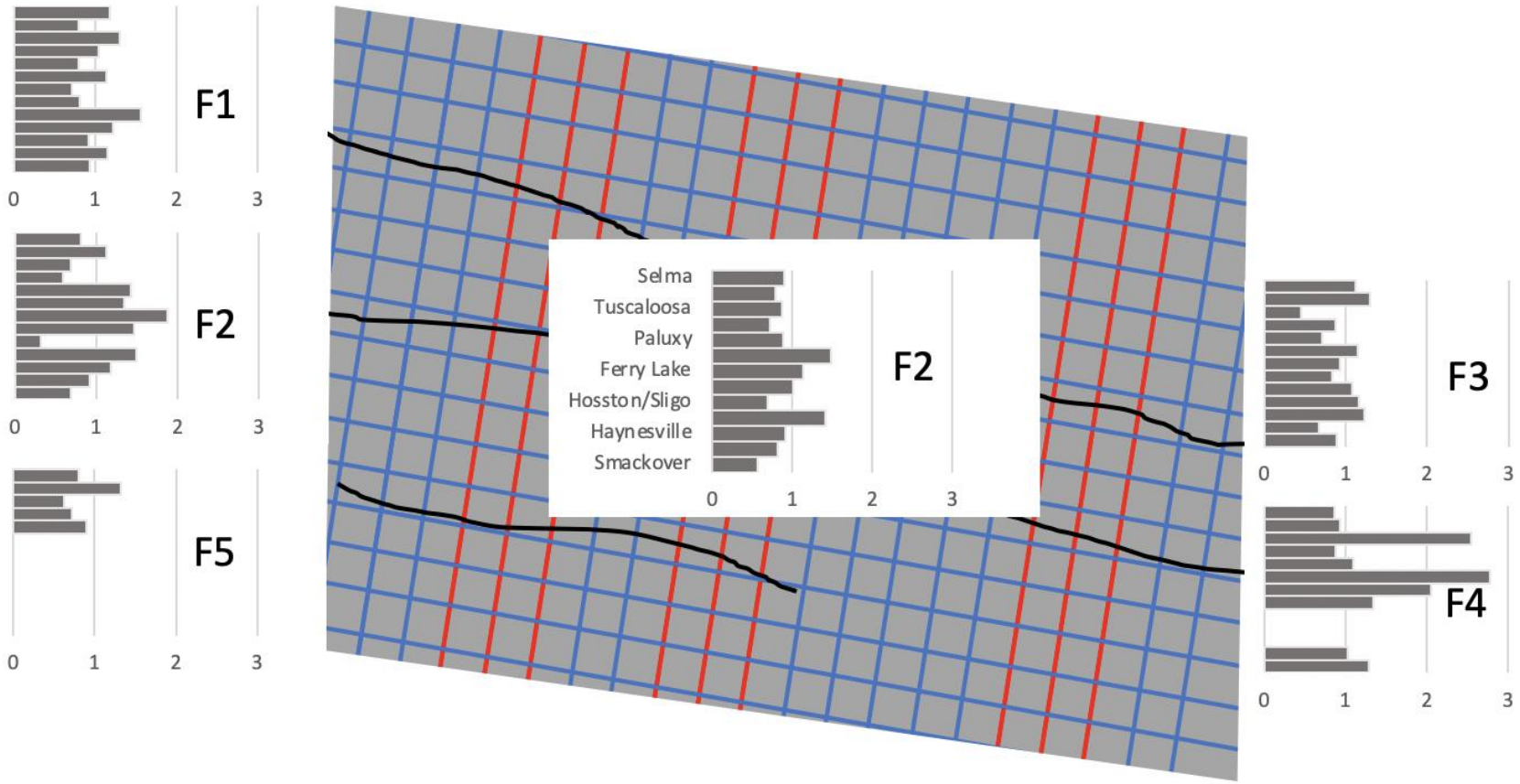

Figure 5.3 *FEI locations in the survey*

and uppermost formations could be assumed to be near “one” and be treated as the baseline, with greater ratios indicating fault movement. However, this study will only look at values greater than one as fault movement.

Several trends in fault movement are apparent when looking at the timing and magnitude of the fault slip. First, slip typically began to occur during the Buckner Anhydrite and Haynesville Formation, though F4 slipped early, during the Smackover Formation, and F2 in lines J, K, and L slipped late, during the Cotton Valley Group. Faults have the highest amount of slip during the Mooringsport Formation. They also have an initial, smaller magnitude peak near the Cotton Valley Group and a resurgence in slip during the Eutaw Formation after a quiet period that followed the main slip event.

F1 and F3 accommodate the smallest, on average, amount of slip, though their initiation and initial peak in movement have greater magnitudes or occur earlier than the other faults, with the exception of the F4 initiation. F4 began slipping the earliest of all faults mapped, and also accommodates the highest amount of slip in both peaks of slip during the Mooringsport Formation and the Tuscaloosa Group. F2 in the J, K, and L lines accounts for little accommodation outside of the first two periods of slip, not even initiating slip until the first peak during the Cotton Valley Group. F2 in the E, F, and G lines has intermediate magnitudes of slip accommodation, and the timing is typical with that of the other faults with the exception of the primary slip event, during which its peak slip accommodation occurs during the Ferry Lake Anhydrite rather than the Mooringsport Formation.

The higher levels of slip in F2 and F4 indicate they accommodated the majority of the extensional strain in this area, resulting in larger expansion ratios, drag folding, and a

better developed hanging wall anticline. That the F4 fault accommodates the most amount of slip could possibly be attributed to its placement in the peripheral fault system. As it is approaching the crux of a change in fault strike, that orientation change may influence accommodation to increase.

Additionally, F2 in lines J, K, and L initiates slip late as compared to in lines E, F, and G, and accommodates little slip outside of peak occurrences. This may indicate the growth of F2, as it initiates in lines E, F, and G in the Haynesville Formation, then propagates eastward to lines J, K, and L, where slip initiates with the first peak in the Cotton Valley Group. It could be during this time that F2 links to F3, as subsequently F3 begins to accommodate very little strain. As slip continues along F2, it remains asynchronous from the E, F, and G lines as compared to the J, K, and L lines. The E, F, and G segment has an earlier peak with greater slip during the Rodessa Formation and Ferry Lake Anhydrite, while the J, K, and L segment has a later peak of lesser slip during the Mooringsport Formation, whereafter it appears to no longer slip. The E, F, and G segment has a tertiary peak during the Eutaw Formation. These differences in slip timing and magnitude suggest that strain was not equally accommodated across all faults, or even across single faults in this region.

5.3 Local Loading

Another of the potential triggers for salt movement is local loading (or lack thereof). No base was mapped for the Norphlet Formation (i.e., top salt) due to evacuation of the Louann Salt from the survey bounds. Therefore, only the Smackover Formation and formations above it can be assessed for local loading. Thicknesses of the

Smackover Formation across the survey are shown in Figure 5.4. In the northwest quadrant of the survey, Smackover Formation thicknesses are notably greater than the rest of the survey. The formation also thins trending eastward, with measurements half the thickness of those observed to the west.

While the discussed measurements are north of the fault system, and therefore should be just north of the salt paleo-boundary, they provide insight to the depositional patterns of the Smackover Formation with minimal to no deformation from the salt. Even south of fault in the southwest corner, the Smackover Formation is thickened, so it is assumed that the overall western thickening of the formation was pre-faulting, with only F4 likely active at this time.

Lateral variation in the thickness of formations may have influenced salt flow or fault activity. Most formations show north/south thickness variation across the fault system, most of which is likely a consequence of increased accommodation space from hanging wall downdrop. East/west variation occurs in all formations aside from the Haynesville Formation, Cotton Valley Group, Rodessa Formation, and Selma Chalk. Roughly, thickening alternates between formations thickened to the west of the survey (i.e., the Smackover, Hosston/Sligo, Paluxy, Washita/Fredericksburg, and Eutaw Formations), to formations thickened to the east of the survey (i.e., the Buckner and Ferry Lake Anhydrites, the Mooringsport Formation, and the Tuscaloosa Group) (Table 6.1). Only F4 (which is in the east half of the survey) appeared to have a timing correlation between high FEI ratios and thickened deposits, with its three highest FEI ratios in three

	A	B	C	D	E	F	G	H	I	J	K	L	M	N	O	P	Q	R	S	T	U	V
1		0.069	0.073	0.069	0.063	0.076	0.078	0.076	0.08	0.069	0.073	0.069	0.061	0.061	0.057	0.057	0.05	0.048	0.05	0.04	0.034	
2	0.065	0.063	0.063	0.065	0.069	0.069	0.069	0.076	0.076	0.065	0.078	0.069	0.067	0.059	0.059	0.055	0.050	0.042	0.034	0.034	0.025	
3	0.063	0.063	0.069	0.065	0.069	0.071	0.073	0.069	0.071	0.065	0.069	0.065	0.061	0.065	0.052	0.057	0.036	0.042	0.036	0.048	0.032	
4	0.063	0.073	0.073	0.071	0.076	0.073	0.071	0.078	0.069	0.069	0.050	0.054	0.063	0.054	0.053	0.052	0.050	0.040	0.025	0.042	0.034	
5	0.073	0.069		0.080	0.084	0.078	0.071	0.076	0.080	0.057	0.048	0.057	0.044	0.061	0.059	0.050	0.038	0.032	0.023	0.046	0.036	0.025
6	0.079		0.052	0.088	0.080	0.078	0.082	0.071	0.080	0.057	0.052	0.048	0.042	0.052	0.059	0.050	0.040	0.036	0.031	0.029	0.023	0.029
7					0.048	0.046	0.074	0.057	0.074	0.059	0.052	0.048	0.046	0.044	0.040	0.040	0.036	0.029	0.027	0.031	0.023	0.040
8			0.017	0.080		0.036	0.061	0.048	0.082	0.052	0.046	0.048	0.046	0.050	0.040	0.042	0.027	0.038	0.025	0.027	0.027	0.029
9		0.071	0.061	0.080	0.082	0.065	0.076	0.090	0.080	0.055	0.048	0.048	0.055	0.052	0.048	0.032	0.036	0.029	0.031	0.029	0.031	0.027
10		0.044	0.073	0.069	0.071	0.073	0.071	0.076	0.067	0.055	0.065	0.055	0.034	0.036	0.034	0.036	0.029	0.023	0.029	0.034	0.040	0.027
11		0.044		0.076	0.086	0.043						0.032	0.042	0.027	0.025	0.027	0.023	0.031	0.027	0.036	0.027	0.029
12		0.057											0.010	0.029	0.034	0.032	0.036	0.031	0.034	0.029	0.027	0.029
13		0.044	0.019		0.038	0.038	0.025	0.040	0.025					0.025	0.034	0.038	0.025	0.034	0.034	0.033	0.027	0.033
14		0.052	0.046	0.053	0.055	0.046	0.046	0.040	0.038	0.023	0.021	0.036			0.031	0.034	0.023	0.042	0.042			
15		0.059	0.052	0.053	0.057	0.055	0.048	0.053	0.044	0.036	0.034	0.029						0.029				
16			0.065	0.059	0.057	0.052	0.046	0.042	0.046	0.042	0.040	0.034	0.013	0.017				0.040				

Figure 5.4 *Smackover Formation thicknesses*

Thickness measurements of the Smackover Formation across the 3D seismic survey. Thicker measurements are shaded darker green, while thinner measurements are shaded lighter green. Measurements two standard deviations or greater away from average are bordered in red.

Table 5.1 *Lateral thickening trends by formation*

Thickening to the...	W	None	E
Selma		X	
Eutaw	X		
Tuscaloosa			X
WashFred	X		
Paluxy	X		
Mooringsport			X
Ferry Lake			X
Rodessa		X	
Hosston/Sligo	X		
Cotton Valley		X	
Haynesville		X	
Buckner			X
Smackover	X		

of the four formations that thickened to the east: the Ferry Lake Anhydrite, the Mooringsport Formation, and the Tuscaloosa Group. There does not appear to be any direct correlation between thickening trends and the remaining faults. However, more localized variation may still have influence FEI ratios.

In all formations, clusters of measurements two standard deviations or greater from the average tend to occur on the downthrown blocks. The largest cluster occurred in the Cotton Valley Group and primarily extends across lines B through H and in M2 fault block. The primary fault affected would be F2, but comparison to its eastern equivalent, F4, is not possible as the Cotton Valley Group has a missing section due to rollover in the F4 downthrown fault block. As such, unfortunately the effect of clustering cannot be accurately assessed regarding its influence on either salt or fault movement.

5.4 Sediment Creep

Lastly, the influence of basin-ward sediment creep should be considered. For sediment creep to influence faulting and/or salt movement, it would need to be observable prior to fault growth, which was determined to be during the Haynesville Formation. The sediments overlying the salt have the potential to creep, as the salt provides an unstable basement for the sediments to detach, whereas those up-dip of the salt (with the Paleozoic rocks acting as the basement) would remain stable from a higher coefficient of friction at the contact. If sediments crept basin-ward, accommodation space would increase at the transition from salt basement to Paleozoic basement as the salt-based sediments mobilized and the Paleozoic based sediments remained in place.

Increased accommodation space during deposition would result in a thicker sediment column and may even result in drag folding along the margin.

Thickening next to the fault scarps on the downthrown blocks is not observed in the Ferry Lake Anhydrite or older formations, and neither is drag folding. Drag folding is observed in formations above the Mooringsport Formation and is likely related to faulting.

5.5 Salt Movement Initiation

The initiation of movement within the Louann Salt has a variety of potential causal factors, with some presented above. Evidence suggests salt movement occurred as early as the Smackover Formation, with local thinning (Hughes, 1968; Mancini and others, 1990) as well as shoaling observed on salt highs within the Smackover Formation (Llinás, 2003). As shoaling is not a formation-wide occurrence, it is thought to have occurred due to uplift of the Smackover Formation along local paleo-highs as the upward-moving salt displaced the Smackover Formation to shallower depths below sea level. Hughes (1968) even suggested salt evacuation initiated with small amounts of Norphlet Formation deposition, while Jackson and Seni (1983) suggest initiation from Jurassic through Early Cretaceous (Cotton Valley Group). Based on evidence of thinning and potential shoaling within the Smackover Formation, it seems salt was evacuating during the deposition of the Smackover Formation.

Overburden density does reach above 2.20 g/cc until, at the earliest, the deposition of the Haynesville Formation, but more likely during the deposition of the Rodessa Formation. As overburden density is less than 2.20 g/cc as an average

overburden until the deposition of the Rodessa Formation, a density inversion could not have been likely to influence the salt to initiate movement. This is not to say that a density inversion did not influence or further exacerbate salt flow once initiated (see below); however, it is supported that a density inversion is not the main cause for initiating salt movement.

The fault system does not see high amounts of accommodation space created during or before the Smackover Formation. While F4 does record initial slip in the Smackover Formation, this would not likely be a significant factor in mobilizing the salt and is more likely passively recording the initiation of salt evacuation, lending more support to salt movement at this time. While most of the faults were not slipping until the Haynesville Formation and the first peak in accommodation space did not occur until the deposition of the Cotton Valley Group, salt movement had already been occurring prior.

Of the potential triggers investigated, local loading is the sole factor that occurs early enough to affect the salt. In recent years, differential loading has been suggested to be a dominant influence in salt movement (Rowan, 2019; Vendeville, 2005; Warren, 2006; Warsitzka and others, 2013). With salt acting as a fluid, a lateral difference in overburden thickness (i.e. differential loading) causes areas of high pressure (under thicker locales) and low pressure (under thinner locales). Differential loading leads to differential pressure, so the salt will be influenced to flow from high pressure areas to low pressure areas. This suggests that the differential loading due to E-W variations in the Smackover Formation thickness could have locally influenced the Louann Salt to initiate salt movement. To induce basin-wide salt flow there must be repeated occurrences of

differential loading across the entire salt periphery, but testing this is beyond the extent of this study, therefore a definitive conclusion cannot be made by this study.

5.6 Model

Models reconstructing the MFS and GFS in North Choctaw Field (Qi and others, 1998) also indicate the northmost faults formed first and faults get younger basin-ward. The imbricate listric faults of the MFS have a northernmost fault with little rotation in the hanging wall, indicating little slip, with basin-ward secondary listric faults exhibiting expansion and folding. While Qi and others (1998) listed the pre-growth strata as extending to the top of the Cotton Valley Group, the first fault in their model was attributed to the initial evacuation of the Louann Salt.

Salt movement was likely occurring before the faults were moving, or the density inversion formed. As salt likely moved soon after sediments were deposited on top of it, fault movement is a passive reaction to salt evacuation and not a main cause. As the faulting is passive and reacting to salt movement, it makes an ideal potential candidate at recording continued salt movement.

The first peak in slip occurred with deposition of the Cotton Valley Group. The largest cluster of anomalously thickened units occurred in the Cotton Valley Group. While this may be a local phenomenon, it is possible that this high increase in load may have locally caused increased lithostatic load and increased slip along the faults. The increased fault slip may also have been influenced by the deposition of the Haynesville Formation due to its higher density. Despite the full overburden not averaging greater than 2.20 g/cc by this time, the Haynesville Formation was deposited with a density

greater than 2.20 g/cc, and the Norphlet Formation compacted to a density greater than 2.20 g/cc with Cotton Valley Group deposition. This may have influenced the salt flow to increase in magnitude, though the overburden had not yet averaged a density inversion. The slip on the faults at this time is increased, but by no means the highest, so this likely created cause for slip but of lower magnitude.

The increase in slip to the primary peak during the Mooringsport Formation begins with the deposition of the Rodessa Formation. The deposition of the Rodessa Formation is when the average overburden density inverts with the salt density. Though density was not a trigger in initiating salt flow, its influence in salt tectonics remains. This density inversion likely exacerbated any movement in the salt. This exacerbation in salt movement was recorded by the faults with the highest peak in slip occurring at this time. The increased accommodation in the faults ends with the Paluxy Formation.

A final pulse of salt movement occurs with the Tuscaloosa Group and Eutaw Formation. This does not have a clear contributing factor, but with the amount of overburden on the salt, there is likely a cumulation of triggers that reactivate the salt to move.

Figure 5.5 shows the chronologic development of the fault system as the salt evacuates from the deposition of the Norphlet Formation through the Cotton Valley Group. Initial basin-ward flow created F4 fault, shortly followed by F1 and F3 which accommodated most of the initial strain. As salt flow continued, F2 formed, whereafter F2 and F4 accommodated the majority of the extensional strain from then on.

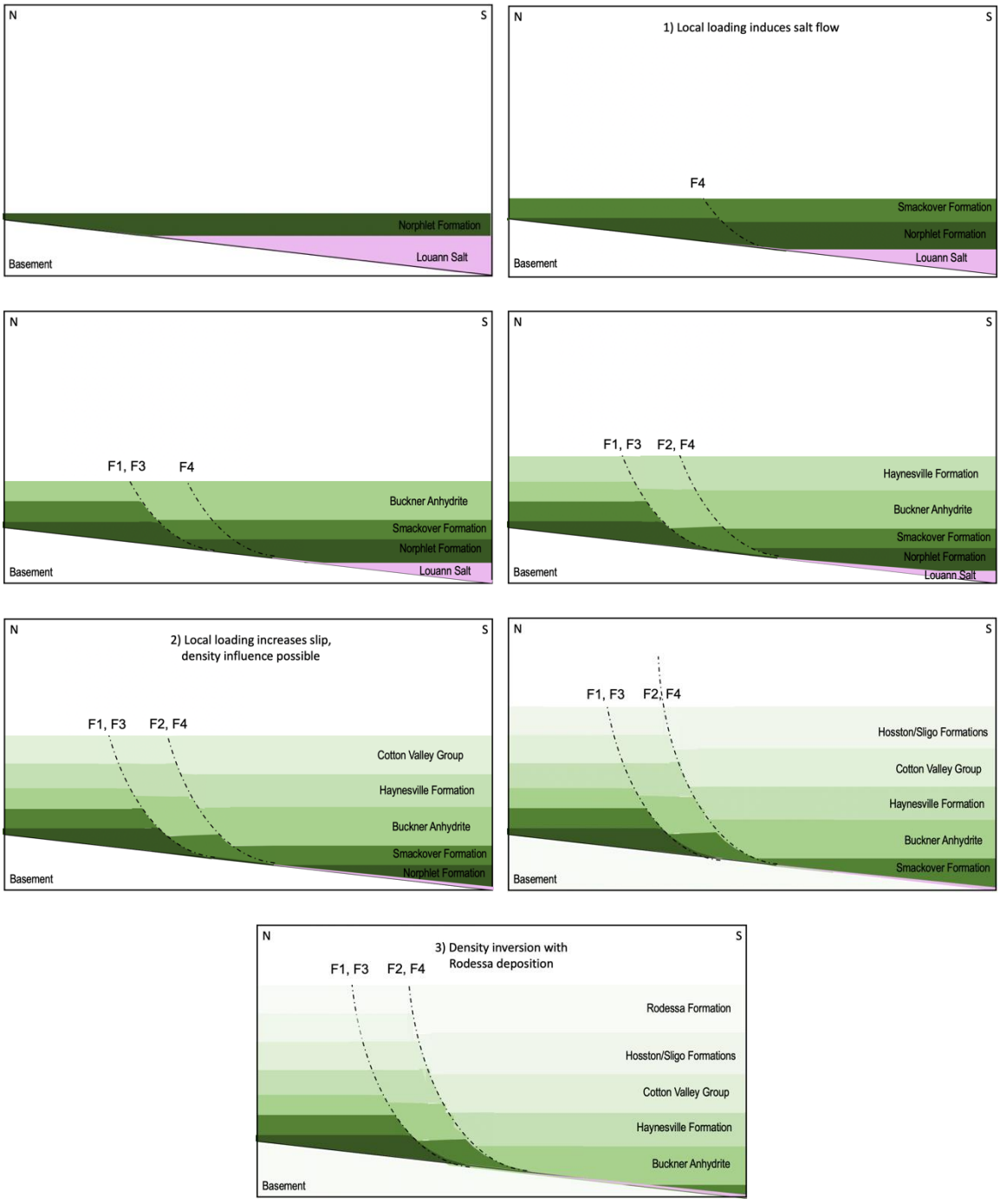

Figure 5.5 *Fault model*

Chronological restoration of the fault systems observed in the seismic survey.

It is likely that these findings can be applied outside of the GFS/MFS/WBFS throughout the rest of the peripheral fault zone. This is most applicable through the Pickens-Gilbertown-Pollard section, as the formations will be most similar to the study area. Further east, such as the Mexia-Talco Fault Zone, the applicability of this study remains, but should be verified with local data due to changes in formations across the Gulf of Mexico.

CHAPTER VI – CONCLUSION

In this study, the focus was to ascertain the relationship between Louann Salt evacuation, deposition, and the peripheral fault zone. The formations and faults within a 3D seismic block were mapped to determine the subsurface geometry in the survey area and well logs were used for formation tops and density. Once mapped in the 3D block, formation thicknesses were measured across the area and both laterally compared and compared across faults. These were then used to determine trends in formation density, local loading, sediment creep, and fault expansion.

Some key generalizations from this study can be made:

1. Density had an average regional inversion with deposition of the Rodessa Formation. This timing coincides with increased expansion indices in F2, F3, and F4.
2. Local loading/differential loading is most likely a key influence in the early stages of salt flow.
3. Extensional strain was accommodated by all faults—however not at the same time or same magnitude— with the majority of strain being accommodated by F4.
4. The peripheral fault zone formed as a passive response to the basin-ward flow of the Louann Salt and provides a record of salt migration which indicates that salt movement was episodic and not one progressive evacuation.

Salt movement is a critical component for many sedimentary basins. Through its ability to quickly generate accommodation space, its capacity to form a variety of diapiric structures, and its tendency to flow, the investigation of salt and its processes are crucial and not to be overlooked. This study suggests salt flow occurs in pulses of movement,

which could influence the degree of accommodation space created in the basin as well as how salt structures form.

Additionally, the greater GOM region and other salt basins such as the North Sea, Persian Gulf, and Campos Basin (Brazil) rely on salt to play a role in most aspects of the hydrocarbon system. With timing being an essential part of the hydrocarbon system, defining and understanding the flow history of salt is vital. Salt basin peripheral fault zones worldwide may have a record of both the timing and magnitude of salt flow, which can be used as a baseline throughout the basin. Further investigation of peripheral fault zones is strongly recommended.

APPENDIX A – Cross Sections

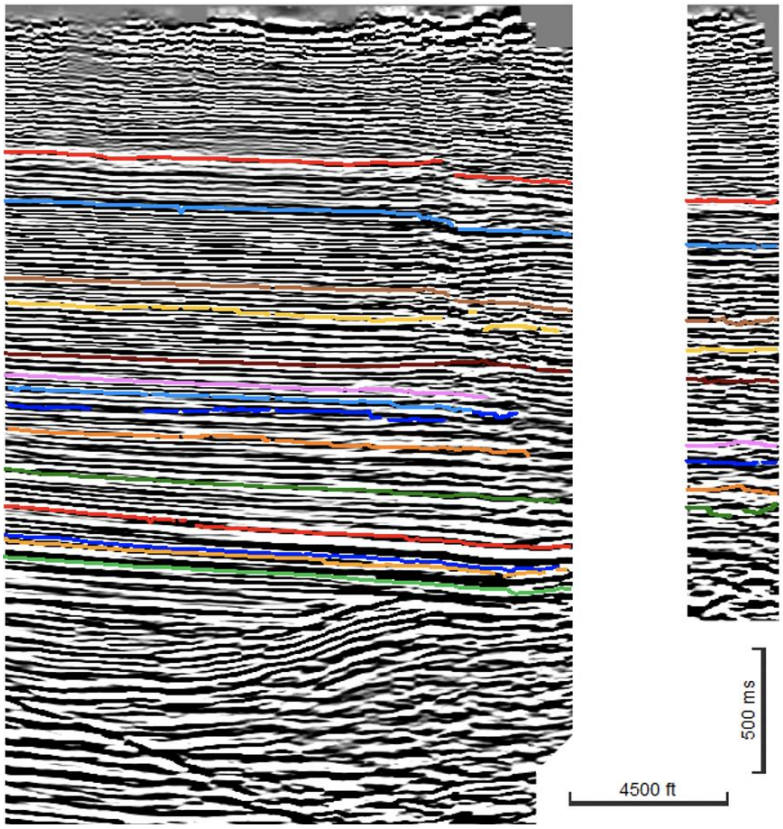

Figure A.1 *Arb line A*

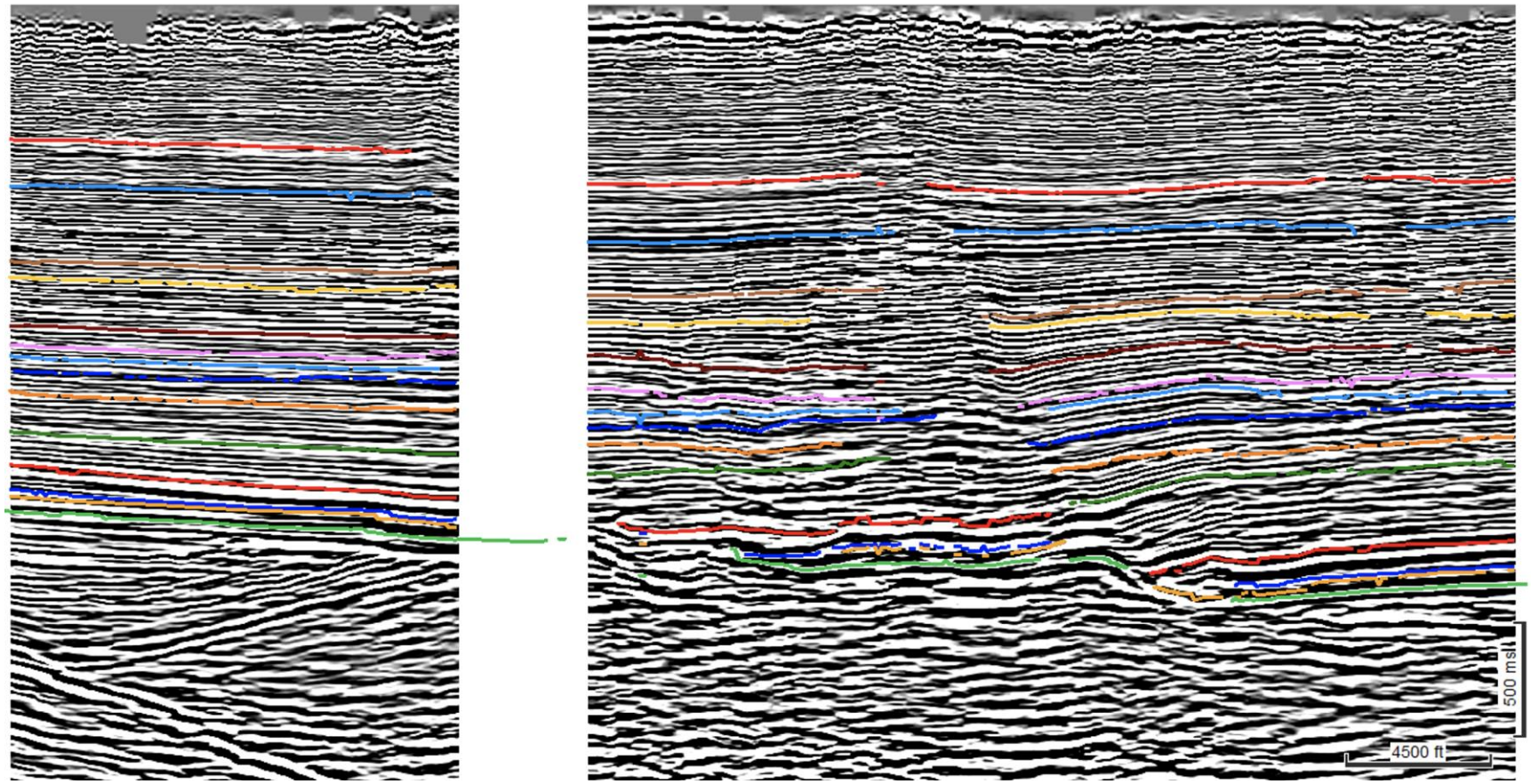

Figure A.2 *Arb line B*

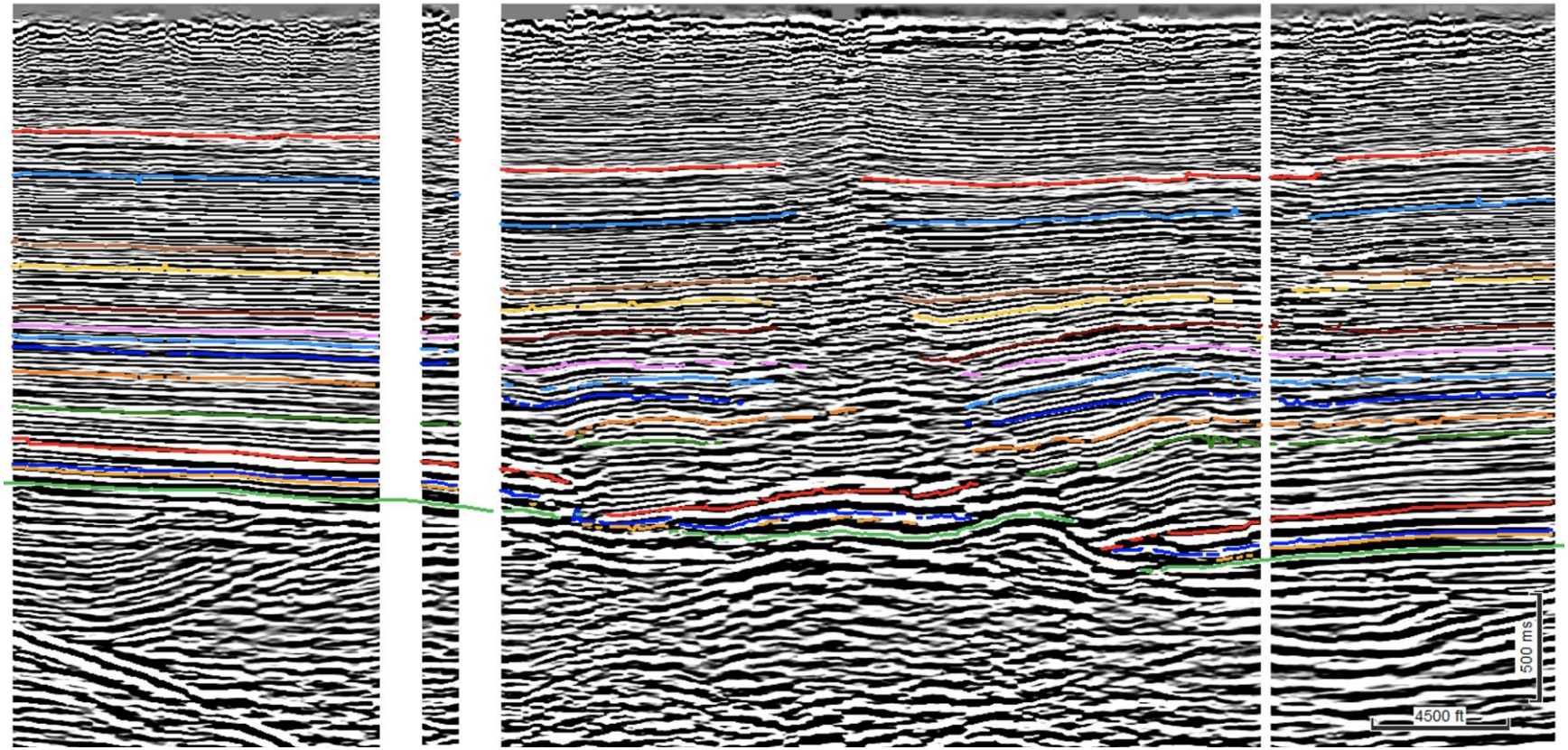

Figure A.3 *Arb line C*

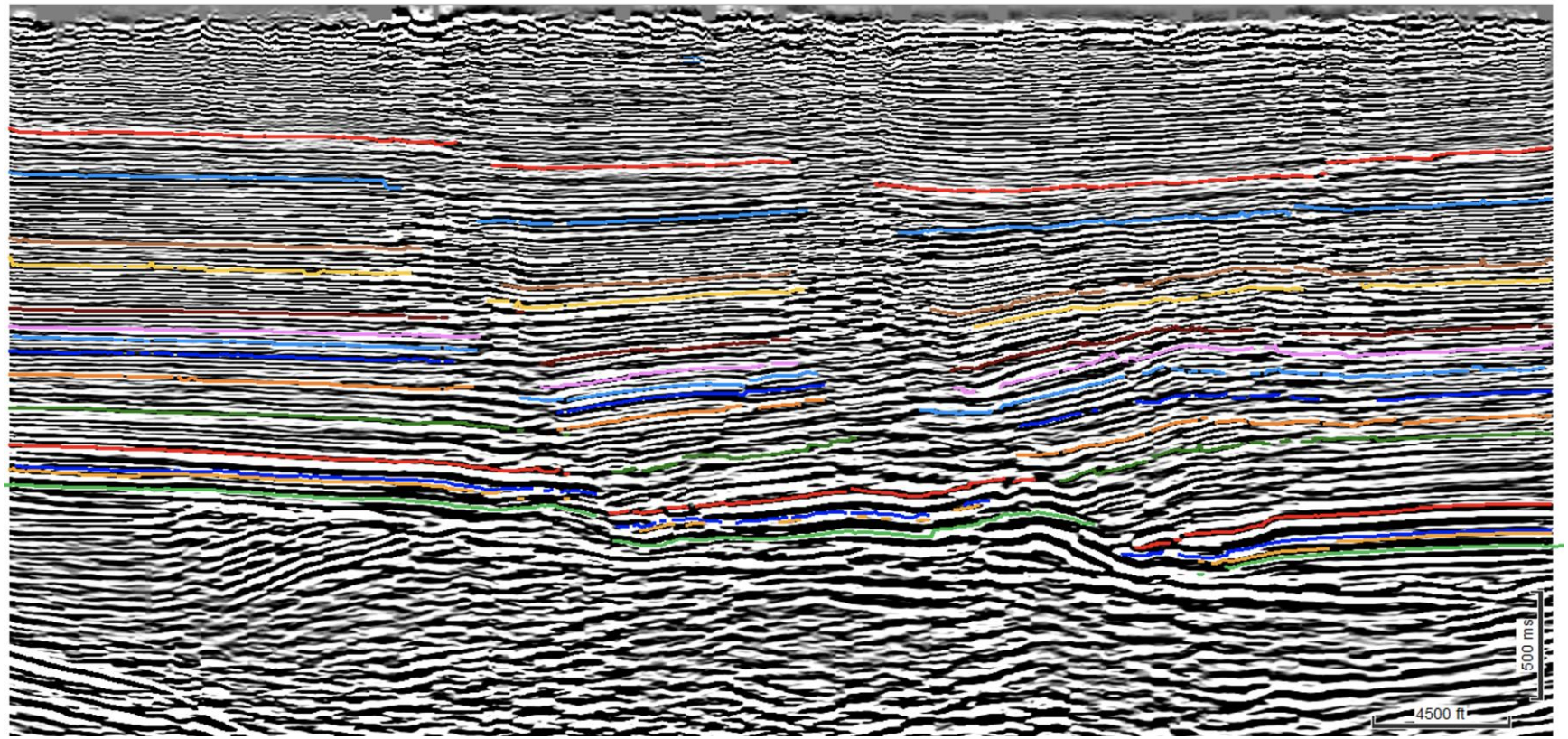

Figure A.4 *Arb line D*

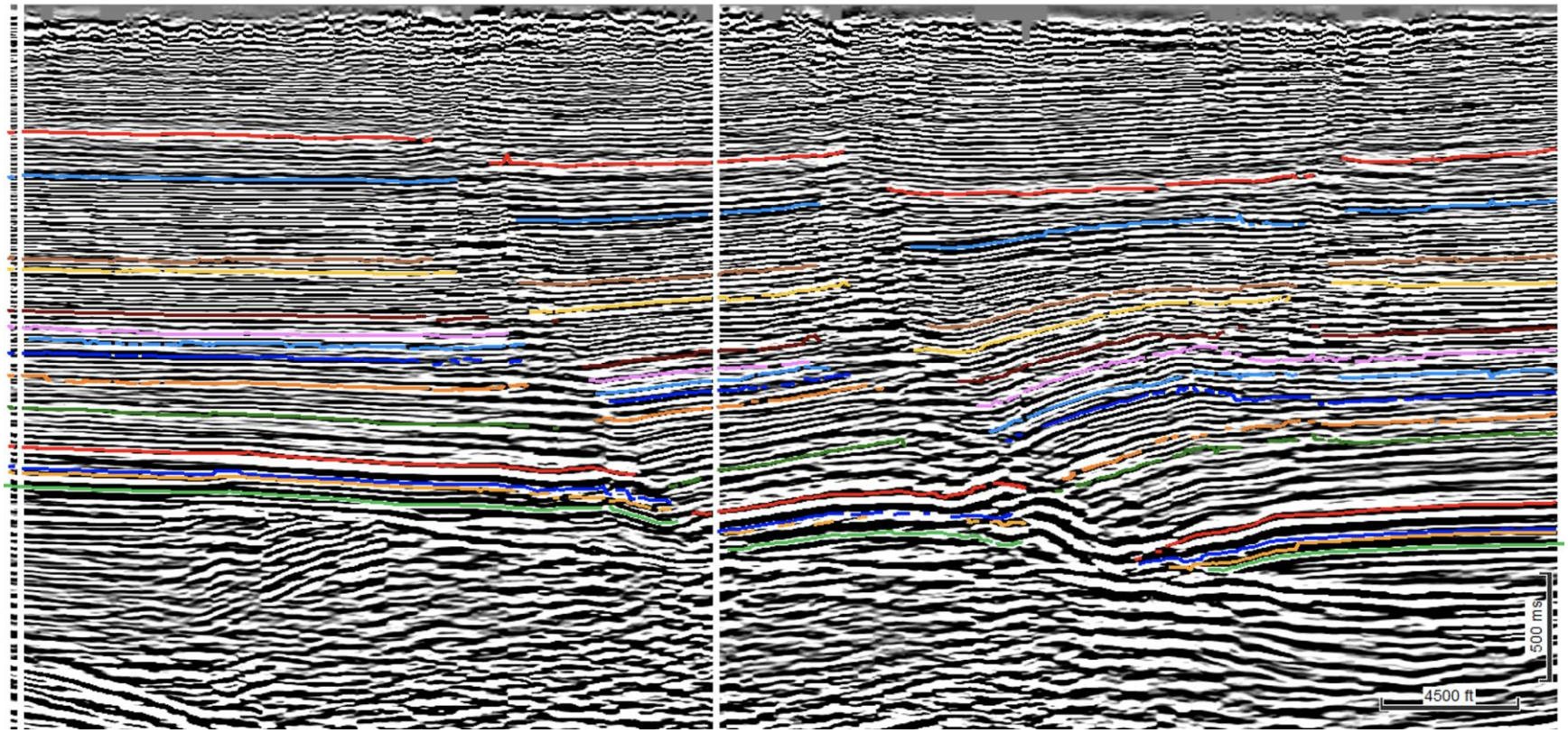

Figure A.5 *Arb line E*

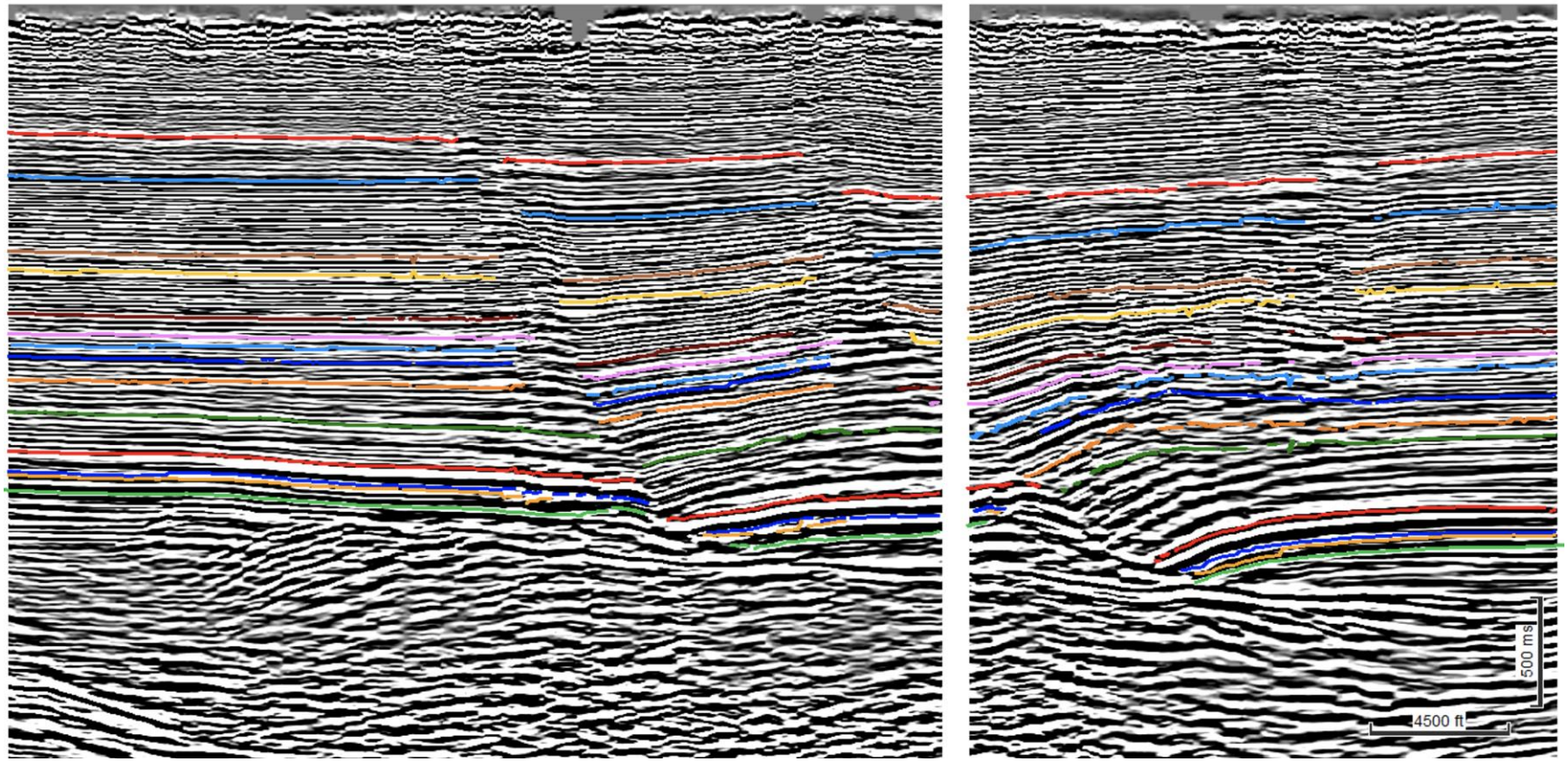

Figure A.6 *Arb line F*

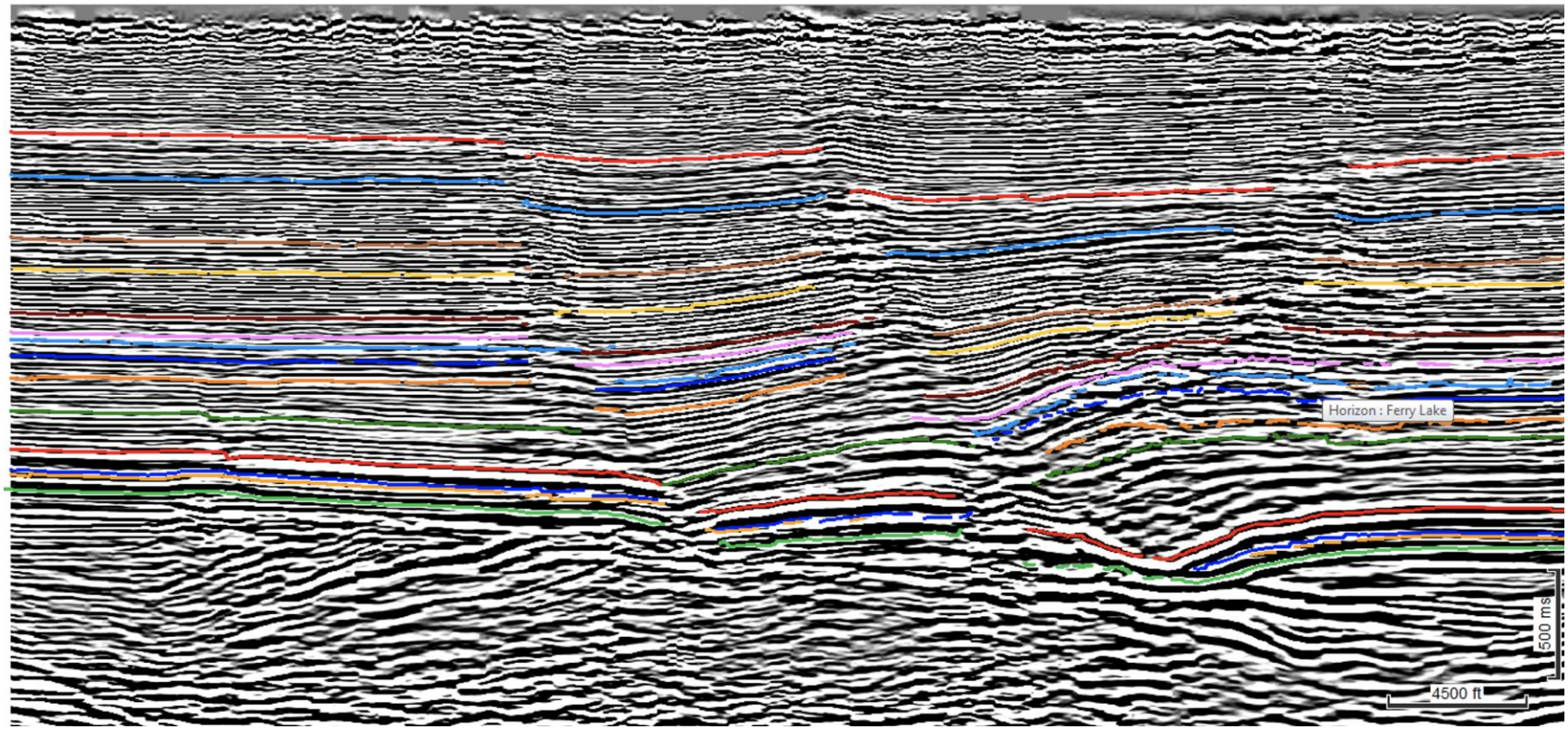

Figure A.7 *Arb line G*

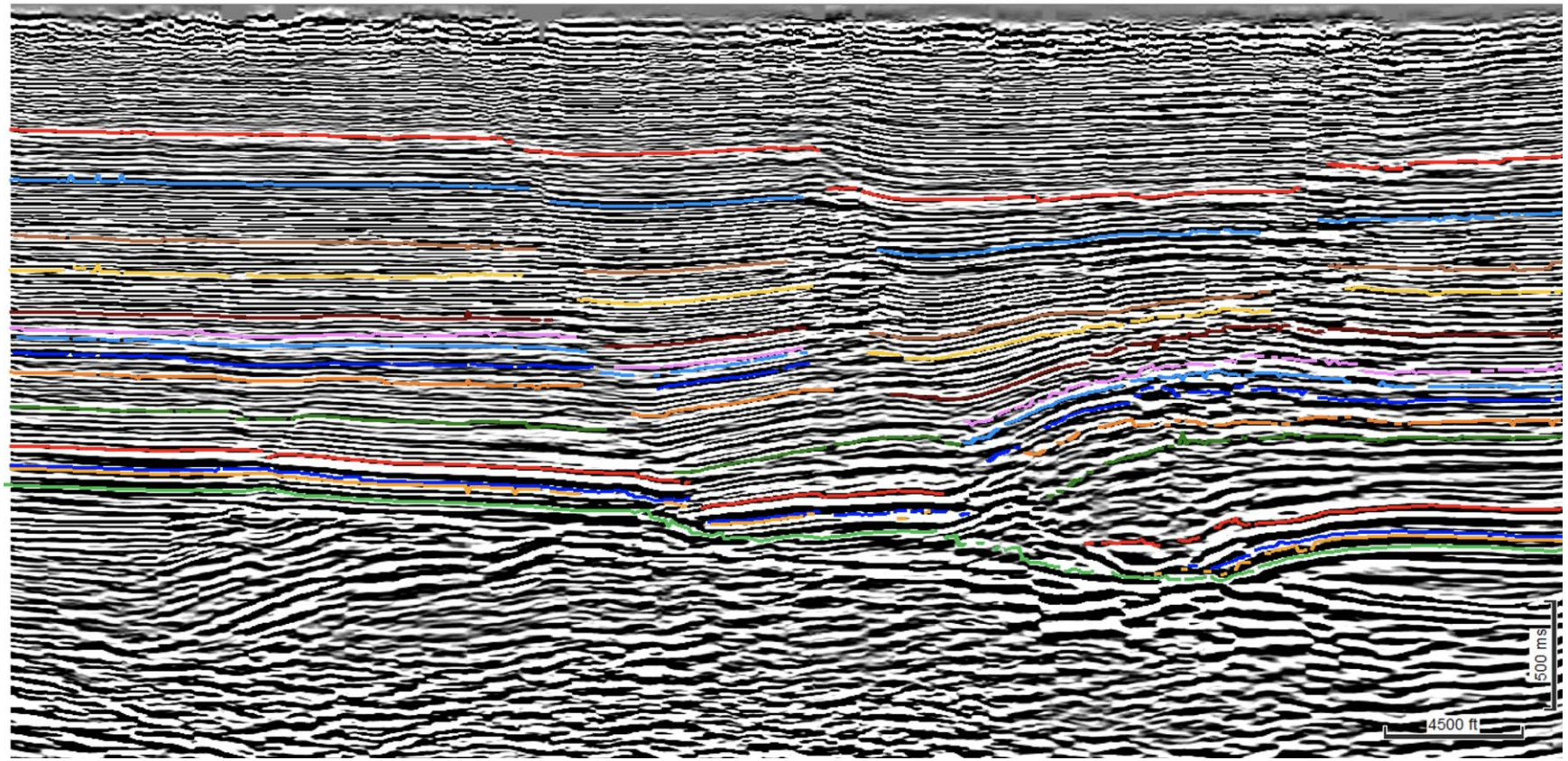

Figure A.8 *Arb line H*

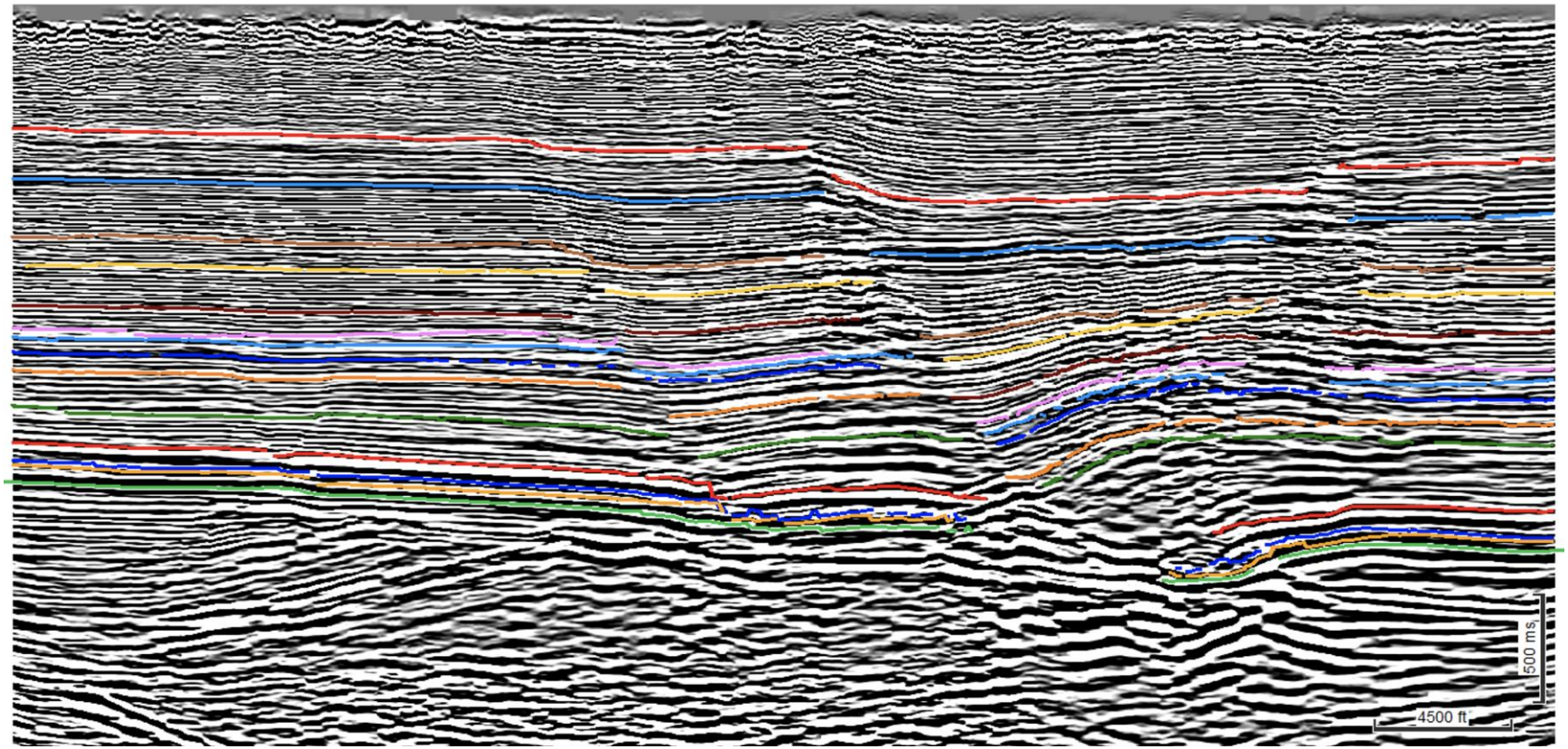

Figure A.9 *Arb line I*

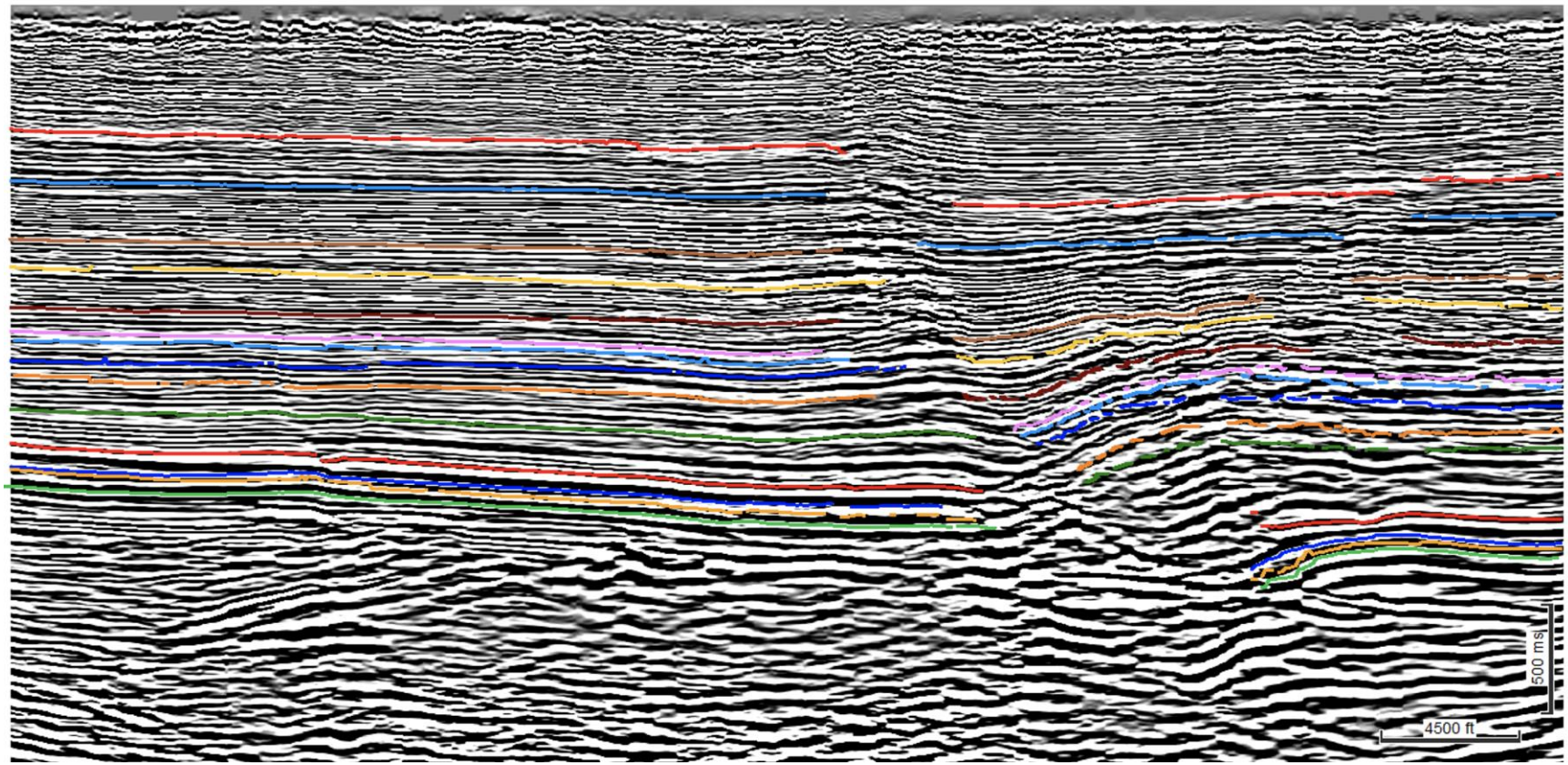

Figure A.10 *Arb line J*

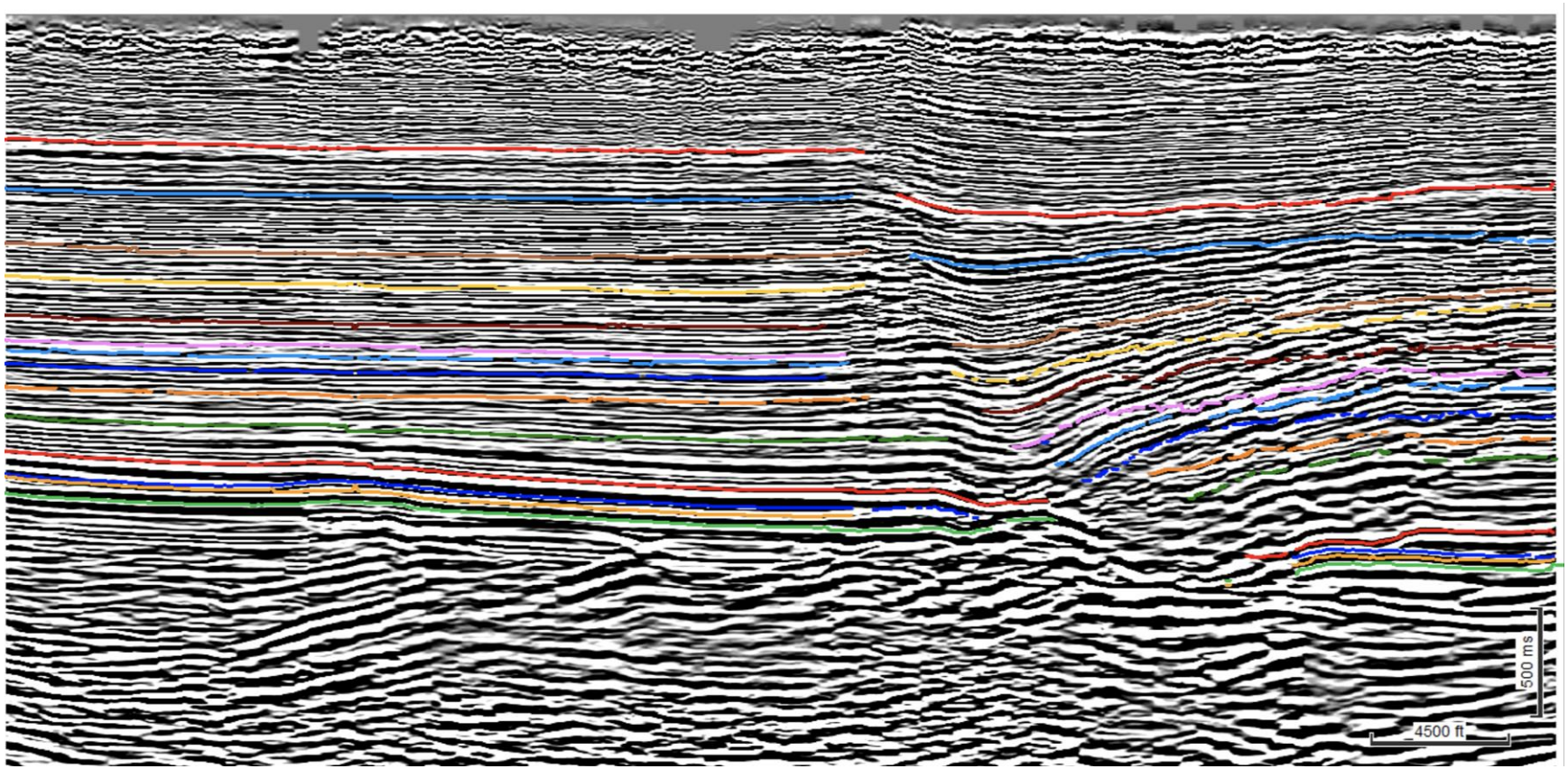

Figure A.11 *Arb line K*

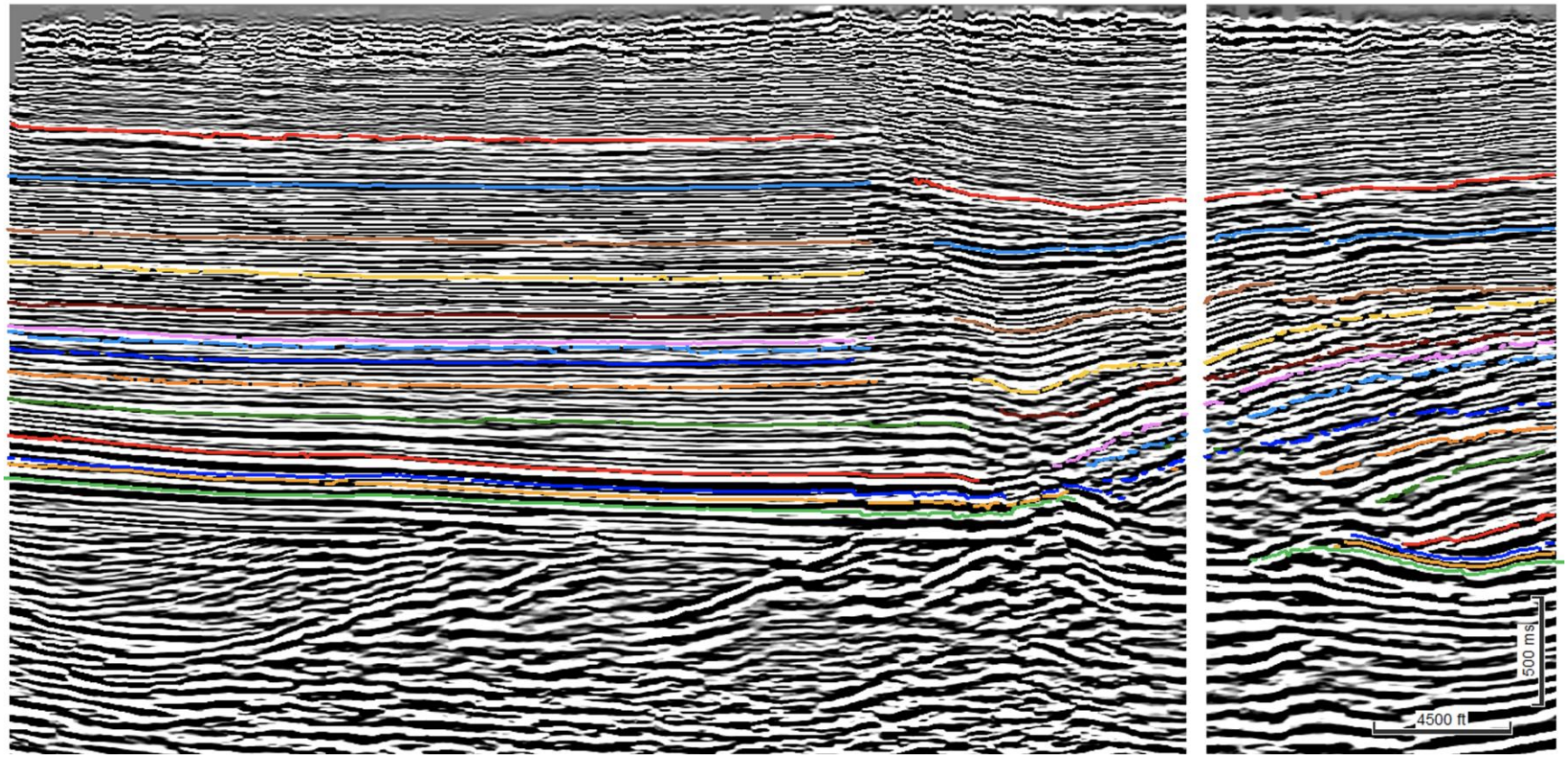

Figure A.12 *Arb line L*

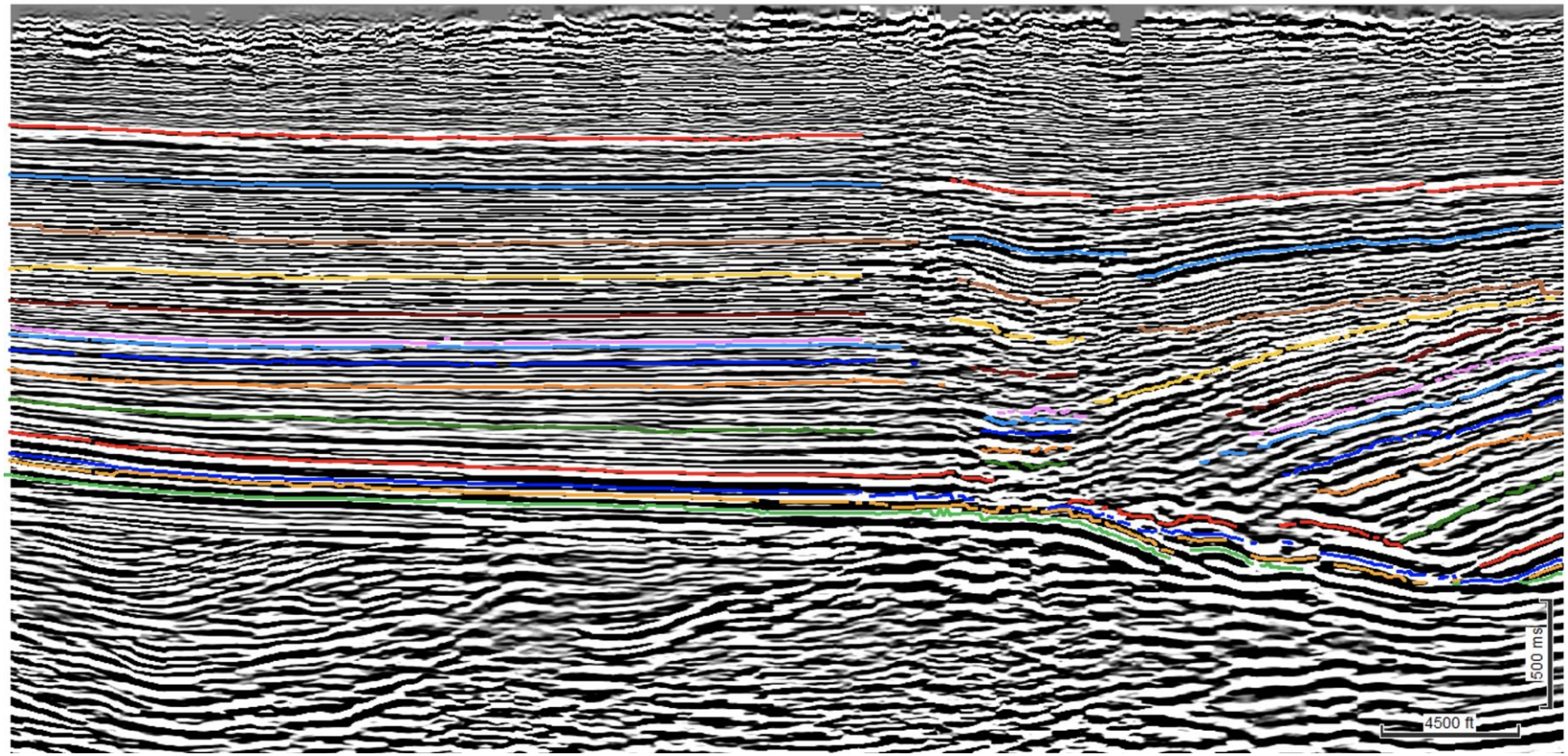

Figure A.13 *Arb line M*

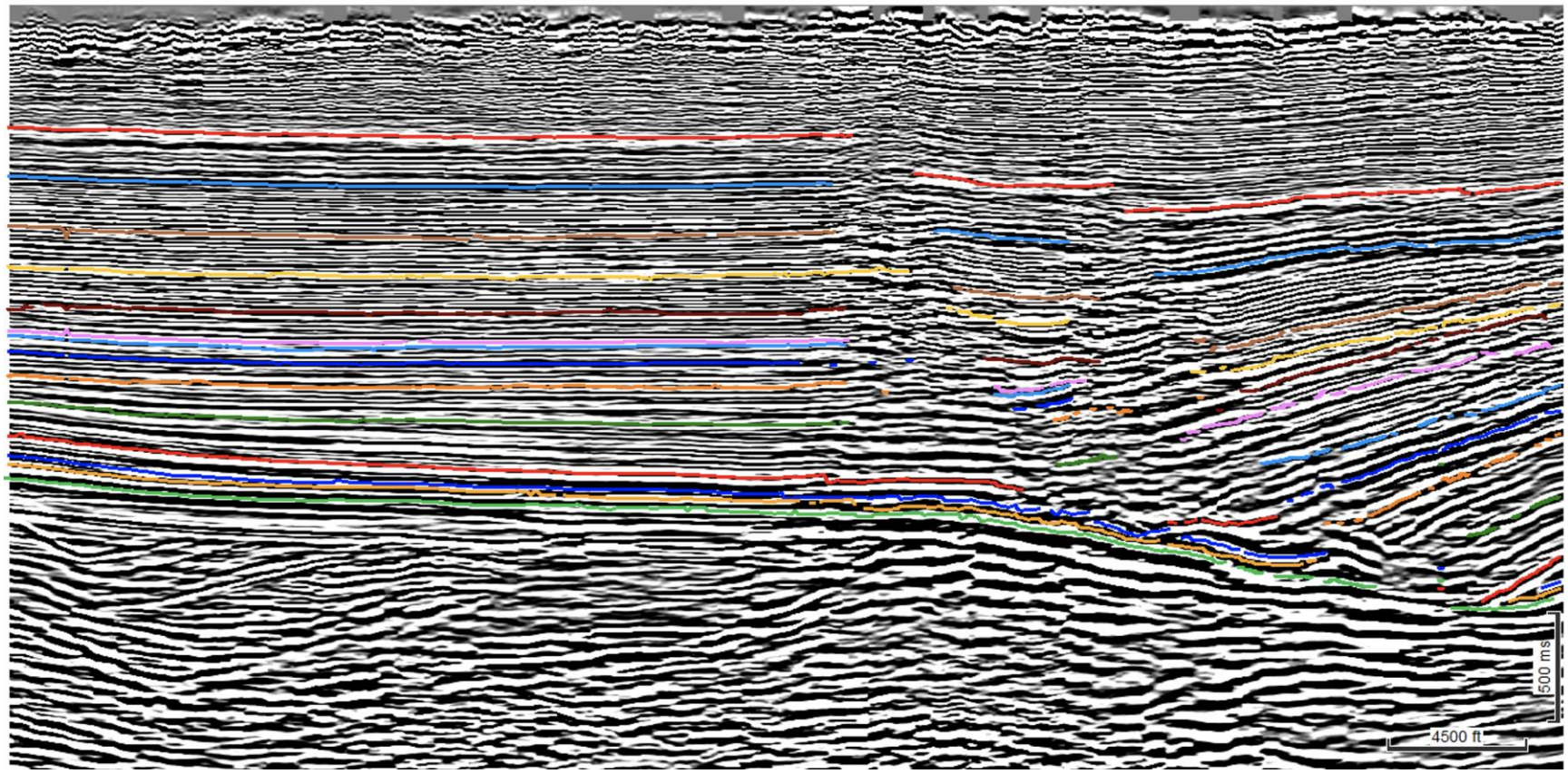

Figure A.14 *Arb line N*

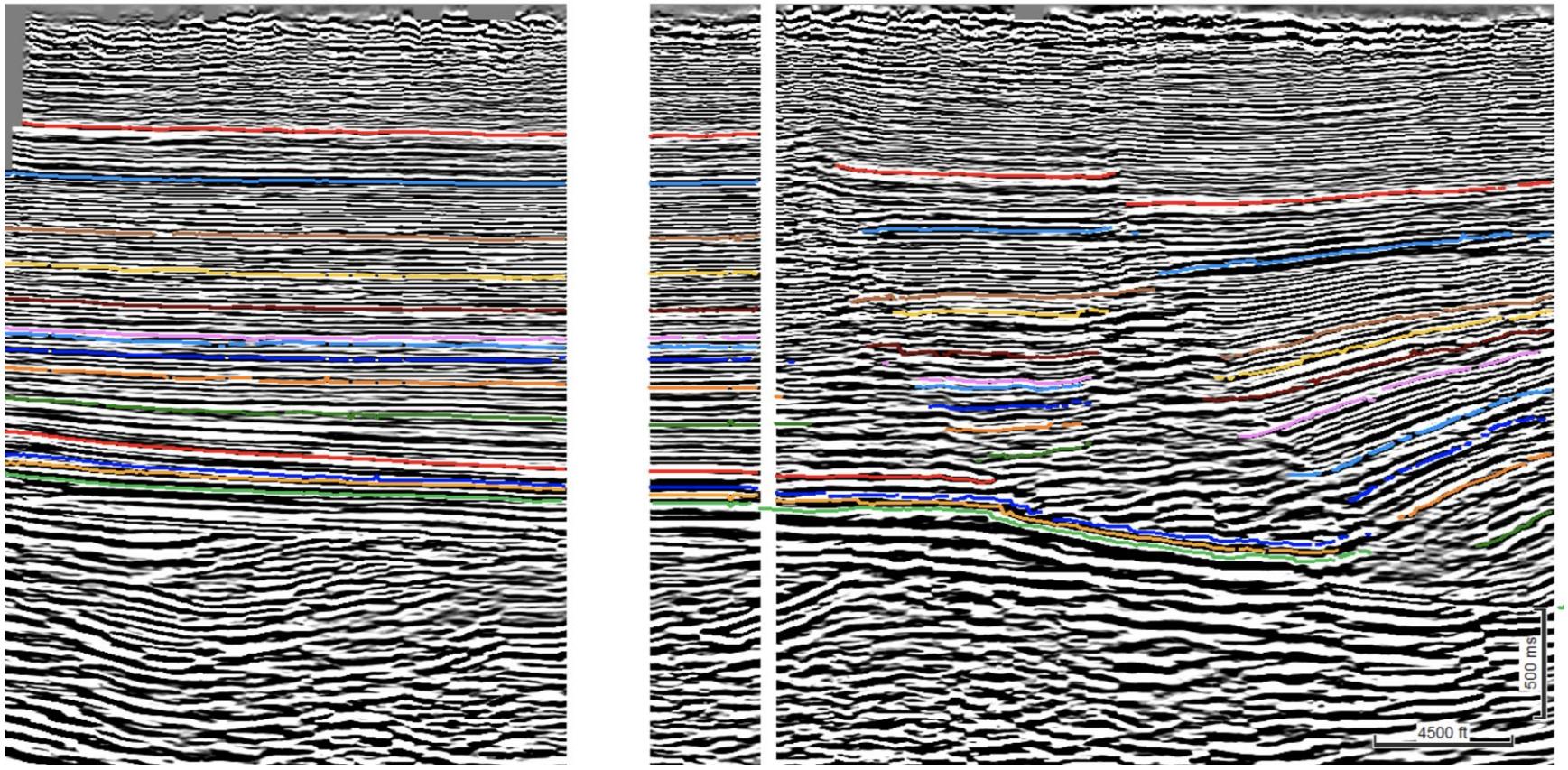

Figure A.15 *Arb line O*

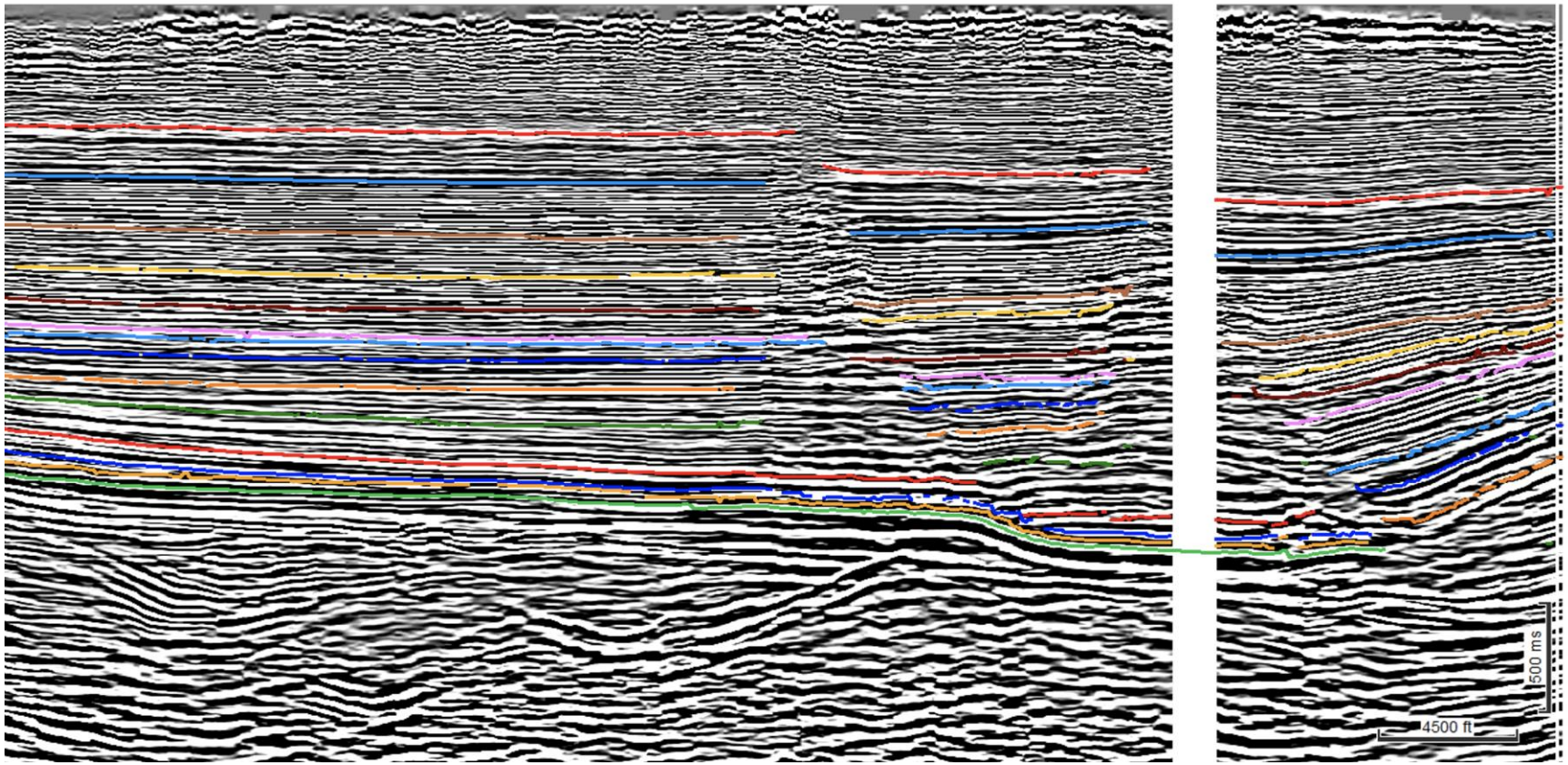

Figure A.16 *Arb line P*

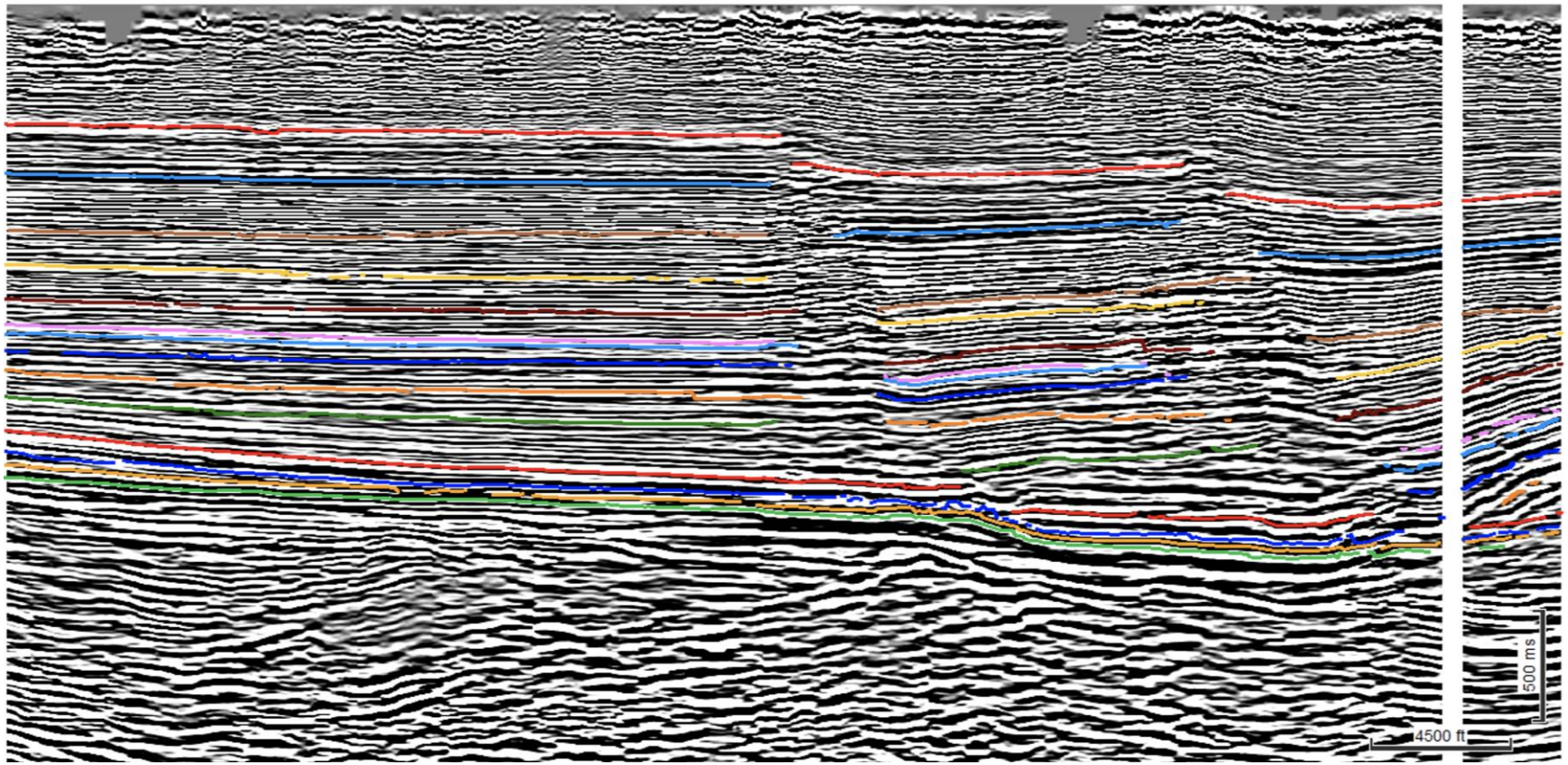

Figure A.17 *Arb line Q*

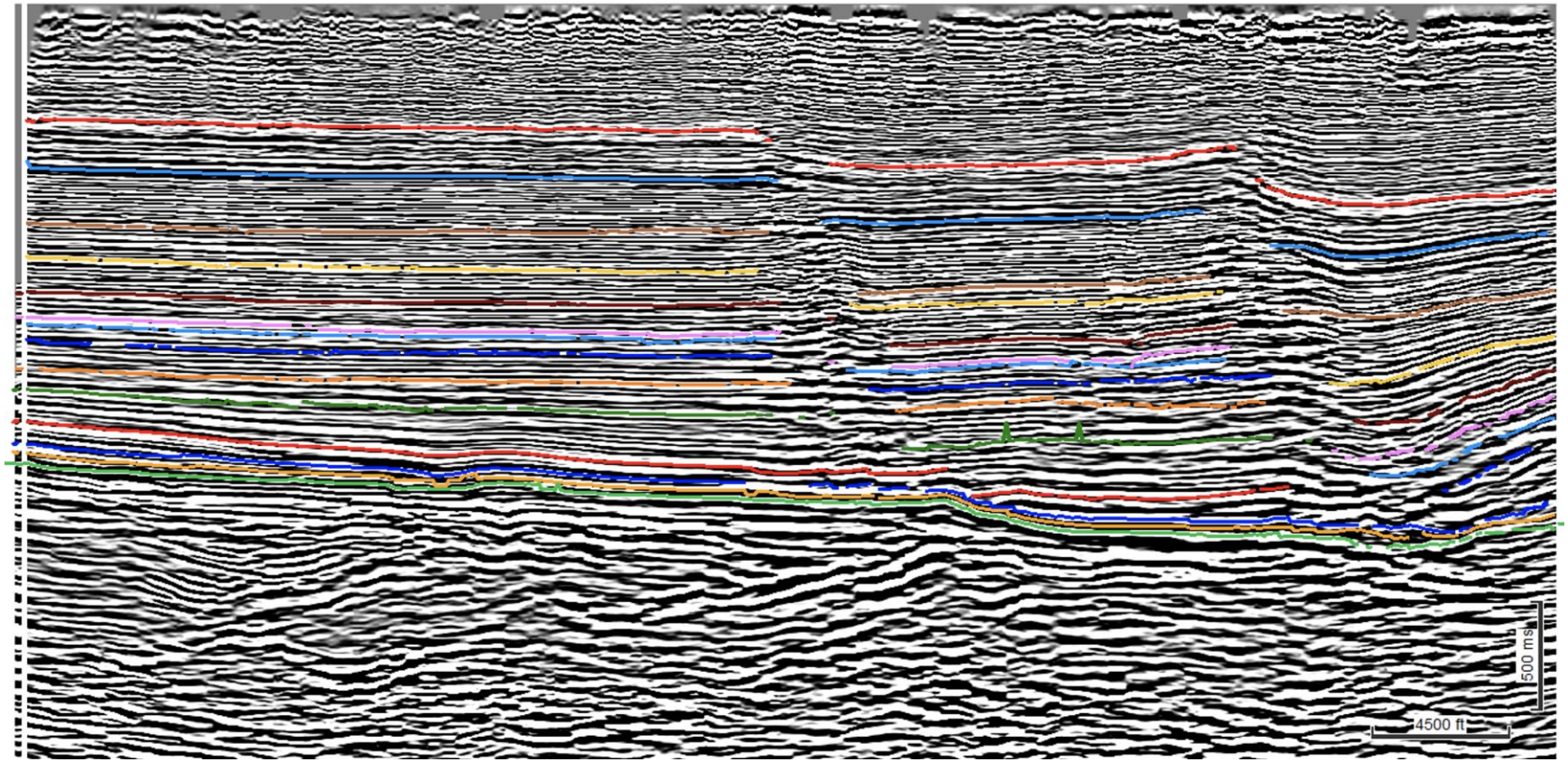

Figure A.18 *Arb line R*

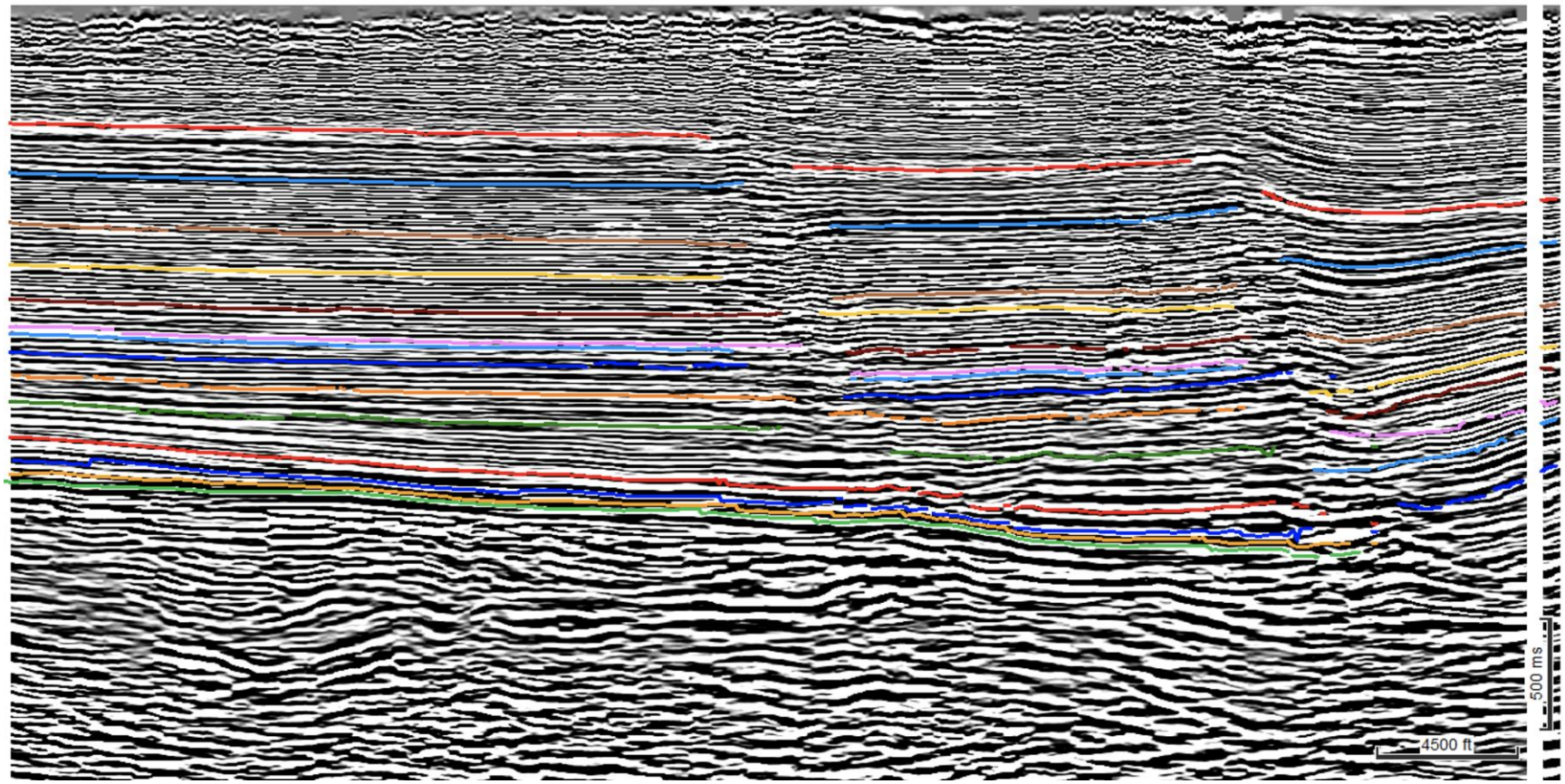

Figure A.19 *Arb line S*

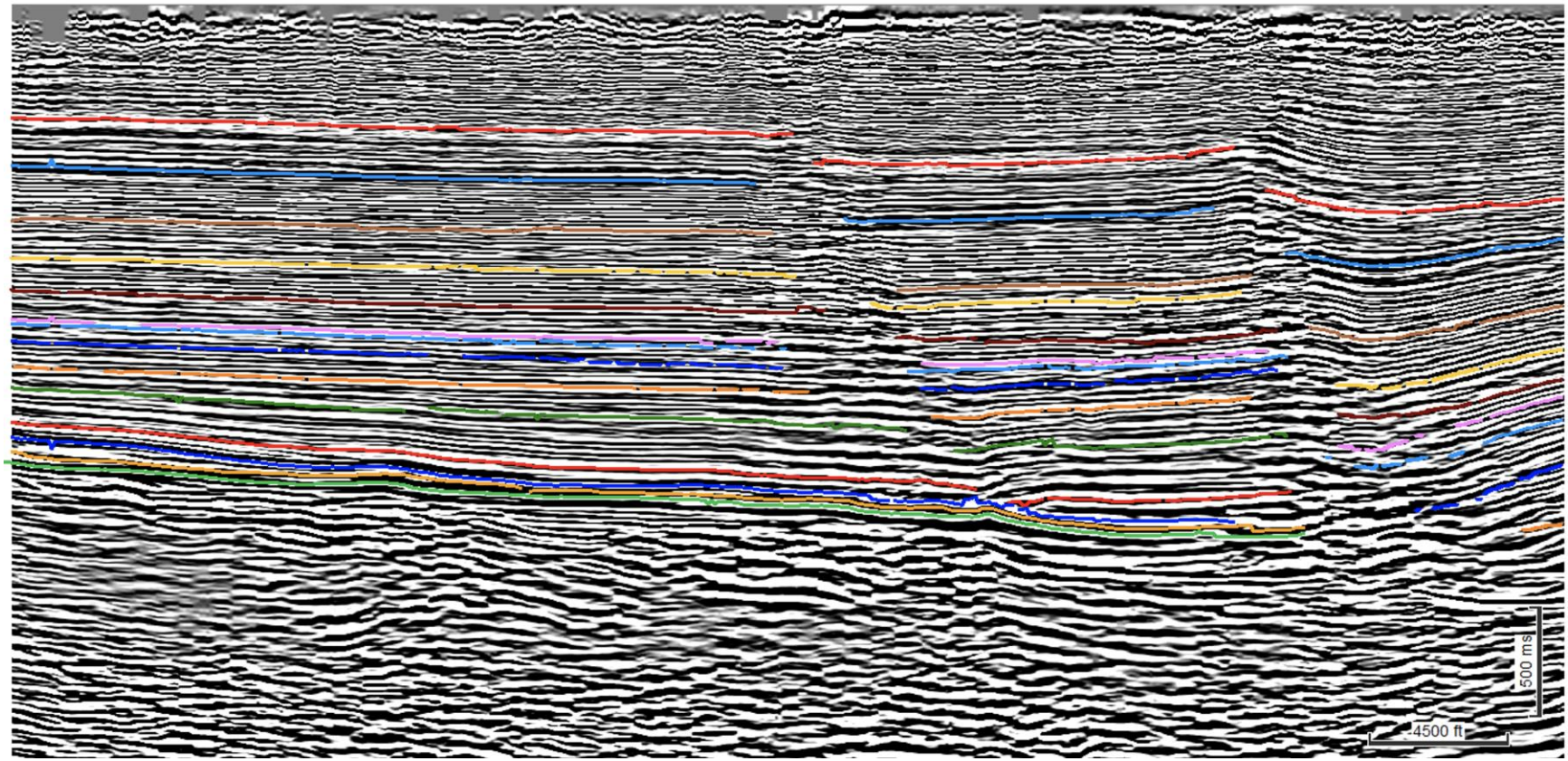

Figure A.20 *Arb line T*

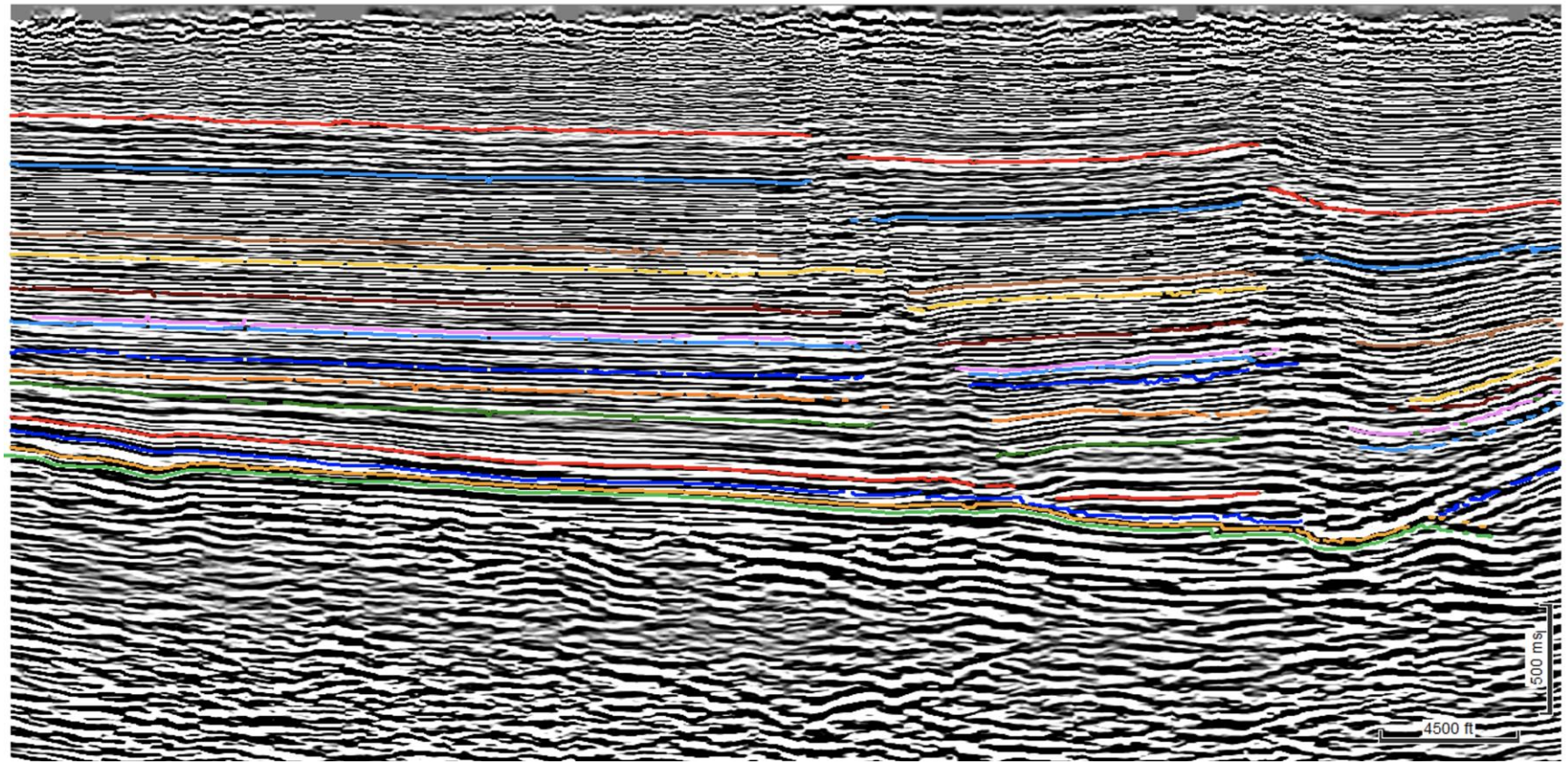

Figure A.21 *Arb line U*

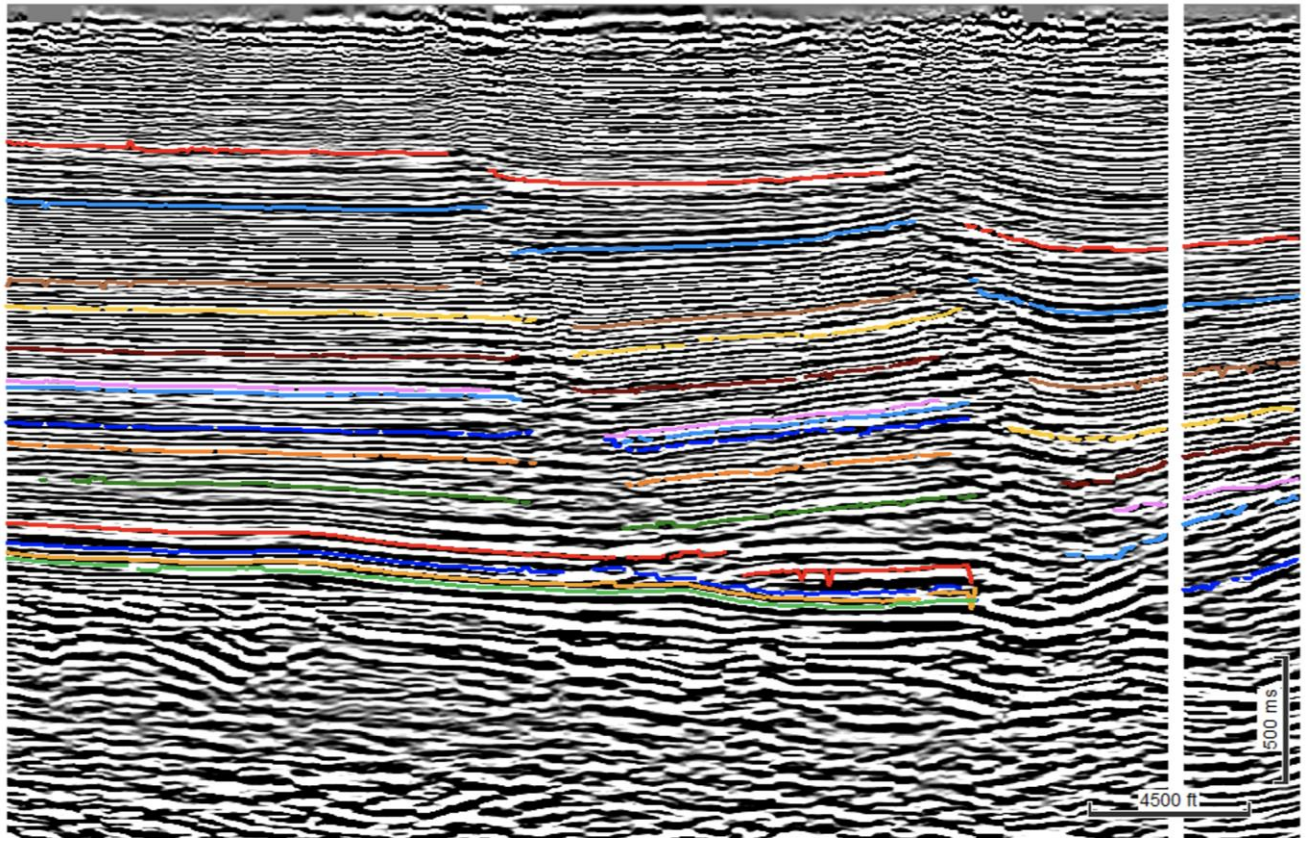

Figure A.22 *Arb line V*

APPENDIX B – Thickness Measurement Charts

Thickness charts for each formation, measured in seconds. Red outlined measurements represent thicknesses two or more standard deviations from the average thickness. Thicker measurements are darker green, thinner measurements are lighter green. Tan represents no measurement take.

	A	B	C	D	E	F	G	H	I	J	K	L	M	N	O	P	Q	R	S	T	U	V
1		0.069	0.073	0.069	0.063	0.076	0.078	0.076	0.08	0.069	0.073	0.069	0.061	0.061	0.057	0.057	0.05	0.048	0.05	0.04	0.034	
2	0.065	0.063	0.063	0.065	0.069	0.069	0.069	0.076	0.076	0.065	0.078	0.069	0.067	0.059	0.059	0.055	0.050	0.042	0.034	0.034	0.025	
3	0.063	0.063	0.069	0.065	0.069	0.071	0.073	0.069	0.071	0.065	0.069	0.065	0.061	0.065	0.052	0.057	0.036	0.042	0.036	0.048	0.032	
4	0.063	0.073	0.073	0.071	0.076	0.073	0.071	0.078	0.069	0.069	0.050	0.054	0.063	0.054	0.053	0.052	0.050	0.040	0.025	0.042	0.034	
5	0.073	0.069		0.080	0.084	0.078	0.071	0.076	0.080	0.057	0.048	0.057	0.044	0.061	0.059	0.050	0.038	0.032	0.023	0.046	0.036	0.025
6	0.079		0.052	0.088	0.080	0.078	0.082	0.071	0.080	0.057	0.052	0.048	0.042	0.052	0.059	0.050	0.040	0.036	0.031	0.029	0.023	0.029
7					0.048	0.046	0.074	0.057	0.074	0.059	0.052	0.048	0.046	0.044	0.040	0.040	0.036	0.029	0.027	0.031	0.023	0.040
8			0.017	0.080		0.036	0.061	0.048	0.082	0.052	0.046	0.048	0.046	0.050	0.040	0.042	0.027	0.038	0.025	0.027	0.027	0.029
9		0.071	0.061	0.080	0.082	0.065	0.076	0.090	0.080	0.055	0.048	0.048	0.055	0.052	0.048	0.032	0.036	0.029	0.031	0.029	0.031	0.027
10		0.044	0.073	0.069	0.071	0.073	0.071	0.076	0.067	0.055	0.065	0.055	0.034	0.036	0.034	0.036	0.029	0.023	0.029	0.034	0.040	0.027
11		0.044		0.076	0.086	0.043						0.032	0.042	0.027	0.025	0.027	0.023	0.031	0.027	0.036	0.027	0.029
12		0.057											0.010	0.029	0.034	0.032	0.036	0.031	0.034	0.029	0.027	0.029
13		0.044	0.019		0.038	0.038	0.025	0.040	0.025					0.025	0.034	0.038	0.025	0.034	0.034	0.033	0.027	0.033
14		0.052	0.046	0.053	0.055	0.046	0.046	0.040	0.038	0.023	0.021	0.036			0.031	0.034	0.023	0.042	0.042			
15		0.059	0.052	0.053	0.057	0.055	0.048	0.053	0.044	0.036	0.034	0.029						0.029				
16			0.065	0.059	0.057	0.052	0.046	0.042	0.046	0.042	0.040	0.034	0.013	0.017				0.040				

Figure B.1 *Smackover Formation thickness measurements (s)*

	A	B	C	D	E	F	G	H	I	J	K	L	M	N	O	P	Q	R	S	T	U	V
1		0.032	0.017	0.029	0.025	0.017	0.019	0.019	0.025	0.017	0.019	0.023	0.038	0.036	0.036	0.044	0.078	0.069	0.078	0.084	0.086	
2	0.021	0.023	0.023	0.025	0.019	0.015	0.019	0.025	0.023	0.023	0.019	0.015	0.025	0.027	0.027	0.036	0.063	0.059	0.069	0.063	0.061	
3	0.018	0.017	0.017	0.017	0.021	0.023	0.025	0.027	0.025	0.027	0.023	0.025	0.027	0.025	0.025	0.029	0.042	0.042	0.042	0.044	0.044	
4	0.019	0.019	0.021	0.019	0.017	0.019	0.027	0.017	0.019	0.027	0.04	0.034	0.025	0.023	0.021	0.023	0.025	0.038	0.04	0.038	0.034	
5	0.019	0.017		0.021	0.021	0.019	0.021	0.019	0.015	0.034	0.04	0.042	0.038	0.025	0.021	0.023	0.029	0.027	0.042	0.019	0.04	0.044
6	0.016		0.029	0.021	0.019	0.025	0.025	0.019	0.021	0.036	0.05	0.042	0.044	0.023	0.025	0.019	0.04	0.044	0.053	0.025	0.032	0.04
7			0.029		0.044	0.025	0.019	0.025	0.025	0.042	0.05	0.04	0.04	0.036	0.034	0.031	0.044	0.044	0.036	0.034	0.031	0.04
8			0.015	0.015	0.025	0.013	0.023	0.015	0.036	0.04	0.042	0.044	0.036	0.04	0.044	0.042	0.042	0.04	0.044	0.038	0.036	0.044
9		0.025	0.019	0.019	0.017	0.038	0.021	0.019	0.017	0.036	0.046	0.048	0.044	0.025	0.023	0.034	0.046	0.048	0.044	0.034	0.044	0.046
10		0.023	0.034	0.025	0.023	0.019	0.029	0.023	0.023	0.05	0.038	0.046	0.05	0.044	0.025	0.046	0.034	0.021	0.023	0.032	0.027	0.044
11		0.019		0.021	0.023	0.015								0.046	0.04	0.015	0.031	0.031	0.025	0.025	0.031	0.025
12		0.031												0.029	0.025	0.034	0.036	0.029	0.032	0.036	0.029	0.032
13		0.031	0.027		0.023	0.027	0.017	0.021	0.025					0.019	0.042	0.036	0.027	0.032	0.034	0.025	0.031	0.023
14		0.021	0.023	0.025	0.019	0.019	0.027	0.025	0.021	0.036	0.032		0.038		0.025	0.032	0.052	0.029				
15		0.017	0.017	0.023	0.017	0.021	0.023	0.017	0.021	0.034	0.032	0.025	0.029					0.025				
16			0.019	0.015	0.015	0.015	0.023	0.023	0.025	0.021	0.019	0.023	0.017	0.021				0.042				

Figure B.2 *Buckner Anhydrite thickness measurements (s)*

	A	B	C	D	E	F	G	H	I	J	K	L	M	N	O	P	Q	R	S	T	U	V
1		0.103	0.094	0.097	0.097	0.101	0.099	0.09	0.08	0.095	0.107	0.105	0.097	0.084	0.09	0.099	0.078	0.082	0.074	0.065	0.063	
2	0.115	0.109	0.099	0.101	0.097	0.097	0.109	0.092	0.088	0.099	0.107	0.103	0.103	0.095	0.094	0.097	0.078	0.086	0.08	0.071	0.076	
3	0.089	0.099	0.094	0.09	0.099	0.09	0.088	0.09	0.092	0.095	0.097	0.101	0.097	0.097	0.09	0.088	0.084	0.084	0.084	0.088	0.08	
4	0.093	0.088	0.092	0.088	0.095	0.084	0.084	0.084	0.09	0.084	0.082	0.095	0.09	0.088	0.088	0.09	0.082	0.084	0.08	0.071	0.073	
5	0.088	0.09		0.086	0.088	0.092	0.084	0.086	0.078	0.086	0.092	0.082	0.08	0.074	0.075	0.071	0.082	0.084	0.078	0.078	0.073	0.08
6	0.079		0.095	0.086	0.088	0.086	0.09	0.084	0.09	0.082	0.088	0.078	0.078	0.069	0.084	0.071	0.076	0.071	0.076	0.082	0.078	0.078
7		0.05	0.04		0.071	0.076	0.088	0.082	0.08	0.078	0.076	0.084	0.076	0.076	0.08	0.069	0.074	0.075	0.076	0.069	0.069	0.074
8		0.101	0.088	0.069	0.088	0.078	0.082	0.082	0.073	0.082	0.095	0.084	0.078	0.074	0.067	0.067	0.071	0.057	0.067	0.078	0.067	0.069
9		0.074	0.092	0.092	0.088	0.076	0.09	0.09	0.078	0.082	0.09	0.08	0.078	0.076	0.092	0.092	0.069	0.078	0.078	0.082	0.069	0.065
10		0.126	0.099	0.095	0.09	0.09	0.095	0.09	0.076	0.092	0.095	0.084	0.096	0.082	0.095	0.074	0.074	0.084	0.086	0.061	0.055	0.057
11		0.126	0.12	0.094	0.099	0.107			0.063								0.08	0.088	0.094	0.086	0.061	0.034
12		0.04														0.082	0.061	0.092	0.097	0.095	0.084	0.086
13		0.109	0.099	0.084	0.088	0.088	0.044	0.113	0.044				0.044			0.071	0.084	0.134	0.143	0.134	0.137	0.078
14		0.115	0.111	0.113	0.107	0.115	0.092	0.092	0.086	0.099	0.038		0.099				0.071					
15		0.111	0.103	0.105	0.116	0.115	0.103	0.107	0.116	0.103	0.088	0.048										
16			0.122	0.12	0.113	0.113	0.115	0.115	0.116	0.109	0.109	0.08	0.076	0.038								

Figure B.3 *Haynesville Formation thickness measurements (s)*

	A	B	C	D	E	F	G	H	I	J	K	L	M	N	O	P	Q	R	S	T	U	V
1		0.145	0.17	0.176	0.183	0.187	0.185	0.176	0.162	0.17	0.157	0.157	0.143	0.153	0.153	0.155	0.147	0.153	0.166	0.168	0.168	
2	0.154	0.162	0.172	0.178	0.176	0.183	0.179	0.178	0.187	0.178	0.172	0.162	0.164	0.162	0.164	0.179	0.17	0.155	0.162	0.17	0.174	
3	0.171	0.174	0.17	0.178	0.185	0.174	0.157	0.168	0.172	0.185	0.183	0.174	0.181	0.185	0.181	0.178	0.181	0.172	0.176	0.185	0.176	
4	0.18	0.176	0.197	0.195	0.193	0.187	0.183	0.179	0.189	0.197	0.166	0.176	0.191	0.199	0.199	0.189	0.199	0.195	0.197	0.191	0.183	
5	0.18	0.187		0.172	0.189	0.187	0.189	0.195	0.202	0.206	0.185	0.187	0.187	0.206	0.22	0.187	0.216	0.208	0.214	0.216	0.212	0.181
6	0.189		0.138	0.189	0.195	0.191	0.195	0.189	0.204	0.193	0.199	0.216	0.193	0.227	0.227	0.195	0.214	0.216	0.229	0.237	0.227	0.193
7		0.218	0.292			0.199		0.204	0.187	0.216	0.216	0.222	0.189	0.229	0.216	0.216	0.231	0.233	0.246	0.233	0.221	0.183
8		0.25	0.292	0.233	0.168	0.258	0.143	0.162	0.168	0.216	0.222	0.229	0.202	0.241	0.218	0.225	0.254	0.256	0.254	0.237	0.242	0.202
9		0.252	0.225	0.206	0.185	0.281	0.168	0.193	0.225	0.227	0.231	0.233	0.21	0.262	0.246					0.233	0.254	0.208
10					0.235	0.309	0.252	0.25	0.225	0.25	0.248	0.243	0.193					0.22	0.172			
11						0.246										0.233	0.212	0.25	0.25	0.241	0.227	0.21
12		0.275	0.319					0.208						0.279		0.246	0.275	0.26	0.254	0.256	0.254	0.248
13		0.384	0.351	0.34	0.338	0.357	0.342	0.327	0.214								0.338	0.241	0.252	0.262	0.241	0.275
14		0.332	0.342	0.342	0.33	0.336	0.359	0.353	0.355	0.359	0.25											
15		0.346	0.33	0.336	0.311	0.315	0.33	0.315	0.298	0.298	0.326	0.118										
16			0.325	0.323	0.325	0.321	0.323	0.328	0.304	0.323	0.344	0.237	0.164	0.122								

Figure B.4 *Cotton Valley Group thickness measurements (s)*

	A	B	C	D	E	F	G	H	I	J	K	L	M	N	O	P	Q	R	S	T	U	V
1		0.179	0.157	0.157	0.151	0.155	0.151	0.162	0.162	0.157	0.141	0.126	0.126	0.122	0.134	0.097	0.111	0.101	0.115	0.099	0.071	
2	0.175	0.178	0.172	0.164	0.145	0.155	0.162	0.149	0.162	0.139	0.145	0.139	0.132	0.149	0.153	0.107	0.113	0.115	0.124	0.111	0.092	
3	0.198	0.181	0.168	0.151	0.147	0.168	0.164	0.149	0.157	0.141	0.151	0.149	0.149	0.147	0.149	0.128	0.122	0.122	0.122	0.124	0.105	
4	0.178	0.185	0.17	0.155	0.147	0.183	0.183	0.172	0.172	0.134	0.132	0.155	0.16	0.164	0.147	0.139	0.12	0.124	0.128	0.132	0.113	
5	0.199	0.191		0.162	0.164	0.195	0.193	0.174	0.187	0.158	0.168	0.164	0.174	0.151	0.151	0.157	0.137	0.128	0.126	0.128	0.103	0.134
6	0.192				0.187	0.189	0.2	0.17	0.195	0.17	0.181	0.162	0.191	0.166	0.168	0.164	0.141	0.132	0.132	0.136	0.099	0.134
7		0.132	0.09	0.208				0.214	0.185	0.17	0.183	0.17	0.197	0.168	0.174	0.17	0.145	0.143	0.139	0.134	0.113	0.128
8		0.088	0.092	0.21	0.304	0.208	0.273	0.235	0.166	0.174	0.174	0.183	0.216	0.174	0.176	0.178	0.141	0.151	0.141	0.149	0.111	0.149
9		0.095		0.214	0.269	0.193	0.275	0.243	0.172	0.162	0.193	0.191	0.223	0.181								0.147
10					0.269	0.229	0.294			0.189	0.183					0.16	0.204	0.193	0.151	0.143		0.162
11		0.143	0.122						0.069				0.071	0.195	0.12	0.155	0.187	0.178	0.176	0.174	0.155	0.174
12		0.126	0.118	0.13	0.05	0.086	0.101	0.12	0.057	0.125							0.176	0.172	0.183	0.185	0.139	0.17
13		0.111	0.078	0.137	0.071	0.111	0.084	0.086	0.067	0.082	0.08						0.147	0.155	0.189	0.172	0.122	0.166
14		0.109	0.099	0.09	0.082	0.094	0.063	0.088	0.076	0.09	0.078											
15		0.105	0.082	0.084	0.086	0.08	0.082	0.073	0.084	0.08	0.08	0.116	0.174									
16			0.08	0.082	0.074	0.071	0.088	0.082	0.094	0.076	0.084	0.107	0.168	0.149	0.153							

Figure B.5 *Hosston and Sligo Formations thickness measurements (s)*

	A	B	C	D	E	F	G	H	I	J	K	L	M	N	O	P	Q	R	S	T	U	V
1		0.086	0.118	0.105	0.109	0.111	0.101	0.088	0.086	0.063	0.103	0.109	0.111	0.107	0.088	0.126	0.103	0.122	0.111	0.116	0.103	
2	0.107	0.099	0.111	0.109	0.118	0.107	0.096	0.099	0.094	0.088	0.111	0.107	0.111	0.103	0.09	0.134	0.109	0.128	0.109	0.113	0.09	
3	0.101	0.101	0.116	0.124	0.126	0.094	0.094	0.065	0.09	0.086	0.111	0.109	0.109	0.101	0.094	0.124	0.13	0.13	0.128	0.122	0.082	
4	0.126	0.126	0.116	0.118	0.122	0.097	0.094	0.067	0.092	0.088	0.107	0.107	0.107	0.109	0.105	0.124	0.12	0.124	0.126	0.13	0.086	
5	0.114	0.12		0.136	0.132	0.105	0.096	0.092	0.092	0.105	0.105	0.105	0.109	0.116	0.107	0.124	0.132	0.13	0.132	0.13	0.09	0.086
6	0.145		0.157		0.113	0.111	0.103	0.095	0.088	0.107	0.111	0.111	0.107	0.111	0.107	0.134	0.136	0.132	0.13	0.122	0.09	0.09
7		0.076	0.13	0.084	0.099	0.078	0.105	0.134	0.071	0.107	0.111	0.103	0.109	0.113	0.128	0.128	0.13	0.134	0.124	0.12	0.095	0.092
8		0.09	0.099	0.084	0.08	0.078	0.101	0.111	0.126	0.12	0.115	0.113	0.099	0.116	0.132	0.139	0.141	0.128	0.149	0.107	0.101	0.097
9		0.107	0.094	0.076	0.071	0.088	0.084	0.12	0.122	0.115	0.113	0.105	0.097	0.103					0.078			0.105
10															0.109	0.111	0.12	0.09	0.124	0.128	0.164	0.13
11		0.136	0.103					0.042	0.134				0.078	0.08	0.105	0.097	0.126	0.088	0.113	0.116	0.13	0.126
12		0.128	0.147	0.149	0.22	0.103	0.088	0.074	0.095	0.088							0.132	0.111	0.105	0.109	0.155	0.126
13		0.155	0.13	0.122	0.199	0.143	0.147	0.147	0.141	0.109	0.088							0.109	0.126	0.111	0.21	0.13
14		0.147	0.111	0.126	0.12	0.118	0.113	0.113	0.111	0.124	0.109	0.13	0.099	0.109								
15		0.153	0.105	0.103	0.103	0.111	0.101	0.101	0.101	0.126	0.092	0.115	0.103	0.097	0.105	0.101				0.139		
16			0.099	0.113	0.116	0.115	0.101	0.099	0.118	0.118	0.12	0.086	0.076	0.082	0.107	0.086	0.088					

Figure B.6 *Rodessa Formation thickness measurements (s)*

	A	B	C	D	E	F	G	H	I	J	K	L	M	N	O	P	Q	R	S	T	U	V
1		0.065	0.048	0.067	0.071	0.05	0.069	0.078	0.071	0.088	0.073	0.063	0.063	0.074	0.078	0.078	0.08	0.086	0.086	0.08	0.126	
2	0.068	0.061	0.059	0.059	0.063	0.052	0.071	0.074	0.067	0.097	0.065	0.086	0.067	0.073	0.069	0.082	0.088	0.078	0.082	0.084	0.145	
3	0.058	0.063	0.061	0.067	0.063	0.071	0.071	0.08	0.071	0.095	0.071	0.069	0.071	0.071	0.069	0.08	0.082	0.084	0.088	0.08	0.141	
4	0.046	0.048	0.059	0.067	0.067	0.069	0.067	0.082	0.059	0.088	0.071	0.063	0.076	0.08	0.078	0.084	0.086	0.082	0.078	0.08	0.141	
5	0.056	0.059		0.057	0.061	0.065	0.078	0.086	0.071	0.071	0.082	0.08	0.08	0.073	0.073	0.073	0.078	0.082	0.076	0.078	0.145	0.147
6	0.065		0.067		0.067	0.069	0.063	0.09	0.074	0.084	0.078	0.065	0.076	0.082	0.063	0.078	0.067	0.078	0.082	0.08	0.145	0.145
7		0.061	0.067	0.053	0.048	0.053	0.046	0.08	0.08	0.082	0.073	0.08	0.082	0.084	0.063	0.082	0.078	0.074	0.084	0.088	0.149	0.139
8		0.065	0.09	0.046	0.05	0.046	0.042	0.059	0.08	0.071	0.076	0.059	0.082	0.08	0.065	0.073	0.082	0.076	0.067	0.09	0.147	0.149
9		0.04	0.086	0.061	0.057	0.038	0.046	0.057	0.067	0.067	0.08	0.063	0.084	0.092					0.073			0.147
10															0.082	0.09	0.067	0.088	0.086	0.09	0.04	0.034
11		0.137	0.092		0.061		0.038	0.042	0.08	0.04			0.063	0.063	0.082	0.09	0.073	0.082	0.082	0.076	0.061	0.048
12		0.132	0.105	0.111	0.059	0.065	0.073	0.065	0.057	0.038	0.034	0.088					0.065	0.08	0.065	0.065	0.069	0.05
13		0.122	0.099	0.12	0.067	0.084	0.073	0.071	0.067	0.08	0.067	0.092						0.084	0.048	0.06	0.048	0.059
14		0.086	0.092	0.109	0.099	0.09	0.076	0.059	0.069	0.078	0.065	0.136	0.092	0.099	0.12	0.086						
15		0.069	0.095	0.107	0.109	0.134	0.063	0.08	0.082	0.082	0.134	0.149	0.094	0.088	0.088	0.08	0.107	0.092	0.202	0.187	0.275	0.187
16			0.092	0.107	0.109	0.139	0.076	0.061	0.086	0.092	0.107	0.191	0.076	0.059	0.111	0.057	0.094	0.074	0.179			

Figure B.7 *Ferry Lake Anhydrite thickness measurements (s)*

	A	B	C	D	E	F	G	H	I	J	K	L	M	N	O	P	Q	R	S	T	U	V
1		0.053	0.053	0.044	0.055	0.052	0.036	0.036	0.046	0.04	0.044	0.04	0.029	0.025	0.025	0.036	0.034	0.034	0.036	0.019	0.025	
2	0.047	0.052	0.048	0.053	0.063	0.059	0.038	0.036	0.048	0.042	0.042	0.038	0.029	0.029	0.027	0.036	0.038	0.038	0.027	0.019	0.027	
3	0.049	0.059	0.05	0.055	0.046	0.042	0.05	0.05	0.048	0.055	0.048	0.038	0.029	0.025	0.025	0.036	0.038	0.04	0.025	0.025	0.027	
4	0.047	0.05	0.05	0.057	0.044	0.05	0.055	0.055	0.05	0.042	0.055	0.04	0.029	0.027	0.023	0.034	0.029	0.025	0.025	0.023	0.021	
5	0.054	0.055		0.061	0.053	0.05	0.046	0.044	0.053	0.038	0.042	0.027	0.023	0.031	0.04	0.032	0.023	0.025	0.025	0.019	0.023	0.029
6	0.044		0.076		0.061	0.055	0.046	0.055	0.036	0.044	0.044	0.031	0.025	0.025	0.038	0.021	0.025	0.023	0.015	0.021	0.023	0.021
7		0.088	0.097	0.057	0.055	0.071	0.076	0.044	0.046	0.036	0.034	0.021	0.027	0.023	0.036	0.032	0.027	0.025	0.023	0.036	0.025	0.025
8		0.063	0.078	0.071	0.055	0.069	0.065	0.029	0.029	0.055	0.029	0.034	0.021	0.023	0.044	0.025	0.031	0.032	0.031	0.034	0.025	0.025
9		0.048	0.076	0.055	0.025	0.038	0.048	0.025	0.029	0.046	0.042	0.036	0.029	0.025					0.032			0.029
10															0.027	0.044	0.029	0.021	0.021	0.023	0.023	0.027
11		0.038	0.126	0.097	0.099	0.101	0.042	0.038	0.023	0.031	0.113		0.034	0.021	0.029	0.036	0.021	0.029	0.023	0.036	0.021	0.029
12		0.04	0.107	0.09	0.097	0.08	0.029	0.042	0.032	0.031	0.067	0.048					0.019	0.042	0.023	0.034	0.023	0.021
13		0.046	0.105	0.116	0.101	0.042	0.061	0.05	0.076	0.033	0.061	0.084	0.053	0.145				0.055	0.031	0.029	0.029	0.029
14		0.067	0.128	0.086	0.074	0.069	0.073	0.054	0.084	0.05	0.057	0.084	0.048	0.17	0.178	0.197			0.159	0.075	0.069	
15		0.073	0.122	0.103	0.078	0.061	0.094	0.057	0.055	0.036	0.069	0.059	0.061	0.174	0.189	0.193	0.042	0.061	0.099	0.103	0.055	0.078
16			0.118	0.094	0.086	0.052	0.107	0.074	0.052	0.025	0.082	0.059	0.061	0.153	0.157	0.174	0.038	0.055	0.073			

Figure B.8 *Mooringsport Formation thickness measurements (s)*

	A	B	C	D	E	F	G	H	I	J	K	L	M	N	O	P	Q	R	S	T	U	V
1		0.088	0.086	0.084	0.078	0.092	0.097	0.08	0.099	0.111	0.115	0.118	0.132	0.126	0.136	0.111	0.113	0.12	0.118	0.143	0.132	
2	0.087	0.09	0.09	0.082	0.084	0.086	0.084	0.08	0.08	0.107	0.111	0.12	0.137	0.147	0.134	0.111	0.118	0.122	0.137	0.137	0.13	
3	0.089	0.09	0.088	0.088	0.09	0.088	0.082	0.086	0.092	0.105	0.109	0.128	0.137	0.143	0.145	0.113	0.115	0.118	0.132	0.162	0.134	
4	0.093	0.092	0.084	0.088	0.09	0.088	0.088	0.088	0.086	0.109	0.109	0.124	0.132	0.134	0.136	0.118	0.128	0.128	0.141	0.17	0.132	
5	0.119	0.082		0.084	0.084	0.088	0.09	0.08	0.094	0.113	0.118	0.128	0.13	0.137	0.128	0.136	0.13	0.141	0.139	0.176	0.134	0.13
6	0.117		0.13		0.082	0.09	0.086	0.076	0.115	0.109	0.118	0.124	0.128	0.134	0.132	0.134	0.128	0.132	0.139	0.17	0.128	0.134
7		0.143	0.143	0.126	0.076	0.067	0.065	0.099	0.116	0.126	0.126	0.126	0.13	0.13	0.132	0.132	0.128	0.143	0.141	0.168	0.124	0.134
8		0.13	0.147	0.097	0.078	0.069	0.046	0.095	0.118	0.151	0.141	0.128	0.128	0.126	0.126	0.143	0.126	0.141	0.141	0.176	0.137	0.134
9		0.139	0.164	0.107	0.107	0.071	0.042	0.076	0.137	0.136	0.143	0.132	0.12	0.141					0.097			0.132
10															0.126	0.082	0.071	0.099	0.101	0.183	0.124	0.164
11		0.141	0.082	0.12	0.107	0.097	0.076	0.071	0.074	0.12	0.147		0.145	0.107	0.115	0.107	0.08	0.09	0.092	0.092	0.139	0.149
12		0.164	0.099	0.09	0.088	0.086	0.05	0.092	0.084	0.109	0.105	0.113					0.101	0.092	0.092	0.084	0.12	0.164
13		0.153	0.103	0.086	0.078	0.107	0.103	0.116	0.097	0.097	0.113	0.097	0.073	0.069	0.16			0.101	0.107	0.086	0.126	
14		0.143	0.128	0.088	0.103	0.128	0.149	0.139	0.137	0.109	0.118	0.044	0.084	0.073	0.103	0.071	0.128		0.092	0.149		0.126
15		0.143	0.111	0.088	0.109	0.103	0.122	0.164	0.153	0.145	0.103	0.061	0.055	0.09	0.088	0.069	0.158	0.088	0.139	0.078	0.059	0.141
16			0.101	0.101	0.099	0.105	0.118	0.166	0.172	0.168	0.113	0.048	0.107	0.109	0.084	0.048	0.153	0.103	0.141			

Figure B.9 *Paluxy Formation thickness measurements (s)*

	A	B	C	D	E	F	G	H	I	J	K	L	M	N	O	P	Q	R	S	T	U	V
1		0.212	0.195	0.212	0.195	0.206	0.202	0.185	0.197	0.185	0.176	0.187	0.176	0.168	0.162	0.153	0.16	0.155	0.159	0.151	0.157	
2	0.205	0.214	0.193	0.21	0.197	0.21	0.21	0.183	0.189	0.183	0.178	0.174	0.17	0.164	0.166	0.158	0.166	0.153	0.162	0.162	0.164	
3	0.212	0.206	0.195	0.195	0.201	0.206	0.208	0.176	0.206	0.193	0.178	0.183	0.174	0.17	0.157	0.16	0.168	0.168	0.17	0.162	0.16	
4	0.199	0.204	0.197	0.202	0.21	0.21	0.208	0.179	0.206	0.178	0.183	0.181	0.172	0.174	0.155	0.151	0.155	0.157	0.166	0.174	0.166	
5	0.186	0.208		0.21	0.21	0.195	0.195	0.189	0.189	0.193	0.181	0.174	0.179	0.174	0.159	0.153	0.145	0.155	0.172	0.172	0.17	0.171
6	0.163		0.128			0.187	0.208	0.199	0.187	0.181	0.185	0.178	0.181	0.166	0.155	0.147	0.162	0.149	0.172	0.172	0.172	0.174
7		0.151	0.122	0.233	0.267	0.284	0.174	0.195	0.164	0.168	0.172	0.178	0.179	0.162	0.172	0.162	0.162	0.16	0.174	0.172	0.168	0.174
8		0.204	0.143	0.235	0.241	0.237	0.155	0.183	0.155	0.168	0.164	0.17	0.185	0.185	0.176	0.155	0.151	0.16	0.176	0.176	0.17	0.168
9		0.21	0.139	0.225	0.214	0.22	0.136	0.187	0.172	0.174	0.174	0.172	0.174	0.168					0.08			0.158
10								0.178							0.185	0.067	0.158	0.176	0.074	0.16	0.189	0.155
11		0.164	0.162	0.17	0.143	0.189	0.084	0.162	0.204	0.164	0.13	0.105	0.162	0.178	0.195	0.082	0.153	0.174	0.174	0.181	0.183	0.168
12		0.138	0.132	0.157	0.113	0.166	0.061	0.105	0.174	0.132	0.092	0.099					0.147	0.162	0.164	0.191	0.162	0.149
13		0.139	0.124	0.132	0.145	0.162	0.065	0.086	0.13	0.118	0.092	0.078	0.143	0.094	0.099	0.17		0.141	0.143	0.185	0.143	
14		0.138	0.168	0.21		0.147	0.109	0.141	0.168	0.176	0.113	0.118	0.138	0.069	0.084	0.113	0.151		0.115	0.143		0.172
15		0.166	0.204	0.227	0.212	0.212	0.082	0.191	0.187	0.172	0.134	0.122	0.116	0.044	0.071	0.097	0.136	0.141	0.084	0.134	0.063	0.118
16			0.225	0.214	0.216	0.216	0.099	0.191	0.187	0.17	0.149	0.134	0.071	0.034	0.063	0.086	0.124	0.143	0.09			

Figure B.10 *Washita and Fredericksburg Formations thickness measurements (s)*

	A	B	C	D	E	F	G	H	I	J	K	L	M	N	O	P	Q	R	S	T	U	V
1		0.078	0.103	0.111	0.046	0.086	0.139	0.158	0.145	0.139	0.149	0.149	0.17	0.189	0.162	0.189	0.157	0.155	0.183	0.183	0.111	
2	0.103	0.078	0.107	0.111	0.057	0.078	0.136	0.151	0.153	0.118	0.143	0.155	0.168	0.189	0.17	0.183	0.164	0.164	0.181	0.178	0.103	
3	0.098	0.084	0.107	0.115	0.057	0.086	0.143	0.158	0.147	0.126	0.143	0.158	0.168	0.191	0.172	0.185	0.166	0.164	0.185	0.185	0.101	
4	0.115	0.086	0.099	0.12	0.061	0.092	0.136	0.153	0.141	0.143	0.143	0.176	0.155	0.176	0.178	0.2	0.174	0.166	0.18	0.176	0.105	
5	0.103	0.08		0.122	0.057	0.09	0.143	0.155	0.143	0.143	0.153	0.164	0.164	0.181	0.17	0.193	0.204	0.176	0.174	0.176	0.103	0.107
6	0.087		0.082	0.097	0.128	0.099	0.136	0.139	0.153	0.151	0.143	0.164	0.151	0.183	0.181	0.179	0.204	0.174	0.159	0.183	0.099	0.116
7		0.118	0.084	0.084	0.122	0.096	0.17	0.155	0.139	0.147	0.155	0.17	0.153	0.193	0.166	0.164	0.206	0.181	0.162	0.185	0.086	0.111
8		0.118	0.084	0.074	0.107	0.107	0.153	0.141	0.13	0.164	0.166	0.164	0.164	0.185	0.168	0.185	0.2	0.181	0.153	0.187	0.097	0.109
9		0.132	0.097	0.088	0.109	0.101	0.143	0.109	0.145	0.155	0.151	0.151	0.162	0.191		0.076			0.084	0.086		0.126
10						0.132		0.095	0.105						0.071	0.074	0.076	0.076	0.082	0.076	0.074	0.101
11		0.048	0.088	0.065	0.099	0.134	0.067	0.078	0.09	0.111	0.137	0.286	0.168	0.128	0.084	0.073	0.063	0.08	0.076	0.076	0.078	0.086
12		0.057	0.059	0.075	0.09	0.128	0.046	0.061	0.099	0.088	0.111	0.256				0.076	0.073	0.084	0.082	0.069	0.076	0.103
13		0.059	0.061	0.101	0.063	0.095	0.059	0.059	0.113	0.08	0.143	0.241	0.181	0.101	0.097	0.16		0.078	0.097	0.076		
14		0.063	0.076	0.086	0.059		0.097		0.101	0.137	0.071	0.126	0.126	0.082	0.076	0.122	0.162		0.227	0.223		0.206
15		0.094	0.067	0.076	0.111	0.118	0.092	0.193	0.13	0.122	0.069	0.09	0.076	0.076	0.09	0.103	0.124	0.214	0.176	0.2	0.208	0.189
16			0.061	0.078	0.115	0.118	0.099	0.187	0.12	0.134	0.086	0.069	0.069	0.084	0.063	0.09	0.103	0.193	0.181			

Figure B.11 *Tuscaloosa Group thickness measurements (s)*

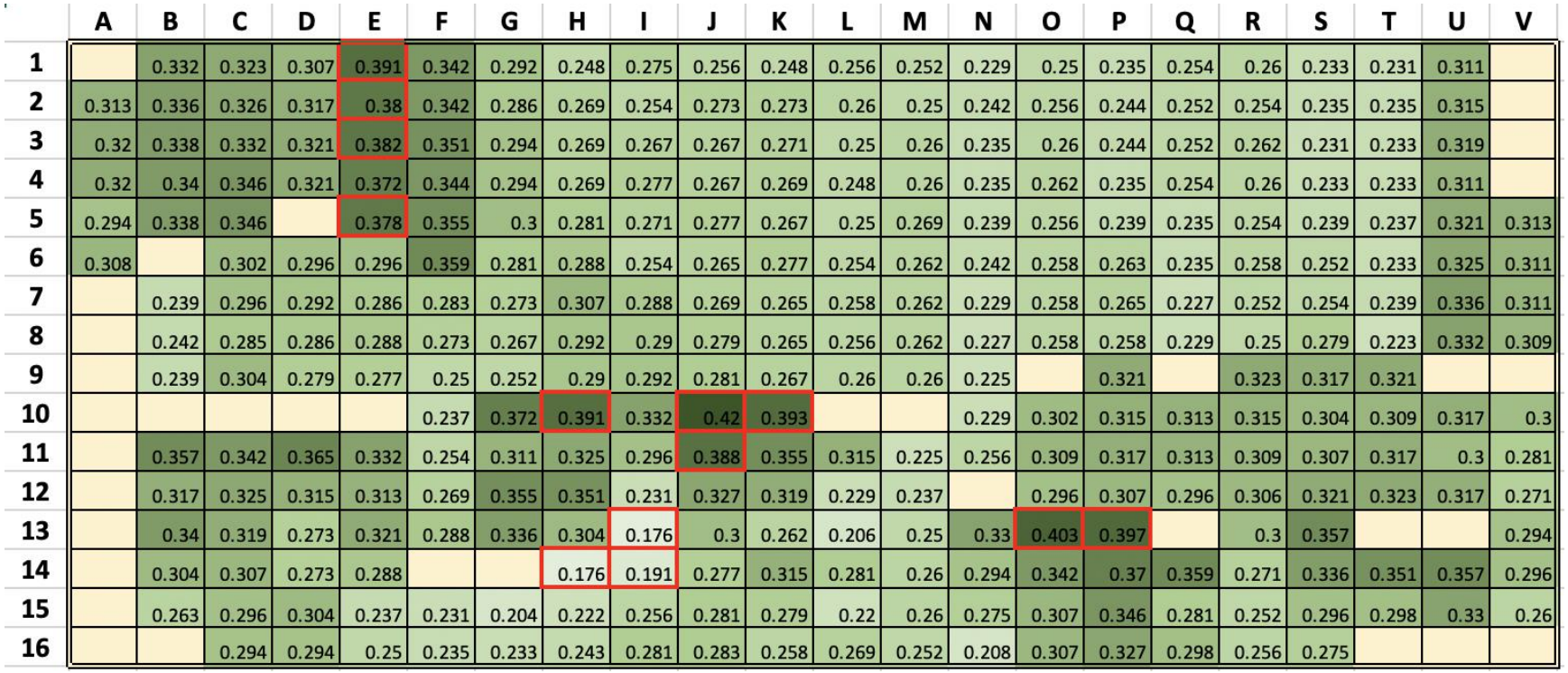

	A	B	C	D	E	F	G	H	I	J	K	L	M	N	O	P	Q	R	S	T	U	V
1		0.332	0.323	0.307	0.391	0.342	0.292	0.248	0.275	0.256	0.248	0.256	0.252	0.229	0.25	0.235	0.254	0.26	0.233	0.231	0.311	
2	0.313	0.336	0.326	0.317	0.38	0.342	0.286	0.269	0.254	0.273	0.273	0.26	0.25	0.242	0.256	0.244	0.252	0.254	0.235	0.235	0.315	
3	0.32	0.338	0.332	0.321	0.382	0.351	0.294	0.269	0.267	0.267	0.271	0.25	0.26	0.235	0.26	0.244	0.252	0.262	0.231	0.233	0.319	
4	0.32	0.34	0.346	0.321	0.372	0.344	0.294	0.269	0.277	0.267	0.269	0.248	0.26	0.235	0.262	0.235	0.254	0.26	0.233	0.233	0.311	
5	0.294	0.338	0.346		0.378	0.355	0.3	0.281	0.271	0.277	0.267	0.25	0.269	0.239	0.256	0.239	0.235	0.254	0.239	0.237	0.321	0.313
6	0.308		0.302	0.296	0.296	0.359	0.281	0.288	0.254	0.265	0.277	0.254	0.262	0.242	0.258	0.263	0.235	0.258	0.252	0.233	0.325	0.311
7		0.239	0.296	0.292	0.286	0.283	0.273	0.307	0.288	0.269	0.265	0.258	0.262	0.229	0.258	0.265	0.227	0.252	0.254	0.239	0.336	0.311
8		0.242	0.285	0.286	0.288	0.273	0.267	0.292	0.29	0.279	0.265	0.256	0.262	0.227	0.258	0.258	0.229	0.25	0.279	0.223	0.332	0.309
9		0.239	0.304	0.279	0.277	0.25	0.252	0.29	0.292	0.281	0.267	0.26	0.26	0.225		0.321		0.323	0.317	0.321		
10						0.237	0.372	0.391	0.332	0.42	0.393			0.229	0.302	0.315	0.313	0.315	0.304	0.309	0.317	0.3
11		0.357	0.342	0.365	0.332	0.254	0.311	0.325	0.296	0.388	0.355	0.315	0.225	0.256	0.309	0.317	0.313	0.309	0.307	0.317	0.3	0.281
12		0.317	0.325	0.315	0.313	0.269	0.355	0.351	0.231	0.327	0.319	0.229	0.237		0.296	0.307	0.296	0.306	0.321	0.323	0.317	0.271
13		0.34	0.319	0.273	0.321	0.288	0.336	0.304	0.176	0.3	0.262	0.206	0.25	0.33	0.403	0.397		0.3	0.357			0.294
14		0.304	0.307	0.273	0.288			0.176	0.191	0.277	0.315	0.281	0.26	0.294	0.342	0.37	0.359	0.271	0.336	0.351	0.357	0.296
15		0.263	0.296	0.304	0.237	0.231	0.204	0.222	0.256	0.281	0.279	0.22	0.26	0.275	0.307	0.346	0.281	0.252	0.296	0.298	0.33	0.26
16			0.294	0.294	0.25	0.235	0.233	0.243	0.281	0.283	0.258	0.269	0.252	0.208	0.307	0.327	0.298	0.256	0.275			

Figure B.12 *Eutaw Formation thickness measurements (s)*

	A	B	C	D	E	F	G	H	I	J	K	L	M	N	O	P	Q	R	S	T	U	V
1		0.204	0.206	0.197	0.199	0.2	0.204	0.229	0.235	0.237	0.242	0.227	0.229	0.227	0.233	0.237	0.233	0.235	0.225	0.225	0.223	
2	0.189	0.193	0.208	0.206	0.204	0.202	0.204	0.237	0.233	0.223	0.231	0.242	0.223	0.227	0.233	0.235	0.233	0.235	0.231	0.229	0.237	
3	0.199	0.204	0.2	0.202	0.212	0.199	0.204	0.233	0.231	0.229	0.229	0.223	0.229	0.229	0.237	0.229	0.218	0.227	0.227	0.233	0.225	
4	0.189	0.195	0.202	0.202	0.193	0.197	0.208	0.235	0.229	0.227	0.225	0.229	0.231	0.229	0.227	0.231	0.231	0.229	0.231	0.233	0.233	
5	0.21	0.193		0.185	0.195	0.195	0.197	0.216	0.216	0.231	0.231	0.216	0.227	0.227	0.235	0.227	0.225	0.229	0.231	0.229	0.223	0.231
6	0.205		0.258	0.262	0.267		0.241	0.195	0.187	0.229	0.229	0.223	0.227	0.231	0.229	0.231	0.225	0.227	0.225	0.229	0.225	0.22
7		0.254	0.258	0.262	0.258	0.26	0.239	0.235	0.227	0.216	0.237	0.225	0.227	0.231	0.225	0.231	0.225	0.227	0.233	0.227	0.216	0.22
8		0.254	0.248	0.241	0.237	0.246	0.231	0.242	0.229	0.225	0.227	0.225	0.214	0.223	0.221	0.229	0.22	0.218	0.216	0.227	0.227	0.227
9		0.258	0.227	0.227	0.227	0.229	0.21	0.231	0.216	0.225	0.231	0.225	0.225	0.229		0.273	0.271	0.263	0.262	0.26	0.292	0.275
10		0.197	0.199	0.214	0.252	0.256	0.248	0.262	0.248	0.195	0.214			0.229	0.26	0.267	0.26	0.252	0.25	0.254	0.258	0.26
11		0.174	0.172	0.168	0.225	0.222	0.233	0.216	0.22	0.2	0.227	0.216	0.283	0.25	0.258	0.252	0.248	0.252	0.25	0.25	0.252	0.246
12		0.168	0.166	0.158	0.168	0.174	0.176	0.185	0.229	0.191	0.17	0.321	0.302	0.3	0.332	0.233	0.258	0.26	0.256	0.262	0.239	0.218
13		0.172	0.164	0.155	0.176	0.178	0.174	0.183	0.235	0.185	0.17	0.273	0.244	0.256	0.286	0.248						0.227
14		0.191	0.197	0.149	0.218	0.164		0.26	0.218	0.2	0.155	0.222	0.239	0.237	0.258	0.227	0.231	0.244	0.246	0.252	0.254	0.254
15		0.187	0.258	0.225	0.225	0.237	0.243	0.265	0.216	0.164	0.195	0.229	0.233	0.233	0.235	0.206	0.199	0.212	0.212	0.216	0.212	0.233
16			0.252	0.242	0.233	0.256	0.248	0.262	0.22	0.166	0.195	0.229	0.202	0.218	0.235	0.2	0.2	0.195	0.185			

Figure B.13 *Selma Chalk thickness measurements (s)*

APPENDIX C – Density Calculations

Step-through of the density calculation process.

Figure C.1 *Modern Formation depths and thicknesses*

STEP 1: Modern formation depths & thicknesses

Depth to...	*Norphlet*	*Smackover*	*Buckner*	*Haynesville*	*Cotton Valley*	*Hosston/Sligo*	*Rodessa*	*Ferry Lake*	*Mooringsport*	*Paluxy*	*Wash/Fred*	*Tusc*	*Eutaw*	*Selma*
Louann Salt	700	1002	1280	1841	3207	3844	4457	4882	5247	5782	6807	7320	8734	9992
Norphlet	0	302	580	1141	2507	3144	3757	4182	4547	5082	6107	6620	8034	9292
Smackover		0	278	839	2205	2842	3455	3880	4245	4780	5805	6318	7732	8990
Buckner			0	561	1927	2564	3177	3602	3967	4502	5527	6040	7454	8712
Haynesville				0	1366	2003	2616	3041	3406	3941	4966	5479	6893	8151
Cotton Valley					0	637	1250	1675	2040	2575	3600	4113	5527	6785
Hosston/Sligo						0	613	1038	1403	1938	2963	3476	4890	6148
Rodessa							0	425	790	1325	2350	2863	4277	5535
Ferry Lake								0	365	900	1925	2438	3852	5110
Mooringsport									0	535	1560	2073	3487	4745
Paluxy										0	1025	1538	2952	4210
Wash/Fred											0	513	1927	3185
Tuscaloosa												0	1414	2672
Eutaw													0	1258
Selma														0

Table C.2 *Porosity at deposition*

STEP 2: Determine porosity at deposition

porosity = initial porosity * e^(-depth*coefficient) becomes: Initial porosity = Porosity / (e^-depth *coefficient)

AVG DEPTH TO SELMA (m) 622

		Norphlet	*Smackover*	*Buckner*	*Haynesville*	*Cotton Valley*	*Hosston/Sligo*	*Rodessa*	*Ferry Lake*	*Mooringsport*	*Paluxy*	*Wash/Fred*	*Tusc*	*Eutaw*	*Selma*
	Thickness	700	302	278	561	1366	637	613	425	365	535	1025	513	1414	1258
	Porosity	0.13	0.138	0.16	0.125	0.145	0.15	0.135	0.16	0.16	0.16	0.18	0.24	0.32	0.14
	Depth	9914	9612	9334	8773	7407	6770	6157	5732	5367	4832	3807	3294	1880	622
	Depth (m)	3022	2930	2845	2674	2258	2063	1877	1747	1636	1473	1160	1004	573	190
	Chosen coefficient	2966	2599	1846	3299	2966	1909	3560	1846	3560	3299	2966	1909	2966	2574
	Initial Porosity =	0.360	0.426	0.747	0.281	0.310	0.442	0.229	0.412	0.253	0.250	0.266	0.406	0.388	0.151

Table C.3 *Thickness at deposition*

STEP 3: Determine thickness at deposition

initial thickness = current thickness (1 + (initial porosity - current porosity))

	Norphlet	*Smackover*	*Buckner*	*Haynesville*	*Cotton Valley*	*Hosston/Sligo*	*Rodessa*	*Ferry Lake*	*Mooringsport*	*Paluxy*	*Wash/Fred*	*Tusc*	*Eutaw*	*Selma*
initial thickness -->	262	119	134	198	485	251	204	162	122	178	339	182	460	388

Table C.4 *Formation thickness and porosity through time*

STEP 4: Determine thickness & porosity at of formations after deposition of each overlying formation

	Norphlet	*Smackover*	*Buckner*	*Haynesville*	*Cotton Valley*	*Hosston/Sligo*	*Rodessa*	*Ferry Lake*	*Mooringsport*	*Paluxy*	*Wash/Fred*	*Tusc*	*Eutaw*	*Selma*	
Initial Porosity = (from above)	0.360	0.426	0.747	0.281	0.310	0.442	0.229	0.412	0.253	0.250	0.266	0.406	0.388	0.151	
Coefficient (from above)	2966	2599	1846	3299	2966	1909	3560	1846	3560	3299	2966	1909	2966	2574	
current thickness = initial thickness / (1 + (initial porosity – [initial porosity*e$^{-depth*coefficient}$)))															
Thickness(m) with deposition of.....	*Norphlet*	*Smackover*	*Buckner*	*Haynesville*	*Cotton Valley*	*Hosston/Sligo*	*Rodessa*	*Ferry Lake*	*Mooringsport*	*Paluxy*	*Wash/Fred*	*Tusc*	*Eutaw*	*Selma*	*Cenozoics*
Norphlet	262	259	255	250	240	236	233	231	229	227	223	221	217	215	211
Smackover	0	119	116	113	107	104	102	101	100	99	97	96	94	93	91
Buckner		0	134	125	109	104	101	98	97	95	92	90	87	86	83
Haynesville			0	198	190	187	185	184	182	181	178	177	174	172	169
Cotton Valley				0	485	473	465	459	455	450	440	436	426	419	410
Hosston/Sligo					0	251	240	233	228	222	213	209	201	196	190
Rodessa						0	204	202	201	199	196	194	190	188	184
Ferry Lake							0	162	158	153	145	142	135	131	126
Mooringsport								0	122	120	118	116	114	112	110
Paluxy									0	178	174	172	167	164	160
Wash/Fred										0	339	334	323	316	306
Tuscaloosa											0	182	168	160	150
Eutaw												0	460	439	414
Selma													0	388	375
														0	622

Table C.4 *(Continued)*

Current porosity = initial porosity * $e^{(-depth*coefficient)}$

Porosity with deposition of.....	Norphlet	Smackover	Buckner	Haynesville	Cotton Valley	Hosston/Sligo	Rodessa	Ferry Lake	Mooringsport	Paluxy	Wash/Fred	Tusc	Eutaw	Selma	Cenozoics
Norphlet	0.360	0.344	0.331	0.311	0.267	0.247	0.232	0.222	0.214	0.203	0.184	0.175	0.153	0.137	0.115
Smackover		0.426	0.405	0.376	0.315	0.288	0.269	0.255	0.244	0.230	0.206	0.193	0.166	0.147	0.120
Buckner			0.747	0.671	0.518	0.456	0.413	0.382	0.360	0.331	0.281	0.258	0.208	0.174	0.131
Haynesville				0.281	0.243	0.226	0.213	0.204	0.198	0.188	0.172	0.164	0.145	0.131	0.112
Cotton Valley					0.310	0.285	0.267	0.254	0.244	0.231	0.208	0.197	0.172	0.153	0.127
Hosston/Sligo						0.442	0.397	0.365	0.344	0.315	0.266	0.243	0.196	0.164	0.123
Rodessa							0.229	0.219	0.211	0.202	0.184	0.175	0.156	0.141	0.121
Ferry Lake								0.412	0.386	0.351	0.293	0.267	0.211	0.175	0.129
Mooringsport									0.253	0.241	0.219	0.209	0.185	0.168	0.143
Paluxy										0.250	0.226	0.214	0.187	0.168	0.142
Wash/Fred											0.266	0.250	0.215	0.191	0.157
Tuscaloosa												0.406	0.319	0.263	0.194
Eutaw													0.388	0.341	0.277
Selma														0.388	0.315

Table C.5 *Formation density through time*

STEP 5: Determine density of formation after deposition of each overlying formation

Density sediments	2.65	2.71	2.71	2.72	2.65	2.68	2.72	2.71	2.72	2.72	2.65	2.65	2.65	2.71	
Density with deposition of.....	***Norphlet***	***Smackover***	***Buckner***	***Haynesville***	***Cotton Valley***	***Hosston/Sligo***	***Rodessa***	***Ferry Lake***	***Mooringsport***	***Paluxy***	***Wash/Fred***	***Tusc***	***Eutaw***	***Selma***	***Cenozoics***
Norphlet	2.070	2.096	2.117	2.149	2.221	2.253	2.276	2.293	2.306	2.323	2.354	2.369	2.404	2.429	2.465
Smackover		1.999	2.034	2.082	2.184	2.229	2.261	2.285	2.302	2.325	2.367	2.387	2.432	2.465	2.510
Buckner			1.462	1.589	1.845	1.948	2.020	2.073	2.108	2.157	2.240	2.279	2.362	2.419	2.492
Haynesville				2.248	2.312	2.341	2.361	2.377	2.388	2.404	2.431	2.445	2.476	2.500	2.533
Cotton Valley					2.150	2.191	2.220	2.241	2.256	2.278	2.315	2.333	2.374	2.403	2.445
Hosston/Sligo						1.955	2.029	2.081	2.116	2.164	2.244	2.281	2.359	2.412	2.479
Rodessa							2.336	2.353	2.365	2.381	2.411	2.425	2.458	2.482	2.517
Ferry Lake								2.022	2.065	2.124	2.221	2.265	2.357	2.417	2.494
Mooringsport									2.294	2.315	2.352	2.369	2.409	2.438	2.479
Paluxy										2.300	2.341	2.361	2.405	2.437	2.482
Wash/Fred											2.221	2.247	2.303	2.343	2.397
Tuscaloosa												1.996	2.136	2.226	2.338
Eutaw													2.025	2.102	2.203
Selma														2.062	2.184

Table C.6 *Average overburden density through time*

STEP 6: Determine average overburden density through time															
total thickness (m)	262	377	506	686	1132	1356	1531	1670	1773	1924	2215	2370	2758	3078	2981.20313
Percent of overburden thickness	***Norphlet***	***Smackover***	***Buckner***	***Haynesville***	***Cotton Valley***	***Hosston/Sligo***	***Rodessa***	***Ferry Lake***	***Mooringsport***	***Paluxy***	***Wash/Fred***	***Tusc***	***Eutaw***	***Selma***	***Cenozoics***
Norphlet	1	0.686	0.504	0.365	0.212	0.174	0.152	0.138	0.129	0.118	0.101	0.093	0.079	0.070	0.071
Smackover		0.314	0.230	0.165	0.094	0.077	0.067	0.061	0.057	0.052	0.044	0.041	0.034	0.030	0.030
Buckner			0.266	0.182	0.097	0.077	0.066	0.059	0.055	0.049	0.041	0.038	0.032	0.028	0.028
Haynesville				0.288	0.168	0.138	0.121	0.110	0.103	0.094	0.080	0.075	0.063	0.056	0.057
Cotton Valley					0.429	0.349	0.304	0.275	0.257	0.234	0.199	0.184	0.154	0.136	0.138
Hosston/Sligo						0.185	0.157	0.139	0.129	0.116	0.096	0.088	0.073	0.064	0.064
Rodessa							0.133	0.121	0.113	0.103	0.088	0.082	0.069	0.061	0.062
Ferry Lake								0.097	0.089	0.079	0.065	0.060	0.049	0.043	0.042
Mooringsport									0.069	0.062	0.053	0.049	0.041	0.036	0.037
Paluxy										0.092	0.078	0.072	0.061	0.053	0.054
Wash/Fred											0.153	0.141	0.117	0.103	0.103
Tuscaloosa												0.077	0.061	0.052	0.050
Eutaw													0.167	0.143	0.139
Selma														0.126	0.126
															0.209
total	1	1	1	1	1	1	1	1	1	1	1	1	1	1	1.2

Table C.6 *(Continued)*

weighted density by above percentage	***Norphlet***	***Smackover***	***Buckner***	***Haynesville***	***Cotton Valley***	***Hosston/Sligo***	***Rodessa***	***Ferry Lake***	***Mooringsport***	***Paluxy***	***Wash/Fred***	***Tusc***	***Eutaw***	***Selma***	***Cenozoics***
Norphlet	2.070	1.438	1.068	0.784	0.471	0.392	0.346	0.316	0.298	0.274	0.237	0.221	0.189	0.169	0.174
Smackover		0.628	0.467	0.343	0.206	0.171	0.151	0.138	0.130	0.120	0.104	0.097	0.083	0.074	0.076
Buckner			0.389	0.290	0.178	0.150	0.133	0.122	0.115	0.106	0.093	0.087	0.075	0.067	0.070
Haynesville				0.648	0.389	0.323	0.286	0.261	0.246	0.226	0.196	0.183	0.156	0.140	0.144
Cotton Valley					0.922	0.765	0.675	0.616	0.579	0.532	0.460	0.429	0.367	0.327	0.336
Hosston/Sligo						0.362	0.318	0.290	0.273	0.250	0.216	0.201	0.172	0.154	0.158
Rodessa							0.312	0.285	0.268	0.246	0.213	0.199	0.170	0.152	0.156
Ferry Lake								0.196	0.184	0.169	0.145	0.135	0.115	0.103	0.106
Mooringsport									0.157	0.145	0.125	0.116	0.099	0.089	0.091
Paluxy										0.213	0.183	0.171	0.146	0.130	0.134
Wash/Fred											0.340	0.317	0.270	0.240	0.246
Tuscaloosa												0.154	0.130	0.115	0.118
Eutaw													0.338	0.300	0.306
Selma														0.139	0.152
															0.456
average overburden density	2.070	2.065	1.924	2.064	2.166	2.163	2.221	2.226	2.251	2.281	2.313	2.309	2.311	2.199	2.722

REFERENCES

Adams, R.L., 2009, Basement tectonics and origin of the Sabine Uplift: Gulf Coast Association of Geological Sciences Transactions, v. 59, p. 3–19.

Andrews, D.I., 1960, The Louann Salt and its relationship to Gulf Coast Salt Domes: Gulf Coast Association of Geological Societies Transactions, v. 10, p. 215–240.

Archer, S.G., Alsop, G.I., Hartley, A.J., Grant, N.T., and Hodgkinson, R., 2012, Salt tectonics, sediments and prospectivity: An introduction: Geological Society Special Publication, v. 363, no. 1, p. 1–6.

Bearden, B.L., Mancini, E.A., and Puckett, T.M., 2000, Salt Anticline Play in the Mississippi Interior Salt Basin: AAPG Bulletin, v. 50.

Benson, D.J., Pultz, L.M., and Bruner, D.D., 1996, The Influence of Paleotopography, Sea Level Fluctuations, and Carbonate Productivity on Depostition of the Smackover and Buckner Formations, Appleton Field, Escambia County, Alabama: Gulf Coast Association of Geological Societies Transactions, v. 46, p. 9.

Bird, D.E., Burke, K., Hall, S.A., and Casey, J.F., 2005, Gulf of Mexico tectonic history: Hotspot tracks, crustal boundaries, and early salt distribution: AAPG Bulletin, v. 89, no. 3, p. 311–328.

Bishop, W.F., 1971, Geology of Upper Member of Buckner Formation, Haynesville Field Area, Claiborne Parish, Louisiana: AAPG Bulletin, v. 55, no. 4, p. 566–580.

Bishop, W.F., 1973, Late Jurassic contemporaneous faults in North Louisiana and South Arkansas: American Association of Petroleum Geologists Bulletin, v. 57, no. 5, p. 858–877.

Branson, E.B., 1915, Origin of thick gypsum and salt deposits: Bulletin of the Geological

Society of America, v. 26, p. 231–242.

Cloos, E., 1968, Experimental analysis of Gulf Coast fracture patterns: AAPG Bulletin, v. 52, no. 3, p. 420–444.

Copeland, C.W., 1968, Facies changes in the Selma group in central and eastern Alabama: Alabama Geological Society.

Copeland, C.W., 1976, Faults in Tertiary rocks of southwestern Alabama: Guidebook for the Annual Field Trip of the Alabama Geological Society, no. 14, p. 16–57.

Cushing, E.M., Boswell, E.H., and Hosman, R.L., 1964, General geology of the Mississippi embayment: Professional Paper, v. 448- B, p. 448.

Dawson, W.C., 1995, Diagenesis of deeply buried Eagle Mills sandstones: Implications for paleo-fluid migration and porosity development: AAPG Bulletin, v. 45.

Dawson, W.C., and Callender, C.A., 1992, Diagenetic And Sedimentologic Aspects Of Eagle Mills-Werner Conglomerate Sandstones (Triassic-Jurassic), Northeast Texas: AAPG Bulletin, v. 42, p. 449–457.

Dobson, L.M., and Buffler, R.T., 1997, Seismic stratigraphy and geologic History of Jurassic rocks, northeastern Gulf of Mexico: AAPG Bulletin, v. 81, no. 1, p. 100–120.

Dockery, III, D.T., and Thompson, D.E., 2016, The Geology of Mississippi: University Press of Mississippi.

Doolan, C.A., Karlsen, A.W., Survey, U.S.G., and Valley, S., 2011, An Assessment of Undiscovered Oil and Gas Resources in Clastic Facies of the Lower Cretaceous Sligo Formation , Eastern U . S . Gulf of Mexico Coastal Plain: Gulf Coast Association of Geological Societies Transactions, v. 61, p. 123–139.

Eddy, D.R., Van Avendonk, H.J.A., Christeson, G.L., and Norton, I.O., 2018, Structure and origin of the rifted margin of the northern Gulf of Mexico: Geosphere, v. 14, no. 4, p. 1804–1817.

Eddy, D.R., Van Avendonk, H.J.A., Christeson, G.L., Norton, I.O., Karner, G.D., Johnson, C.A., and Snedden, J.W., 2014, Deep crustal structure of the northeastern Gulf of Mexico: Implications for rift evolution and seafloor spreading: Journal of Geophysical Research: Solid Earth, v. 119, no. 9, p. 6802–6822.

Enomoto, C.B., Scott, K.R., Valentine, B., Hackley, P.C., Dennen, K., and Lohr, C., 2012, Preliminary evaluation of the shale gas prospectivity of the Lower Cretaceous Pearsall Formation in the onshore Gulf Coast region, United States: Gulf Coast Association of Geological Societies, v. 62, p. 93–115.

Eoff, J.D., Dubiel, R.F., Pearson, O.N., and Whidden, K., 2015, Geologic Framework for the Assessment of Undiscovered Oil and Gas Resources in Sandstone Reservoirs of the Upper Jurassic – Lower Cretaceous Cotton Valley Group , U . S . Gulf of Mexico Region: GCAGS Transactions, v. 65, p. 93–105.

Esposito, R.A., Pashin, J.C., and Walsh, P.M., 2008, Citronelle Dome: A giant opportunity for multizone carbon storage and enhanced oil recovery in the Mississippi Interior Salt Basin of Alabama: Environmental Geosciences, v. 15, no. 2, p. 53–62.

Forgotson, Jr., J.M., 1954, Regional stratigraphic analysis of the Cotton Valley Group of the Upper Gulf Coastal Plain: Transactions--Gulf Coast Association of Geological Societies, v. 4, p. 143–154.

Forgotson, Jr., J.M., 1957, Stratigraphy of Comanchean Cretaceous Trinity Group:

AAPG Bulletin, v. 41, no. 10, p. 2328–2363.

Forgotston, Jr., J.M., 1963, Depositional History and Paleotectonic Framework of Comanchean Cretaceous Trinity Stage, Gulf Coast Area: AAPG Bulletin, v. 47, no. 1, p. 69–103.

Fossen, H., 2016, Structural Geology: Cambridge University Press, Cambridge.

Halbouty, M.T., and Hardin, Jr., G.C., 1956, Genesis of Salt Domes of Gulf Coastal Plain: AAPG Bulletin, v. 40, no. 4.

Hammes, U., and Frébourg, G., 2012, Haynesville and Bossier mudrocks: A facies and sequence stratigraphic investigation, East Texas and Louisiana, USA: Marine and Petroleum Geology, v. 31, no. 1, p. 8–26.

Hammes, U., Hamlin, H.S., and Ewing, T.E., 2011, Geologic analysis of the Upper Jurassic Haynesville Shale in east Texas and west Louisiana: AAPG Bulletin, v. 95, no. 10, p. 1643–1666.

Hardin, F.R., and Hardin, G.C., 1961, Contemporaneous Normal Faults of Gulf Coast and Their Relation to Flexures: AAPG Bulletin, v. 45, no. 2, p. 238–248.

Heydari, E., 2000, Sedimentological characteristics of the Upper Cretaceous Demopolis Chalk, Mississippi: GCAGS Transactions, v. 50, no. 1991, p. 429–438.

Hosman, R.L., 1996, Regional stratigraphy and subsurface geology of Cenozoic deposits, Gulf Coastal Plain, south-central United States: US Geological Survey Professional Paper, no. 1416 G.

Hudec, M.R., and Jackson, M.P.A., 2007, Terra infirma: Understanding salt tectonics: Earth-Science Reviews, v. 82, no. 1–2, p. 1–28.

Hughes, D.J., 1968, Salt tectonics as related to several Smackover fields along the

northeast rim Gulf of Mexico Basin: Transactions--Gulf Coast Association of Geological Societies, v. 18, p. 320–330.

Hunt, B., Robinson, D.M., Weislogel, A.L., and Ewing, R.C., 2017, Sediment source regions and paleotransport of the Upper Jurassic Norphlet Formation, eastern Gulf of Mexico: AAPG Bulletin, v. 101, no. 9, p. 1519–1542.

Jackson, M.P.A., and Hudec, M.R., 2017, Salt Tectonics: Principles and Practice: Cambridge University Press, 498 p.

Jackson, M.P.A., and Seni, S.J., 1983, Geometry and evolution of salt structures in a marginal rift basin of the Gulf of Mexico, east Texas: Geology, v. 11, p. 131–135.

Jin, G., Groshong, R.H., and Pashin, J.C., 2009, Growth trishear model and its application to the Gilbertown graben system, southwest Alabama: Journal of Structural Geology, v. 31, no. 9, p. 926–940.

Johnson, J.R., Meylan, M.A., and Ufnar, D.F., 2006, Evolution of a Salt Diapir within the Mississippi Salt Basin , USA : Interaction of Salt Migration and Sediment Deposition: GCAGS, v. 56, no. 5, p. 309–322.

Kim, Y., Lee, C., and Lee, Y., 2018, Numerical analysis of sedimentary compaction: Implications for porosity and layer thickness variation: Journal of the Geological Society of Korea, v. 54, no. 6, p. 631–640.

Kimball, C.E., Anderson, E.G., Sartin, A.A., and Young, L.M., 1989, Petrology and hydrocarbon potential of the Ferry Lake Anhydrite, Caddo-Pine Island Field, Caddo Parish, Louisiana: Transactions--Gulf Coast Association of Geological Societies, v. 39.

Ko, J., 2014, Reviews of Brown Dense shale oil / gas system of the lower Smackover

Formation in north Louisiana, U.S.A.: Journal of the Korean Society of Mineral and Energy Resource Engineers, v. 51, no. 5, p. 729–749.

Liu, K., 2005, Onshore to Offshore , Northeastern Gulf of Mexico Area: GCAGS, v. 55, p. 431–441.

Llinás, J.C., 2003, Petroleum Exploration for Upper Jurassic Smackover Carbonate Shoal and Microbial Reefal Lithofacies Associated with Paleohighs, Southwest Alabama: GCAGS/GCSSEPM Transactions, v. 53, p. 462–474.

Mancini, E.A., and Mink, R.M., 1985, Upper Jurassic Norphlet Hydrocarbon Potential Along Regional Peripheral Fault Trend in Mississippi, Alabama, and the Florida Panhandle: ABSTRACT: AAPG Bulletin, v. 69.

Mancini, E.A., Mink, R.M., Payton, J.W., and Bearden, B.L., 1987, Environments of deposition and petroleum geology of Tuscaloosa Group (Upper Cretaceous), South Carlton and Pollard Fields, southwestern Alabama: American Association of Petroleum Geologists Bulletin, v. 71, no. 10, p. 1128–1142.

Mancini, E.A., Parcell, W.C., Puckett, T.M., and Llinas, J.C., 2001a, Topical Report 4 — Basin and petroleum migration modelling of the Mississippi Interior Salt Basin:

Mancini, E.A., and Puckett, M.T., 2000, Sequence Stratigraphy and Petroleum Potential of Lower Cretaceous Strata, Mississippi Interior Salt Basin: GCAGS Transactions, v. 50.

Mancini, E.A., Puckett, T.M., and Parcell, W.C., 1999, Modeling of the Burial and Thermal Histories of Strata in the Mississippi Interior Salt Basin: Gulf Coast Association of Geological Societies Transactions, v. 49.

Mancini, E.A., Puckett, T.M., Parcell, W.C., and Llinás, J.C., 2001b, Basin Analysis of

the Mississippi Interior Salt Basin and Petroleum System:, accessed at DOE Report.

Mancini, E.A., and Soens, D.D., 1994, Paleoenvironments of the Tombigbee Sand Member of the Eutaw Formation (Upper Cretaceous) of Eastern Mississippi and Western Alabama: ABSTRACT: AAPG Bulletin, v. 44, p. 421–430.

Mancini, E.A., Tew, B.H., and Mink, R.M., 1990, Jurassic Sequence Stratigraphy in the Mississippi Interior Salt Basin of Alabama: Gulf Coast Association of Geological Societies Transactions, v. 40, p. 521–529.

Mann, S.D., 1988, Subaqueous Evaporites of Buckner Member, Haynesville Formation, Northeastern Mobile County, Alabama: ABSTRACT: AAPG Bulletin, v. 38, p. 187–196.

Mann, C.J., and Thomas, W.A., 1964, Cotton Valley Group (Jurassic) nomenclature, Louisiana and Arkansas: Transactions--Gulf Coast Association of Geological Societies, v. 14, p. 143–152.

Martin, R.G., 1978, Northern and eastern Gulf of Mexico continental margin: Stratigraphic and structural framework: AAPG Special Publications, p. 21–42.

Mink, R.M., and Mancini, E.A., 1995, Lower Cretaceous and Upper Jurassic Oil Reservoirs of the Updip Basement Structure Play: Southwest Alabama: ABSTRACT: AAPG Bulletin, v. 45.

Moore, T., 1983, Cotton Valley Depositional Systems of Mississippi: AAPG Bulletin, v. 33.

Munyan, A.C., 1943, Subsurface Stratigraphy and Lithology of Tuscaloosa Formation in Southeastern Gulf Coastal Plain: AAPG Bulletin, v. 27, no. 5, p. 596–607.

Nunnally, J.D., and Fowler, H.F., 1958, Lower Cretaceous Stratigraphy of Mississippi:

Mississippi State Geological Survey Bulletin, v. 79.

Obid, J.A., 2005, Upper Jurassic Sequence Stratigraphy, Onshore to Offshore Alabama, Eastern Gulf of Mexico: Gulf Coast Association of Geological Societies Transactions, v. 55, p. 593–607.

Pashin, J.C., Groshong, Jr., R.H., and Jin, G., 1998a, Structural Modeling of a Fractured Chalk Reservoir: Toward Revitalizing Gilbertown Field, Choctaw County, Alabama: AAPG Bulletin, v. 48.

Pashin, J.C., Raymond, D.E., Rindsberg, A.K., Alabi, G.G., and Caroll, R.E., 1998b, Area Balance and Strain in an Extensional Fault System: Strategies for Improved Oil Recovery in Fractured Chalk, Gilbertown Field, Southwestern Alabama: DOE Report.

Payeur, T., Weimer, P., Gutterman, W., Zimmermann, E., and Cumella, S., 2017, Stratigraphic Evolution of Upper Jurassic Strata, Northeastern Deepwater Gulf of Mexico: Preliminary Results: GCAGS, v. 67, p. 235–257.

Petty, A.J., 1995, Ferry Lake, Rodessa, and Punta Gorda Anhydrite Bed Correlation, Lower Cretaceous, Offshore Eastern Gulf of Mexico: AAPG Bulletin, v. 45.

Petty, A.J., 2010, Stratigraphy and Petroleum Exploration History of the Smackover Formation (Oxfordian), Northeastern Gulf of Mexico: Gulf Coast Association of Geological Societies Transactions, v. 60, p. 583–596.

Pindell, J., Graham, R., and Horn, B., 2014, Rapid outer marginal collapse at the rift to drift transition of passive margin evolution, with a Gulf of Mexico case study: Basin Research, v. 26, no. 6, p. 701–725.

Pittman, J.G., 1984, Correlation of Beds Within the Ferry Lake Anhydrite: Gulf Coast

Association of Geological Societies Transactions, v. 35, p. 251–260.

Puckett, T.M., and Mancini, E.A., 1999, Stratigraphic Framework of the Mesozoic Sediments of the Mississippi Interior Salt Basin: Gulf Coast Association of Geological Societies Transactions, v. 49, p. 25.

Qi, J., Pashin, J.C., and Groshong, Jr., R.H., 1998, Structure and Evolution of North Choctaw Ridge Field, Alabama, a Salt-Related Footwall Uplift Along the Peripheral Fault System, Gulf Coast Basin: AAPG Bulletin, v. 48.

Quarles, Jr., M., 1953, Salt-ridge hypothesis on origin of Texas Gulf Coast type of faulting: Bulletin of the American Association of Petroleum Geologists, v. 37, no. 3, p. 489–508.

Raymond, D., 1989, Eagle Mills Formation of the Alabama coastal plain: Guidebook for the Annual Field Trip of the Alabama Geological Society, p. 75–92.

Raymond, D.E., Osborne, W.E., Copeland, C.W., and Neathery, T.L., 1988a, Alabama Stratigraphy: Geological Survey of Alabama Circular, v. 140, p. 102.

Raymond, D.E., Osborne, W.E., Copeland, C.W., and Neathery, T.L., 1988b, Waveland Field, an Analyses of Facies, Diagenesis, and Hydrodynamics in Mooringsport Reservoirs: Geological Survey of Alabama Circular, v. 31, p. 19–30.

Reese, D., 1975, Post Ferry Lake Lower Cretaceous clastics of South Mississippi and producing trends: Transactions--Gulf Coast Association of Geological Societies, v. 25, p. 192–195.

Rhodes, J.A., and Maxwell, G.B., 1993, Jurassic Stratigraphy of the Wiggins Arch, Mississippi: AAPG Bulletin.

Rives, J.S., 1961, The Hosston Formation of the San Marcos Arch: South Texas

Geological Society Bulletin.

Roberts, J.L., and Lock, B.E., 1988, Rodessa Formation, Bossier Parish, Louisiana: Lithofacies Analysis of Hydrocarbon-Productive Shallow-Water Clastic-Carbonate Sequence: AAPG Bulletin, v. 38.

Rowan, M.G., 2019, Conundrums in loading-driven salt movement: Journal of Structural Geology, v. 125, no. March 2018, p. 256–261.

Salvador, A., 1991, Triassic-Jurassic, *in* Salvador, A. ed., The Geology of North America: The Gulf of Mexico Basin: Geological Society of America, Boulder, Colorado, p. 131–180.

Schmoker, J.W., and Schenk, C.J., 1994, Regional Porosity Trends of the Upper Jurassic Norphlet Formation in Southwestern Alabama and Vicinity, with Comparisons to Formations of Other Basins: AAPG Bulletin, v. 78, no. 2, p. 166–180.

Scott, K.R., Hayes, W.E., and Fietz, R.P., 1961, Geology of the Eagle Mills formation: Gulf Coast Association of Geological Societies Transactions, v. 11, no. 1, p. 1–14.

Shah Alam, A.H.., and Pilger, Jr., R.H., 1988, Salt tectonics and Cretaceous uplift, westernmost central Mississippi Salt Basin, Madison Parish, Louisiana: Transactions--Gulf Coast Association of Geological Societies, v. 38, p. 225–230.

Swanson, S.M., Enomoto, C.B., Dennen, K.O., Valentine, B.J., Lohr, C.D., and Survey, U.S.G., 2013, Geologic Model for the Assessment of Undiscovered Hydrocarbons in Lower to Upper Cretaceous Carbonate Rocks of the Fredericksburg and Washita Groups, U.S. Gulf Coast Region: Gulf Coast Association of Geological Societies Transactions, v. 63, p. 423–437.

Sydboten, Jr., B.D., and Bowen, R.L., 1987, Depositional Environments and Sedimentary

Tectonics of the Subsurface Cotton Valley Group, West Central Ms: Gulf Coast Association of Geological Societies Transactions, v. 37, p. 239–245.

Talbert, S.J., and Atchley, S.C., 2000, Sequence Stratigraphy of the Lower Cretaceous (Albian) Fredericksburg Group , Central and North Texas A sequence stratigraphic framework is provided ABILENE: Gulf Coast Association of Geological Societies Transactions, v. 50, no. 2000.

Tew, B.H., Mink, R.M., Mann, S.D., Bearden, B.L., and Mancini, E.A., 1991, Geologic Framework of Norphlet and Pre-Norphlet Strata of the Onshore and Offshore Eastern Gulf of Mexico Area: Gulf Coast Association of Geological Societies Transactions, v. 41, no. 1, p. 590–600.

Thomson, A., 1978, Petrography and Diagenesis of Hosston Sandstone Reservoirs at Bassfield, Jefferson Davis County, Mississippi: ABSTRACT: Gulf Coast Association of Geological Societies Transactions, v. 28.

Thorsen, C.E., 1963, Age of growth faulting in the southern Louisiana.: Transactions-Gulf coast association of geological societies, v. 13, p. 103–110.

Tonietto, S.N., and Pope, M.C., 2013, Diagenetic Evolution and its Influence on Petrophysics Properties of the Jurassic Smackover Formation Thrombolite and Grainstone Units of Little Cedar Creek Field, Alabama: GCAGS Journal, v. 2, p. 62–82.

Valentine, B.J., Hackley, P.C., Enomoto, C.B., Bove, A.M., Dulong, F.T., Lohr, C.D., and Scott, K.R., 2014, Reprint of “Organic petrology of the Aptian-age section in the downdip Mississippi Interior Salt Basin, Mississippi, USA: Observations and preliminary implications for thermal maturation history”: International Journal of

Coal Geology, v. 136, p. 38–51.

Vendeville, B.C., 2005, Salt tectonics driven by sediment progradation: Part I - Mechanics and kinematics: AAPG Bulletin, v. 89, no. 8, p. 1071–1079.

Wade, W.J., and Moore, C.H., 1993, Jurassic Sequence Stratigraphy of Southwest Alabama: Gulf Coast Association of Geological Societies Transactions, v. 43, p. 431–443.

Walthall, B.H., and Walper, J.L., 1967, Peripheral Gult rifting in northeast Texas: The American Association of Petroleum Geologists Bulletin, v. 51, no. 102–110.

Warren, J.K., 2006, Salt Tectonics, *in* Evaporites: Sediments, Resources and Hydrocarbons: Springer, Berlin, Heidelberg.

Warsitzka, M., Kley, J., and Kukowski, N., 2013, Salt diapirism driven by differential loading - Some insights from analogue modelling: Tectonophysics, v. 591, p. 83–97.

Wilson, G. V., Kidd, J.T., and Shannon, S.W., 1976, Relationships of surface and subsurface faults in Choctaw and Clarke Counties, Alabama: Alabama Geological Society, p. 58–79.

Winter, C.V., 1954, Pollard Field, Escambia County, Alabama: Transactions--Gulf Coast Association of Geological Societies, v. 4, p. 121–142.

Worrall, D.M., and Snelson, S., 1989, Evolution of the northern Gulf of Mexico, with emphasis on Cenozoic growth faulting and the role of salt, *in* The Geology of North America: An overview: The Geological Society of America, p. 97–137.

Xiao, H.-B., and Suppe, J., 1989, Role of compaction in listric shape of growth normal faults: American Association of Petroleum Geologists Bulletin, v. 73, no. 6, p. 777–786.